*CO2 Injection in an Oil Reservoir with Gas Cap
(Compositional Simulation Case at Heidrun Field Norway)*

Master of Science Thesis

By
Zein Wijaya

Supervisor:
Prof. Jon Kleppe (NTNU)
Vidar Haugse Phd (Statoil)

Trondheim, June 2006

HOVEDOPPGAVEN/DIPLOMA THESIS/MASTER OF SCIENCE THESIS

Kandidatens navn/ The candidate's name: Wijaya, Zein

Oppgavens tittel, norsk/Title of Thesis, Norwegian:

Oppgavens tittel, engelsk/Title of Thesis, English: CO_2 Injection in An Oil Reservoir with Gas Cap (Compositional Simulation Case at Heidrun Field)

Utfyllende tekst/Extended text:

Project outline:

A potential problem with CO_2 injection in oil reservoirs with gas caps is that gas cap may be contaminated by Co_2. This could be an issue on the Heidrun field where downdip using CO_2-WAG is considered. Compositional reservoir simulations should be performed to investigate if the injected CO_2 will form a stable CO_2 layer below the hydrocarbon gas cap or if the CO_2 will be mixed with the hydrocarbon gas before or during the production of the gas cap.

The candidate will start with an existing black oil sector model (from Heidrun field). The sector model (or a part of it) should first be converted to a compositional model (Eclipse300) using an existing equation of state. A number of predictions should be performed, starting with down dip WAG at constant reservoir pressure followed by depletion of the gas cap.

The candidate should try to optimize the amount of gas that can be produced before CO_2 breakthrough by considering different alternatives for gas production wells. Other sensitivities like gas production rate and diffusion should be evaluated.

Studieretning/Area of specialization: Petroleum Technology

Fagområde/Combination of subjects: Reservoir Engineering

Tidsrom/Time interval:

Faglærer/Teacher
Professor Jon Kleppe

SKJEMAET TAS INN SOM SIDE 1 I HOVEDOPPGAVEN/PLEASE USE THIS FORM AS PAGE 1 IN THE THESIS

ACKNOWLEDGEMENTS

I would like to thank to Statoil Rotvoll Norway for their permission to use this data. I also want to express my sincerest gratitude to my supervisors in Statoil and NTNU: Vidar Haugse PhD, Alf Sebastian Lackner PhD, Prof Jon Kleppe and Jan Ivar Jensen for their personal and academic guidance throughout the whole work of this thesis and also for their fresh ideas and insights when discussing every topic in this thesis.

I also thank to Quota Programme for giving me financial support in two years studying at the Department of Petroleum Engineering and Applied Geophysics, Norwegian Science and Technology University (NTNU), Trondheim Norway.

I would like to give many thanks to the office staff at IPT, NTNU and all my friends for their friendship and 'smart' discussion in this latest two years.

Finally I want to dedicate this thesis to my family especially my wife (Lenny) and my daughters (Shania and Yasmin) that encourage me to finish this thesis.

Trondheim, June 2006

Zein Wijaya

STATOIL   **NTNU**

ABSTRACT

A potential problem with CO_2 Injection in oil reservoirs with gas caps is that gas cap may be contaminated by CO_2. This could be an issue on the Heidrun Field where down dip using CO_2-WAG is considered. Compositional reservoir simulations should be performed to investigate if the injected CO_2 will form a stable CO_2 layer below the hydrocarbon gas cap or if the CO_2 will be mixed with the hydrocarbon gas before or during the production of the gas cap.

The project thesis will be started with an existing black oil sector model (from Upper Tilje Formation in Segment H and I form Heidrun field). The sector model (or a part of it) should first be converted to a compositional model (Eclipse 300) using an existing equation of state. A number of predictions should be performed, starting with down dip WAG at constant reservoir pressure followed by depletion of the gas cap. The project thesis will discuss also how to optimize the amount of gas that can be produced before CO_2 breakthrough by considering different alternatives for gas production wells. Other sensitivities like gas production rate, well location, changing perforation interval and diffusion should be evaluated.

LIST OF CONTENTS

LIST OF FIGURES

LIST OF TABLES

1. INTRODUCTION

The Heidrun field was discovered on March 1985. The field lies in The Haltenbanken area, located in block 6507/07 of the Norwegian sector of the North Sea (See **Figure 1** in Appendix A). The field is being developed with a Tension Leg Platform (TLP). The platform is anchored to the seabed at 350 m (1150 ft) water depth. The average reservoir depth is 2375 m (7800 ft) subsea. The hydrocarbon bearing strata are predominantly unconsolidated sands which exhibit varied sedimentology, mineralogy and permeability through the section.

The Heidrun reservoirs are divided into the following main groups: Åre, Tilje and Fangst, where Fangst has the best reservoir qualities. Reservoir quality is generally high to very high, with porosity around 25 – 30%, and weighted average horizontal permeability around 277 mD. Overall the field is characterized by a high sand production tendency due to poorly consolidated reservoir sandstone.

The reservoir pressure and temperature are around 267 bar and 85°C respectively, at datum (2550 m TVD SS). The oil gravity is between 21 – 35° API. The initial pressure at the Heidrun field is hydrostatic and pressure support is therefore needed early in the life of the field. A combination of gas injection and water injection is used in the Fangst group while water injection is the main recovery method in the Tilje and Åre formations. WAG will be used in Upper Tilje for some of the segments, but the limited gas handling capacity limits the use of gas as an IOR method. Several studies have looked at gas injection in Lower Tilje and Åre, but they all conclude that water injection is the best recovery method

The Heidrun field started production on October 1995, ten wells were pre-drilled; nine producers and one gas injection well. Continuous drilling of new wells will be performed to the end of 2014, according to the current well plan. The initial reserve estimate was 118 million Sm^3 oil and 13.2 billion Sm^3 gas [17].

1.1   Geological Structure

The Heidrun field is formed by a large fault bounded structural closure dipping towards south, and is dissected by numerous minor normal faults with typical throws of less than 80 m. These faults have been grouped into the following three sets, which defines most of the major Heidrun fault segments (See **Figure 2** in Appendix A):

1.   Faults striking NNE - SSW.

2.   Faults striking N - S.

3.   Faults striking ESE - WNW.

The following seven horizons have been subject to seismic mapping: Sea Floor, Base Cretaceous Unconformity (BCU), Top Fangst Gp. (TFa), Top Ror Fm. (TRo), Top Tilje 4 Zone (TT4), Intra Åre 2B (IÅ2B), Coal Marker 1 and Coal Marker 2. This is illustrated in the seismic cross-sections in **Figure 3** (in Appendix A).

The erosional event of BCU of late Cretaceous age forms the topography of most of the Heidrun field, with increasing erosion from the central part of the field to the north. This causes a considerable variation in the seismic quality and character of the BCU event, dependent of changes in lithology and fluid (oil vs. gas) below the unconformity.

1.2   Geological Stratigraphy

The stratigraphy and sedimentary facies of the Heidrun reservoirs are shown in **Figure 4** (in Appendix A). Basically the stratigraphy of Heidrun reservoirs are divided into the following main groups: Åre, Tilje and Fangst. For this thesis project, we only discuss about Tilje formation.

The Tilje Formation in the Heidrun Field has an average thickness of 120 metres and was deposited in a shallow marine to paralic setting where tidal processes often dominated the depositional environment and this has in many cases resulted in very heterolithic lithologies.

The Upper Tilje (T3 &T4) has a higher sand content and significantly better reservoir properties than the Lower Tilje (T1&T2). The Tilje Formation is overlain by the marine Ror Formation which consists of shale and siltstone which grades to very fine sand both near the base and in the upper part. The average thickness of the Ror Formation is 60m. The Ror Formation is hydrocarbon filled in the sandier section in the same depth interval as the Tilje and Fangst reservoirs. It is however not included in the Heidrun Field reservoirs because of its inherent low permeability.

2. RESERVOIR CHARACTERIZATION HEIDRUN FIELD

Reservoir Characterization is an important step to be taken before doing reservoir simulation. This step is needed to identify uncertainty range that we have in reservoir. This means in this step, we try to assess the range of reservoir performance given our understanding of the subsurface uncertainties.

In this section, we will try to explain data that we used for simulating Heidrun field in term of rock properties, fluid properties, initial pressure and water oil contact (WOC) / gas oil contact (GOC). For this part, the author only discusses reservoir characterization from Upper Tilje formation in H and I segment from Heidrun field. These segments will be used as reservoir model in compositional simulation study.

2.1 Rock Properties

Regarding rock properties, the author tries to evaluate some reservoir uncertainties in reservoir rock Heidrun field (Upper Tilje formation in H and I segment) like:

➤ Porosity Distribution
➤ Permeability Distribution
➤ Relative Permeability
➤ Capillary Pressure

2.1.1 Porosity Distribution

Porosity is a measure of a rock's storage capacity. In reservoir simulation, the main important parameter is related to interconnected pore space For understanding porosity distribution data in Heidrun field, The author made histogram distribution from geological model to identify minimum (P10), centre (P50) and maximum (P90) porosity data for Upper Tilje formation (Segment H and I) Heidrun field. Based on histogram porosity data distribution in **Figure 5** (Appendix A)**,** it can be concluded that:

➢ Minimum porosity range (P10) in Heidrun field (H and I Segment): 7.03 %

➢ Mean porosity range (P50) in Heidrun Field (H and I Segment): 24.95 %

➢ Maximum porosity range (P90) in Heidrun field (H and I Segment) : 36.11 %

In the flow equations used in reservoir simulation, porosity appears as one of the parameters that scales the volume of fluids present in the reservoir at any time. During production, this volume is depleted, and reservoir pressure drops. The higher the reservoir's porosity, the less this pressure decline will be over time.

2.1.2 Permeability Distribution

Absolute permeability is a measure of a rock's ability to transmit fluid. For a hydrocarbon reservoir to be commercial, it must not only be porous, but also permeable. Permeability is analogous to conductivity in heat flow. Since it is a measure of resistance to flow, a higher permeability reservoir experiences less pressure drop than a corresponding low permeability reservoir. Regarding permeability data distribution in Upper Tilje Formation from Heidrun Field, the author tries to review permeability data in grid block model and make histogram permeability distribution. Based on histogram permeability distribution in **Figure 6** (Appendix A)**,** it can be concluded that:

➢ Minimum permeability range (P10) in Heidrun Field (H and I Segment) : 1 mD

➢ Mean permeability range (P50) in Heidrun Field (H and I Segment) : 1150.1 mD

➢ Maximum permeability range (P90) in Heidrun Field (H and I Segment) : 9260 mD

Similar to porosity, the permeability of a reservoir could be a function of pressure. Permeability is a key parameter controlling the propagation of transients created by conditions imposed at the well. It does not determine ultimate recovery, but rather the rate of this recovery.

For Heidrun Field, Permeability is generally high to very high, with weighted average horizontal permeability around 1150.1 mD. Based on log observation and analysis indicate that the quality of Heidrun reservoir, e.g. porosity and permeability increase towards to the northern crest of the structure (See **Figure 6** in Appendix A).

2.1.3 Relative Permeability

When two or more immiscible fluids flow simultaneously through a porous medium, they compete and do not move at equal velocity. This results on the one hand from interactions between the fluids and the rock, and on the other from interactions among the fluids themselves. As previously mentioned, this manifests itself in interfacial tensions. Interfacial tensions are not transport properties, and so we cannot use them directly to qualitatively characterize relative motion. We can, however, observe the relative ease with which each of the two competing fluids go through the porous medium—that is, we can measure the *relative permeability*. Relative permeability appears prominently in the flow equations used in reservoir simulation.

2.1.3.1 The Concept of Relative Permeability

The concept of relative permeability is an attempt to extend Darcy's law for single phase flow of fluid through porous media to account for simultaneous flow of several phases. In this regime, the flow of each phase is governed by the microscopic pressure gradient of each phase and the fraction of overall permeability that is associated with it. Relative permeability is a manifestation of microscopic forces and physical factors governing pore level movement and distributions of fluids. Whenever two or more phases are present within the pore space, their distribution is governed by the balance of capillary forces between fluid components and the rock, and by the wetting characteristics of the rocks. These two forces coupled with inertial forces due to pressure

gradients combine to determine how easily each phase moves within the porous material, hence the concept of relative permeability.

Relative permeability relations are usually reported as functions showing the variations of the relative permeability as a function of the saturations of the fluid. In addition, it is necessary to define residual saturations which normally indicate the smallest saturation for a given phase to become mobile. Relative permeability for a given fluid is fraction between 0 and 1. Since the wetting phase does not flow at or below its irreducible saturation, it follows that its relative permeability is 0 in that saturation range. Likewise for the non-wetting phase, its relative permeability is 0 for saturations equal / below the residual value. For two phase flow in porous media, the relative permeability of both wetting and non-wetting phases is usually plotted versus the wetting phase saturation. These curves are called as relative permeability curves. This curve can be generated by using some correlations (like: **Corey or Verma Correlation).** For Heidrun field, the recommended relative permeability curves for water and oil is given by "Frode's formula" [18]:

A. For Oil – Water Set:

$$kro = kro(Swi)\frac{Son^{a1}}{Son^{a1} + a2(1 - Son)^{a3}} \quad \text{.....................................(1)}$$

$$krw = krw(Sor)\frac{Swn^{b1}}{Swn^{b1} + b2(1 - Swn)^{b3}} \quad \text{...............................(2)}$$

Where: $\quad Swn = \dfrac{Sw - Swi}{(1 - Swi - Sorw)}$ ....(3)

$$Son = 1 - Swn \quad \text{...(4)}$$

Krw(Sor) = Relative permeability to water at residual oil saturation.
Suggested values are 0.1 - 0.2 for water wet,
0.3 - 0.4 for intermediate wettability, or > 0.5 for oil wet.

Kro(Swi) = Relative permeability to oil at irreducible water saturation.
Suggested values are 0.8 - 1.0 for water wet, or < 0.6 for oil wet.

Swi   = Irreducible water saturation.

Sorw   = Residual oil saturation during a water flood.
Suggested values are < 0.30 for water wet, 0.40 for intermediate wettability, or > 0.45 for oil wet.

a1, a2, a3 =   Fitting parameters

b1, b2, b3 =   Fitting parameters

The optimized values of fitting parameters were determined using a simulating annealing logarithm and depend on rock type.

B. For Gas – Oil Set:

The Corey equations have been used to generate the relative permeability curves for gas and oil:

$$For \quad S_g \ < \ S_{gcr} \ :$$
$$K_{rg} \ = \ 0$$

$$For \ S_g > 1 - S_{org} - S_{wcon} \ :$$
$$K_{rog} = 0$$

$For\ S_g \geq S_{gcr}$:

$$K_{rg} = K_{rgro} \left(\frac{S_g - S_{gcr}}{1 - S_{gcr} - S_{oirg} - S_{wcon}} \right)^{N_G} \quad \dots\dots\dots\dots\dots\dots\dots\dots\dots\dots\dots\dots(5)$$

$For\ S_g \leq 1 - S_{org} - S_{wcon}$:

$$K_{rog} = K_{rocg} \left(1 - \frac{S_g - S_{gcon}}{1 - S_{org} - S_{wcon} - S_{gcon}} \right)^{N_{og}} \quad \dots\dots\dots\dots\dots\dots\dots\dots\dots(6)$$

Where:

Krgro   = Relative permeability to gas at residual oil saturation.
       Suggested values are 0.2 - 1.0 for light oils, or < 0.1 for some heavy oils.

Krocg   = Relative permeability to oil at connate gas saturation.
       Input value should be the same as Krocw

Sgcon   = Connate gas saturation.
       Suggested values are 0.0 - 0.05 except for special cases such as foamy oil.

Sgcr   =   Critical gas saturation.
       If otherwise unknown, suggested values are same or greater than connate gas saturation.

Sorg   =   Residual oil saturation during a gas flood.
       Suggested values are 0.25 - 0.50

Soirg   =   Irreducible gas saturation.
       If otherwise unknown, suggested values are same or less than residual oil saturation during a gas flood(Sorg).

Ng   = Gas relative permeability exponent.

Nog   = Oil relative permeability exponent in the gas - oil curves.

For three phase flow, relative permeability is calculated from two sets of two phase curves. If water, oil and gas are flowing simultaneously, the following sets of relative permeability curves are used (See **Figure 7** in appendix A):

1. Oil–water set: where oil is the non wetting phase and water is the wetting phase
2. Gas–oil set: where gas is the non wetting phase and oil plus irreducible water are the wetting phase. This means that oil is the wetting phase while irreducible water is considered to be a part of rock solid.

The two relative permeability oil curves in **Figure 7** are two phase curves. However, as indicated above, in a three phase flow situation, the oil relative permeability would be a function of both water and gas saturations. Plotting it in a triangular diagram, so that each saturation is represented by one of the sides, we can define an area of mobile oil limited by the system's maximum and minimum saturations (which not necessarily are constants). Inside this area, *Iso - kro* curves may be drawn, as illustrated in **Figure 8** (Appendix A). In principle, *Kro* may be measured in the laboratory. However, due to the experimental complexity of three-phase experiments, we most of the time construct it from two phase oil-water *Krow* and two phase oil-gas *Krog* . The simplest approach is to just multiply the two:

$$Kro= Krow.\ Krog \quad ....(7)$$

However, since some of the limiting saturations in three phase flow not necessarily are the same as for two phase flow, this model is not representative. For instance, the minimum oil saturation, *Sor,* for three phase flow is process dependent and a very difficult parameter to estimate. The so-called *Stone-models* may be used for construction of three-phase relative permeability curves. A variety of other models exist, but these have been the most commonly used models. For the purpose of illustration, we will describe Stone's model 1 and model 2.

For **Stone's model 1**, we define normalized saturations as

$$S_{oD} = \frac{S_o - S_{or}}{1 - S_{wir} - S_{or}}$$

.... (8)

$$S_{wD} = \frac{S_w - S_{wir}}{1 - S_{wir} - S_{or}}$$

....(9)

$$S_{gD} = \frac{S_g}{1 - S_{wir} - S_{or}}$$

....(10)

Then we define the functions:

$$\beta_w = \frac{k_{row}}{1 - S_{wD}}$$

....(11)

$$\beta_g = \frac{k_{rog}}{1 - S_{gD}} \cdot$$

....(12)

The three phase oil relative permeability as constructed my Stone´s model 1 may now be defined as:

$$k_{ro} = S_{oD}\, \beta_w \beta_g$$

.... (13)

Please note that the above formulas assume that end point relative permeability is 1. If this is not the case, the relative permeability formula must be modified accordingly.

Stone's model 2 does not require the estimation of *Sor,* as it attempts to estimate it implicitly by its formulation.

The model simply is:

$$k_{ro} = (k_{rog} + k_{rg})(k_{row} + k_{rw}) - (k_{rw} + k_{rg})$$ .... (14)

In this model, *Sor* is defined at the point where *Kro* becomes negative. The two models of Stone predict quite different *kro's* in many cases, and one should be very careful in selecting which model to use in each situation.

2.1.3.2 The Relative Permeability of Heidrun Field

In Heidrun full field simulation model, there are introduced five sets of relative permeability curves. These relative permeability curves have been created based on network modeling. The different sets apply to zones of different absolute permeability. The report "Heidrun Relative permeability and capillary pressure recommendations" by Wibeke Hammervold Thomas and Egil Boye Petersen is a newly finished report which gives a recommended water/oil/gas relative permeability for the Garn, Ile, Tilje (Upper Tilje and Lower Tilje) and Åre formation. Especially for Tilje formation, basically there are 4 types of relative permeability curves (Tilje 3.1, Tilje 3.2, Tilje 3.3 and Tilje 3.4). In Tilje 3.2 the recommendations for a more water-wet case are used, and in Tilje 3.1 and Tilje 3.3-3.4 the curves representing a less water-wet case are used

The relative permeability curves in the segment model H and I are the same as the recommended curves set from the report mentioned above. Three different sets relative permeability curves are being used in simulation model for H and I segment. In the Tilje formation, the recommended plug scale oil-water relative permeability curves cannot be used directly in the simulation model. Because it is also difficult to get near a good history match by using the recommended plug scale relative permeability curves. The upscaling study indicate that some upscaling in relative permeability curve is needed in the Tilje formation

Regarding this, the author tries to make plot of **upscaling relative permeability curves for Tilje formation** in oil water system and gas oil system. These relative permeability curves were differentiated based on region in Heidrun geological model. Basically, there are 44 regions in Heidrun field where those regions were determined

based on imbibition number (IMBNUM) and saturation number (SATNUM), see **Figure 9** in Appendix A. Heidrun geologic model define IMBNUM and SATNUM in determining regions because Heidrun field used relative permeability hysteresis. In relative permeability hysteresis, relative permeability curves will show hysteresis between drainage processes (wetting phase decreasing) and imbibition processes (wetting phase increasing). For this case, IMBNUM (Imbibition number) will specify which saturation table is to be used for each grid block cell for imbibition processes. In the other side, SATNUM (saturation number) will specify which saturation table is to be used for drainage processes and equilibration in each grid block cell.

The plot of Tilje Formation Relative permeability curves can be seen in **Figure 10 -** Appendix A (for oil water system) and in **Figure 11 -** Appendix A (for gas oil system). From those charts, we can see that the endpoint for those relative permeability curves depend on irreducible saturation (For Upper Tilje: Sorw = 0.2 and Sorg=0.26). In this case, gas oil relative permeability curves are straight lines with Sorg=0.26.

Successful simulation of a multiphase system hinges on adequate relative permeability information. Since relative permeability is a function of saturation, which varies over a reservoir's life, the best way to get adequate information is to incorporate relative permeability models into the reservoir simulator. The data from relative permeability curves above will be used as input in reservoir simulator for Heidrun field. Based on past experience in reservoir simulation study, relative permeability data have been shown to affect the result of numerical simulations more than any other input parameter because this data is very critical in history-matching study (to match oil, water and gas production)

2.1.4 Capillary Pressure

2.1.4.1 The Concept of Capillary Pressure

Reservoir fluid flow is a fundamentally complex process. Fluid movement depends not only on the fluids themselves, but also on how the fluids interact with the porous medium, which in effect is a huge capillary network. When two immiscible fluids

are in contact inside a fine pore tube, a curved interface exists between them. Under static condition, the pressure within the phase on the concave side of the interface is higher than it is on the convex side to keep the interface from moving (see **Figure 12** in Appendix A). This pressure difference is balanced by the interfacial tension acting along the circumference of the interface. The fluid on the convex side of the interface has more affinity to wet the solid surface of the pore tube and is designated as the wetting phase. The other fluid is non-wetting phase. Capillary pressure is the pressure difference that exists across the interface of two immiscible fluids in a capillary (porous) system. In this case the pressure difference is between the non-wetting and the wetting phases across the interface. It can be expressed by equation:

$$P_c = \frac{2\gamma WN}{R} \cos\theta$$

.... (15)

Where:

P_c = Capillary Pressure

γWN = Wetting/non-wetting phase Interfacial Tension

R = Radius of the tube

Θ = Angle of contact between the solid surface and liquid

For a water-oil system with water as the wetting phase:

$$P_{cwo} = p_o - p_w$$ ....(16)

And for gas-oil system with oil as the wetting phase:

$$P_{cgo} = p_g - p_o$$ ....(17)

It should be obvious from expressions above that it is possible for the capillary pressure to be negative.

2.1.4.2 The Capillary Pressure of Heidrun Field

Regarding capillary pressure data in simulation model for H and I segment Heidrun field, the simulation is run with zero capillary pressure.

2.1.5 Fluid Contact (WOC and GOC)

Before running simulation in Heidrun field, the author tries to identify Water Oil Contact (WOC) and Gas Oil Contact (GOC). This data need to be known firstly because this data will be used as main consideration when we put injector and producer well in grid block system. The listed fluid contacts are based on observations in wells, and calculated contacts from pressure gradients. Unfortunately some segments have not been tested by wells. Consequently there is a significant uncertainty related to the distribution of fluid contacts across the field. This is accounted for in the uncertainty analysis.

Interpreted common fluid contacts are the basis for the fluid regimes. An integrated analysis of observation data (RFT data, logs) and pressure gradient calculation indicate fluid contact for H and I segment Heidrun field in **Table 1** below:

Reservoir / Contact	Gas Oil Contact (GOC)	Water Oil Contact (WOC)
Upper Tilje	2300 m (H Segment) 2305.5 m (I Segment)	2491.5 m (H Segment) 2488 m (I Segment)
Lower Tilje	2313 m (H Segment) 2305.5 m (I Segment)	2470 m (H Segment) 2488 m (I Segment)

Tabel 1: Gas Oil Contact and Water Oil Contact Depth in Upper and Lower Tilje Formation (H and I Segment) – Heidrun Field

The location of these fluid contacts in Heidrun geological model (H and I segment) can be seen in **Figure 13** (Appendix A).

2.1.6 Fluid Properties (Black Oil PVT Data)

Fluid properties, like rock properties, significantly affect fluid flow dynamics in porous media. Unlike rock properties, however, fluid properties exhibit significant pressure dependency. Therefore, it is often necessary in reservoir simulation to estimate these properties using correlations and/or equations of state.

The Heidrun reservoir fluids were first evaluated by **Simonsen** in 1987. In 1994, a more comprehensive study of the fluid system in the Heidrun reservoir was carried out by **Meisingset,** in order to provide the necessary input to reservoir simulation models. The study was based on data from exploration wells. **Meisingset** concluded that at least five main kinds of PVT properties could be observed among the investigated oil. Degree of biodegradation was regarded as main factor differ the fluid system. The fluid systems were grouped in five PVT groups, and the properties of each group were expressed on reservoir simulation input format (Eclipse 100 input files).

Since 1994, new PVT data has become available through analysis of oil collected from a number of production wells. This extension of the range and amount of PVT data available has made it possible to create a revised improved set of PVT models for the Heidrun reservoir fluid. Basically, each reference sample was described by an individual Equation of State (EOS), where the different EOS was developed by matching the measured properties of the reference samples. Currently based on formation and geographical placement, the fluid systems have been grouped into six PVT groups with different depth trends and two dummies group [5]. Two dummies group were created in PVT regions to make smooth and constant extrapolation for lower and higher density oil when reservoir model tries to extrapolate API versus depth from segment to segment in black oil simulation model. For Upper Tilje - H and I segment Heidrun field, PVT data that will be used is PVT data in group 1 (PVTNUM=1), see **Figure 14** in Appendix A.

The properties of the reservoir oil vary substantially both vertically and laterally over the field. This is modelled by using a non-constant RS, and API tracking. Initial density (API) and solution gas content (RS) are modelled with API vs. depth and RS vs. depth tables for each equilibration region, and thereby determine the fluid properties at any given point in the Heidrun reservoir, see **Figure 15** in Appendix A.

2.1.6.1   Gas Properties

In calculating gas properties such as density, compressibility and formation volume factor, we often use the real gas law as our basis. The properties of interest in the gas flow equation are *density*, *compressibility factor*, *compressibility*, *formation volume factor* and *viscosity*. Density appears in the gravity term, and it is often neglected. The compressibility factor introduces an important non-linearity, in that it appears in the formation volume factor. Gas viscosity is also strongly dependent on pressure, and needs to be calculated as pressure varies spatially and temporally.

Heidrun is an oil field that has gas cap, so for this field, we try to review PVT Gas that will be used as data input to run simulation. Gas density in Upper Tilje formation Heidrun field is about 0.922 kg/m³· For the other gas properties, the author tries to make correlation plot Bg and μg versus pressure (See **Figure 16** in Appendix A). These gas properties data will be used as data input in compositional simulation for Upper Tilje formation (H and I segment) at Heidrun field.

2.1.6.2   Oil Properties

Oil properties that appear in the governing flow equations for the oil phase are *density*, *compressibility*, *formation volume factor*, *viscosity* and *solubility of gas in oil*. In the absence of gas, these oil properties can be treated as constants, because the compressibility of gas-free oil is very small. However, the presence of dissolved gas in oil necessitates the use of appropriate correlations to determine the variation of these properties with pressure and temperature. Theoretically, an infinite amount of gas can dissolve in oil, provided that adequate pressure is available. Accordingly, if pressure is available, it is conceivable that there will be no free gas (undersaturated reservoirs). If pressure is not sufficient some of the gas will exist in the Free State (saturated reservoirs).

For Heidrun field, because the reservoir is saturated reservoir, we make correlation plot between Bo, and μo versus pressure with different GOR (See **Figure 17** in Appendix A). Thirty two (32) representatives Heidrun oil samples have been used in the current study to develop PVT model with API varying from 21 − 35. Based on that

study, the PVT properties of the fluid system can be described by use of six black oil PVT tables. Then reservoir model will interpolate between these six PVT tables by use of the API tracking function in the Eclipse 100 reservoir simulation software (with regard to depth dependency of API gravity and GOR).

For oil density, because there are 6 PVT regions and two dummies group in Heidrun field, we have eight different oil densities in PVT data. Especially for Upper Tilje Formation - Segment H and I, the oil density is **851 kg/m³** (group 1 in PVT data).

2.1.6.3 Water Properties

Since gas solubility in water is very small compared to oil, for most practical cases, we assume constant values for these properties that come into play in the water flow equation. For Heidrun field simulation, we use water properties data below:

Pressure, bara	Bw	Cw, bara^{-1}	μw, cp	ρw, kg/m³
245	1.03	4.94E-05	0.38	1033

Tabel 2: Water Properties Data for Heidrun Field

2.1.7 Reference Pressure and Initial Temperature

Based on the analysis of recombination RFT and log data from wells in Heidrun field, we estimate reference pressure for Upper Tilje formation – H and I segment - Heidrun field is 267.17 bara at datum depth 2550 meter. The initial reservoir temperature for Upper Tilje formation Heidrun field is 85 °C.

2.1.8 Equation of State (EOS) Model

Cubic equations of state (EOS's) are simple equations relating pressure, volume, and temperature (PVT). They accurately describe the volumetric and phase behavior of

pure compounds and mixtures, requiring only critical properties and acentric factor of each component. The same equation is used to calculate the properties of all phases, thereby ensuring consistency in reservoir processes that approach critical conditions (e.g., miscible-gas injection and depletion of volatile-oil/gas-condensate reservoirs). Problems involving multiphase behavior, such as low-temperature CO2 flooding, can be treated with an EOS, and even water-/hydrocarbon-phase behavior can be predicted accurately with a cubic EOS. One of the tools usually used in petroleum engineering to give comprehensive evaluation of the potentiality of the reservoir is reservoir simulation. Simulation will give accurate result if uses an accurate description of the reservoir fluid phase behavior and the appropriate reservoir model. This section gives the description about the EOS model. Basically there are 4 (four) common cubic EOS that have been known in petroleum industry.

Those cubic EOS are:
- ➢ Van Der Walls EOS
- ➢ Soave-Redlich-Kwong (SRK EOS), (Soave, 1972)
- ➢ Peng-Robinson (PR EOS), (Peng and Robinson, 1976)
- ➢ . Modified Peng-Robinson (PR78 EOS), (Peng and Robinson, 1978)

 All equations may be used with or without Peneloux volume correction (Peneloux et al., 1982). A constant or a temperature dependent Peneloux correction may be used. The temperature dependent volume correction is determined to comply with the ASTM 1250-80 correlation for volume correction factors for stable oils (Pedersen et al., 2002). In this section, the author only discuss about SRK equation with Peneloux volume correction because this equation will be used to develop EOS model in Heidrun field.

2.1.8.1 The Concept of EOS (SRK Peneloux EOS)

The Soave Redlich Kwong (SRK) Equation is the most widely used Redlich Kwong (RK) EOS proposed to date even tough it grossly overestimates liquid volumes

and underestimates liquid density of petroleum mixtures. The present use of the SRK EOS results from historical and practical reasons. It offers an excellent predictive tool for system requiring accurate predictions of VLE (Vapor Liquid Equilibrium) and vapor properties. Volume correction is highly recommended, if not mandatory, when liquid densities are needed from the EOS. The Pedersen et al for C_{7+} characterization method is recommended when the SRK EOS is used.

Basically, The SRK equation takes the form:

$$P = \frac{RT}{V-b} - \frac{a(T)}{V(V+b)}$$

....(18)

where P is the pressure, T the temperature, V the molar volume, R the gas constant and a and b are equation of state parameters, which for a pure component are determined by imposing the critical conditions

$$\left(\left(\frac{\partial P}{\partial V}\right)_T = \left(\frac{\partial^2 P}{\partial V^2}\right)_T = 0\right)_{\text{crit. point}}$$

....(19)

The following relation is then obtained for parameter a of component i at the critical point

$$a_{ci} = \Omega_a \frac{R^2 T_{ci}^2}{P_{ci}}$$

....(20)

and for parameter b:

$$b_i = \Omega_b \frac{R T_{ci}}{P_{ci}}$$

....(21)

Where

$\Omega_a = 0.42748$

$\Omega_b = 0.08664$

T_{ci} is the critical temperature of component i and P_{ci} the critical pressure. Values for T_c, P_c and may be seen from the pure component properties. All the values except those for salts are taken from Reid et al. (1977). The values for the salts are chosen to ensure that these components remain in the aqueous phase (Sørensen et al., 2002).

The temperature dependence of the a-parameter is expressed in the form of a term $a_i(T)$, which multiplied with a_{ci} gives the final expression for the a-parameter of the SRK-equation

$$a_i(T) = a_{ci}\alpha_i(T)$$ ....(22)

The parameter α is by default obtained from the following expression

$$\alpha_i(T) = \left(1 + m\left(1 - \left(\frac{T}{T_c}\right)^{0.5}\right)\right)^2$$ ....(23)

Where:

$$m_i = 0.480 + 1.574\,\omega_i - 0.176\,\omega_i^2$$ ....(24)

It is seen that $\alpha_i(T)$ equals 1 at the critical temperature at which temperature $a_i(T)$ therefore becomes equal to a_{ci}. ω is the acentric factor that is defined as follows (Pitzer, 1955):

$$\omega_i = -\log_{10} P_{ri}^{Vap}\Big|_{T_r=0.7} - 1$$

....(25)

where P_{ri}^{vap} is the reduced vapor pressure of component i (vapor pressure divided by critical pressure)

With Peneloux volume correction, the SRK equation takes the form:

$$P = \frac{RT}{V-b} - \frac{a}{(V+c)(V+b+2c)}$$

....(26)

The SRK molar volume, $\acute{\upsilon}$, and the Peneloux molar volume, V, are related as follows:

$$V = \acute{\upsilon} - c$$ ....(27)

The b parameter in the Peneloux equation $\widetilde{b}$ is similarly related to the SRK b-parameter as follows:

$$b = \widetilde{b} - c$$ ....(28)

The parameter c can be regarded as a volume translation parameter and is given by the following equation

$$c = c' + c''\ (T - 288.15) \dotfill (29)$$

where T is the temperature in K. The parameter c' is the temperature independent volume correction and c'' the temperature dependent volume correction. Per default the temperature dependent volume correction c'' is set to zero unless for C_{7+} pseudo-components. In general, the temperature independent Peneloux volume correction for defined organics and "other organics" is found from the following expression

$$c' = 0.40768 \frac{RT_c}{P_c} \left(0.29441 - Z_{RA}\right) \dotfill (30)$$

where Z_{RA} is the Racket compressibility factor

$$Z_{RA} = 0.29056 - 0.08775\ \omega \dotfill (31)$$

For some components, e.g. H_2O, MEG, DEG, TEG, and CO_2, the values have been found from pure component density data. For heavy oil fractions c is determined in two steps. The liquid density is known at 15°C/59°F from the composition input. By converting this density (ρ) to a molar volume $V = M/\rho$, the c' parameter can be found as the difference between this molar volume and the SRK molar volume for the same temperature. Similarly c'' is found as the difference between the molar volume at 80°C/176°F given by the ASTM 1250-80 density correlation and the Peneloux molar volume for the same temperature, where the Peneloux volume is found assuming c=c'.

2.1.8.2 Compositional (EOS) Model Heidrun Field

In a compositional model, reservoir fluids in communication should be described by a single EOS. Otherwise, oil with constant composition may change properties when

flowing through the reservoir. Heidrun Field EOS Model (for 23 pseudo components) was developed by performing the following procedures:

❖ Data collection and quality check

❖ Entering of compositions and experimental data into PVTsim software packages

❖ Tune SRK Peneloux equation of state (EOS) and match it to the experimental data (Tune to Constant Composition Expansion (CCE), Differential Liberation (DL) and a swelling test with CO_2)

❖ Export data from PVTsim to eclipse 100 and 300 format. The example of fluid composition for data input in Eclipse 300 format can be seen in **APPENDIX C**

The SRK Peneloux equation of stats (EOS) has been used in this work for PVT modelling purposes. Each EOS did not use the same correlation for viscosity, which cannot be used in a composition reservoir simulation model. A simplified approach was used in this study, where two typical Heidrun reservoir oils were used to set up compositional models with less variation in oil properties than in the black oil model. A light and a heavy Heidrun reference samples were chosen for this study. For light oil, The Corresponding States (CS) viscosity model has been used, while the Lorence Bray Clarke (LBC) model has been used for heavy oil. The light oil is denoted PVT2 in the black oil model [5]. This oil is from Tilje 3B in well 6507/7-A-22 and has an API of 30.9. The heavy sample is the PVT5 from Tilje 1C in well 6507/7-A-22, which has an API of 22.4. This compositional model was generated by Calsep (software provider) with converting previous compositional model to PVTsim version used in this study (version 11).

For getting match between SRK Peneloux EOS models with experimental data, some steps were carried out in PVTsim environment.

Those steps are:

➢ Reduce the number of components was used (Pseudoize the 30 components fluid characterizations for both PVT2 and PVT5)

➢ Characterization of the grouped components (SRK Peneloux EOS)

➢ Manual adjustment of Peneloux parameters to tune the density

> Tuning by regression for :

> - o Critical temperature of the C_{10+} components
> - o Critical pressure of the C_{10+} components
> - o Accentric factor of the C_{10+} components
> - o Critical volume of the C_{10+} components
> - o Interaction parameter between C_1 and C_{20+} components

The example of tuning model parameters for each component in PVT model 1 can be seen in **Table 3** below. In table below, tuning of the Peneloux parameter is quantified by showing both old (Old Pen) and new (New Pen) values. The interaction parameters (Kij) are set by default to 0 in the SRK-P EOS. Only the values after tuning are therefore shown.

PVT model:	PVT1, 34.6 API										
EoS:	SRK-P										
Visc. Mod	CS										
Grouping met	Standard										
Tuning:											
Comp:	Tc [%]	Pc [%]	Acc. fac. [%]	Vc [%]	Old Pen.	New Pen.	New C1 Kij	New C2 Kij	New C3 Kij	New C4 Kij	New C5 Kij
N2	-10.0	0.0	0.0	0.0	0.92	0.92	0.0	0.0	0.0	0.0	0.0
CO2	-2.0	0.0	0.0	0.0	3.29	3.29	0.0	0.0	0.0	0.0	0.0
C1	0.0	0.0	0.0	0.0	0.63	3.00	0.0	0.0	0.0	0.0	0.0
C2	0.0	0.0	0.0	0.0	2.63	3.00	0.0	0.0	0.0	0.0	0.0
C3	0.0	0.0	0.0	0.0	5.06	5.06	0.0	0.0	0.0	0.0	0.0
iC4	0.0	0.0	0.0	0.0	7.29	7.29	0.0	0.0	0.0	0.0	0.0
nC4	0.0	0.0	0.0	0.0	7.86	7.86	0.0	0.0	0.0	0.0	0.0
iC5	0.0	0.0	0.0	0.0	10.93	10.93	0.0	0.0	0.0	0.0	0.0
nC5	0.0	0.0	0.0	0.0	12.18	12.18	0.0	0.0	0.0	0.0	0.0
C6	0.0	0.0	0.0	0.0	17.98	17.98	0.0	0.0	0.0	0.0	0.0
C7	0.0	0.0	0.0	0.0	6.68	6.68	0.0	0.0	0.0	0.0	0.0
C8	0.0	0.0	0.0	0.0	14.66	14.66	0.0	0.0	0.0	0.0	0.0
C9	0.0	0.0	0.0	0.0	22.51	22.51	0.0	0.0	0.0	0.0	0.0
C10	-0.1	0.9	13.0	0.0	30.55	30.55	0.0	0.0	0.0	0.0	0.0
C11	-0.1	0.9	13.0	0.0	36.03	36.03	0.0	0.0	0.0	0.0	0.0
C12	-0.1	0.8	12.9	0.0	40.76	40.76	0.0	0.0	0.0	0.0	0.0
C13	-0.1	0.9	12.9	0.0	44.05	44.05	0.0	0.0	0.0	0.0	0.0
C14	-0.1	0.9	12.9	0.0	46.30	46.30	0.0	0.0	0.0	0.0	0.0
C15	-0.1	0.9	12.9	0.0	47.74	47.74	0.0	0.0	0.0	0.0	0.0
C16	-0.1	0.9	13.0	0.0	48.91	48.91	0.0	0.0	0.0	0.0	0.0
C17	-0.1	0.9	12.9	0.0	48.26	48.26	0.0	0.0	0.0	0.0	0.0
C18	-0.1	0.9	13.0	0.0	47.79	47.79	0.0	0.0	0.0	0.0	0.0
C19	-0.1	0.8	12.9	0.0	46.44	46.44	0.0	0.0	0.0	0.0	0.0
C20	-0.1	0.9	12.9	0.0	44.54	44.54	0.0	0.0	0.0	0.0	0.0
C21	-0.1	0.9	12.9	0.0	42.00	42.00	0.0	0.0	0.0	0.0	0.0
C22	-0.1	0.9	12.9	0.0	38.83	38.83	0.0	0.0	0.0	0.0	0.0
C23	-0.1	0.9	12.9	0.0	35.18	35.18	0.0	0.0	0.0	0.0	0.0
C24	-0.1	0.8	12.9	0.0	31.59	31.59	0.0	0.0	0.0	0.0	0.0
C25	-0.1	0.8	13.0	0.0	27.41	27.41	0.0	0.0	0.0	0.0	0.0
C26	-0.1	0.9	12.9	0.0	22.80	22.80	0.0	0.0	0.0	0.0	0.0
C27	-0.1	0.9	12.9	0.0	17.56	17.56	0.0	0.0	0.0	0.0	0.0
C28-C29	-0.1	0.9	13.0	0.0	10.15	10.15	-0.1	0.0	0.0	0.0	0.0
C30-C31	-0.1	0.9	13.0	0.0	-1.03	-1.03	-0.1	0.0	0.0	0.0	0.0
C32-C33	-0.1	0.8	13.0	0.0	-13.54	-13.54	-0.1	0.0	0.0	0.0	0.0
C34-C36	-0.1	0.8	12.9	0.0	-30.41	-30.41	-0.1	0.0	0.0	0.0	0.0
C37	-0.1	0.8	12.9	0.0	-42.61	-42.61	-0.1	0.0	0.0	0.0	0.0
C38-C39	-0.1	0.9	12.9	0.0	-52.50	-52.50	-0.1	0.0	0.0	0.0	0.0
C40-C43	-0.1	0.9	13.0	0.0	-72.53	-79.79	-0.1	0.0	0.0	0.0	0.0
C44-C48	-0.1	0.9	12.9	0.0	-104.95	-115.44	-0.1	0.0	0.0	0.0	0.0
C49-C80	-0.1	0.9	12.9	0.0	-177.20	-194.92	-0.1	0.0	0.0	0.0	0.0

Tabel 3: Example Tuning Parameters for Heidrun PVT Model no 1 [5]

The result of comparison between calculation Heidrun PVT Model and experimental data are shown in **Figure 18 , Figure 19** and **Figure 20** in Appendix A. From that chart, it looks that we can get close match for relative volume in CCE test, solution gas (Rs), gas volume factor (Bg), gas deviation factor (Z factor) and oil viscosity (μo). The match is not good for oil density. But overall, we can say that Heidrun EOS model is good enough to be used in compositional simulation model. Heidrun phase behaviour chart itself can be seen in **Figure 21** (Appendix A)

A simple approach was used to initialize the sector model, where the mole fraction for each component was linear with depth in oil zone. The compositional gradient was based on two points: the reference sample at the depth of sampling and saturated oil at the GOC. The composition of saturated oil was estimated by swelling the reference sample with injection gas. This approach gives a small variation in API with depth, while saturation pressure and GOR decreases with depth. The composition in the gas cap was found from the incipient of the oil at GOC. Gas composition in Heidrun Field mostly dominated by N_2-C_1 (86.16 % mole). The detailed of gas composition can be seen in **Table 4** below.

Component Name	Mole Composition (%)
N2-C1	8.62E-01
CO2	1.23E-02
C2	5.24E-02
C3	2.03E-02
C4	2.27E-02
C5	1.12E-02
C6	3.40E-03
C7	4.12E-03
C8-C9	6.21E-03
C10-C11	2.53E-03
C12-C13	1.60E-03
C14-C15	9.19E-04
C16-C17	4.18E-04
C18-C19	1.69E-04
C20-C21	4.95E-05
C22-C23	2.28E-05
C24-C25	1.08E-05
C26-C29	6.60E-06
C30-C33	9.43E-07
C34-C38	2.06E-07
C39-C44	3.42E-08
C45-C54	5.43E-09
C55-C80	1.36E-09

Tabel 4: Gas Composition in Upper Tilje Formation - H and I Segment Heidrun Field (Based on Correlation Depth Sample to Depth 2299.9 m and 2304.9 m)

Gas composition for Upper Tilje formation (H and I segment) in table above was analyzed based on correlation from depth sample 2281.4 m to depth 2299.9 m (H segment) and 2304.9 m (I segment). This correlation analysis has been verified by Phazecomp software and the result is matched.

For undersaturated oil composition in Upper Tilje formation - Heidrun field can be seen in **Table 5** below. This undersaturated oil composition was analyzed based on sample that was taken from depth 2393 m.

Component Name	Mole Composition (%)
N2-C1	4.33E-01
CO2	9.84E-03
C2	5.85E-02
C3	3.55E-02
C4	2.63E-02
C5	1.65E-02
C6	1.41E-02
C7	2.81E-02
C8-C9	6.11E-02
C10-C11	4.38E-02
C12-C13	4.64E-02
C14-C15	4.49E-02
C16-C17	3.45E-02
C18-C19	2.79E-02
C20-C21	1.72E-02
C22-C23	1.47E-02
C24-C25	1.26E-02
C26-C29	2.01E-02
C30-C33	1.48E-02
C34-C38	1.32E-02
C39-C44	1.04E-02
C45-C54	9.56E-03
C55-C80	7.19E-03

Tabel 5: Oil Composition (Undersaturated Oil) in Upper Tilje Formation - H and I Segment Heidrun Field (Based on Depth Sample at 2393 m)

3. CO$_2$ FLOODING CONCEPT

CO$_2$ flooding is one of successful EOR (Enhanced Oil Recovery) method applied in oil fields. When considering a candidate reservoir for CO$_2$ flooding, the first question historically asked is whether or not CO$_2$ is miscible with the in place crude at reservoir

temperature and obtainable reservoir pressure. However for CO_2 flooding, multiple contact or dynamic miscibility is only one of the recovery mechanism and enhancements which should be considered. Others include:

- ➢ Oil swelling with CO_2
- ➢ Extraction or vaporization of oil into the CO_2 rich phase
- ➢ Reduction of oil viscosity for improved mobility ratio
- ➢ Reduction in residual oil saturation due to a reduction in CO_2 – oil interfacial tension

While features such as these, as well as less favourable aspects such as CO_2 loss to the aqueous phase and water blockage of oil from contact with CO_2 are subjects for study in the laboratory, other characteristics such as unstable frontal advance due to viscous fingering and gravity tonguing are less suitable for laboratory investigation. In addition, scale up to reservoir condition involves question concerning the reservoir characterization as well as questions concerning operating alternatives. Examples of these field performance considerations include:

- ➢ Oil recovery performance
- ➢ CO_2 required per barrel of oil recovered
- ➢ Vertical and areal conformance
- ➢ Efficiency of mobility control alternatives
- ➢ Effect of injection and production well strategies
- ➢ Effect of pressure level and gradients
- ➢ Effect of stratification and dip
- ➢ Effect of process alternatives such as:
  - • Continuous CO2 injection
  - • WAG (water alternate with gas)
  - • Reservoir blow down
  - • CO2 slug followed by flue gas

3.1 Basic Concept

The principles of miscibility are fundamental to understanding how CO_2 flood work. Carbon dioxide is effective in improving oil recovery for two reasons: density and viscosity. At high pressure, CO_2 forms a phase whose density is close to that of a liquid, even though its viscosity remains quite low. Under miscible condition, the specific gravity of this dense CO_2 typically is around 0.7 to 0.8 g/cm^3, not much less than for oil and far above that of a gas such as methane, which is about 0.1 g/cm^3. Dense phase CO_2 has the ability to extract hydrocarbon components from oil more easily than if it were in the gaseous phase (and thus at lower pressure) [1]. The viscosity of CO_2 (0.05 to 0.08 cp) typically lower than that of fresh water (0.7 cp) or oil (1.0 to 3.0 cp). Although the low viscosity of the gas relative to the oil can be detrimental to sweep, CO_2 can improve recovery by reducing the oil viscosity.

3.1.1 Mechanisms for CO_2 Miscibility with Oil

In general, miscibility between fluids can be achieved through two mechanisms: first contact miscibility and multiple contact miscibility. When two fluids become completely miscible, they form a single phase; one fluid can completely displace the other fluid, leaving no residual saturation. A minimum pressure is required for two fluids to be miscible.

A clear example of first contact miscibility is ethanol and water. Regardless of the proportions of the two fluids, they immediately form one phase with no observable interface. Butane and crude oil also are first contact miscible and butane might make an ideal solvent for oil.

In the multiple contact miscible process that takes place with CO_2 and crude oil where CO_2 and oil are not miscible on first contact but require many contact in which components of the oil and CO_2 transfer back and forth until the oil enriched CO_2 cannot be distinguished from the CO_2 enriched oil (See **Figure 22** in Appendix A). Zick call this process a condensing / vaporizing mechanism. Multiple contact miscibility between CO_2 starts with dense phase CO_2 and hydrocarbon liquid. The CO_2 first condenses into the oil,

making it lighter and often driving methane out ahead of the "oil bank". The lighter components of the oil then vaporize into the CO_2 rich phase, making it denser, more like the oil, and thus more easily soluble in the oil. Mass transfer continues between the CO_2 and oil until the resulting two mixtures become indistinguishable in term of fluid properties. At that point, there is no interface between the CO_2 and oil and one hydrocarbon phase results [1]. **Figure 22 (**in Appendix A) illustrates the condensing / vaporizing mechanism for miscibility. During oil displacement, there is gradation in composition from pure CO_2 on the left (injection side) to virgin oil on the right (production side). The vaporizing region occurs upstream of the condensing region. Every contact in the process involves a miscible displacement, even though pure CO_2 is not miscible with original oil.

In the next section, the author will try to explain first contact miscibility and multiple contact miscibility process more detail by using conceptual phase behaviour ternary diagram to illustrate equilibrium condition.

3.1.1.1 First Contact Miscibility

First contact miscibility means that the injected solvent can mix with the reservoir oil in all proportions and produce a single phase fluid. Referring to **Figure 23** in Appendix A, the condition for first contact miscibility can be determined as follows:

❖ If the solvent is represented by the light component, then a tangent drawn from the top of point S to the two phase envelope will determine the oil compositions, on the bottom side of ternary diagram, which are miscible with that solvent

❖ If the reservoir oil composition is represented by point M on the diagram, then a tangent from that point to the two phase envelope will determine the solvent compositions which are miscible with that oil.

It follows that the range of oil compositions which are miscible with the light pseudo component, or solvent compositions which are miscible with particular oil, can be extended if the two phase region is decreased in size. This can be achieved by increasing

the pressure or decreasing the temperature. Of course, for decreasing the temperature is not possible since reservoir temperature is fixed. On the other hand, the two phase regions obtained with practical levels of injection pressure could be quite large such that the plait point disappears. In such case, first contact miscibility with the light component is not possible. The range of solvent compositions miscible with given oil will also decrease.

3.1.1.2 Condensing Gas Drive Miscibility

Condensing gas drive is one type of the developed miscibility. In this case, the reservoir oil composition is to the left of the limiting tie line within the ternary diagram (see **Figure 24** in Appendix A). Injection gases with compositions between A and B in **Figure 24** still can miscibly displace the reservoir oil even though they are not first contact miscible with it. In this situation, dynamic miscibility results from the insitu transfer of intermediate molecular weight hydrocarbons, predominantly ethane through butane, from the injected gas into the reservoir oil.

For example, assume that gas of composition B is injected to displace the oil in **Figure 24**. Gas composition B is defined by extending the limiting tie line through the plait point P until it intersects the right side of triangle. The right side of the triangle represents all mixture of methane and intermediate molecular weight hydrocarbons. Oil and gas B are not miscible initially, because most of their mixture falls within the two phase region. Suppose mixture M_1 within the two phase region results after the first contact of reservoir oil by gas B. According to the tie line passing through M_1, liquid L_1 and gas G_1 are in equilibrium at this point in the reservoir. Subsequent injection of additional gas B pushes the mobile equilibrium gas G_1 ahead into the reservoir, leaving Equilibrium liquid L_1, for gas B to contact. Gas B and liquid L_1, mix to give a new overall mixture M_2 at this location. However, Equilibrium gas G_2 and equilibrium liquid L_2 result from mixture M_2 and liquid L_2 lies closer to the plait point than the liquid L_1 left after the first contact. By continued injection of gas B, the composition of liquid at the well bore is altered progressively in a similar manner along the bubble point curve until it reaches the plait point composition. The plait point fluid is directly miscible with injection gas. By

this multiple contacting mechanism, reservoir oil is enriched with intermediate molecular weight hydrocarbons until it becomes miscible with the injected gas. This mechanism for the in-situ generation of miscibility is called variously the condensing gas drive process or the enriched gas drive process.

3.1.1.3 Vaporizing Gas Drive Miscibility

Vaporizing gas drive is another type of multi contact miscibility. **Figure 25** in Appendix A illustrates the mechanism of vaporizing gas drive miscibility. In this example, Reservoir oil A contains a high percentage of intermediate molecular weight hydrocarbons and its composition lies on the extension of the limiting tie line through the plait point. Injection gas and reservoir are not initially miscible. Consequently, the injection gas initially displaces oil immiscibly away from the well bore but leaves some oil undisplaced behind the gas front. Suppose the relative proportions of injection gas and undisplaced oil after this first contact is such as to give the overall composition M_1. According to the tie line passing through M_1, liquid L_1 and gas G_1 are in the equilibrium at this point in the reservoir. Subsequent injection of gas into the reservoir pushes the equilibrium gas G_1, left after the first contact, further into the reservoir, where it contacts fresh reservoir oil. Liquid, L_1 is left behind as residual oil saturation. As a result of this second contact, a new overall composition, M_2 is reached with corresponding equilibrium gas and liquid G_2 and L_2. Further injection causes gas G_2 to flow ahead and contact fresh reservoir oil and the process is repeated. In this manner, the composition of gas at the displacing front is altered progressively along the dew point curve until it reaches the plait point composition. The plat point fluid is directly miscible with the reservoir oil.

Although this description for the miscibility mechanism of the vaporizing gas drive process was given for multiple batch contacts of gas and oil, the process of gas enrichment is, of course, continuous; a transition zone of contiguously miscible composition is established from reservoir oil composition to injected gas composition. As long as the reservoir oil composition lies on or to the right of limiting tie line, miscibility can be attained by the vaporizing gas drive mechanism with injected gas that has a composition lying to the left of the limiting tie line.

If the oil composition should lie to the left of the limiting tie line, gas enrichment will occur only to the composition of equilibrium gas lying on the tie line that can be extended to pass through the oil composition. For example, if Reservoir oil B in **Figure 25** (Appendix A) were being displaced, the injection gas would be enriched to the composition of equilibrium gas G_2 but could not be enriched past this composition, since any further contacting of reservoir oil by gas G_2 would result only in mixtures that lie on the tie line passing through G_2. The requirement that the oil composition must lie to the right of the limiting tie line also implies that only oils that are undersaturated with respect to methane can be miscibly displaced by injection gas. Thus, oil of composition L_2 on the bubble point curve of **Figure 25** could not develop vaporizing gas drive miscibility with injection gas.

3.1.2 Effect of Pressure on CO_2 Flood Oil Recovery

Miscibility development between CO_2 and oil is a function of both temperature and pressure, but for an isothermal reservoir, the only concern is pressure. As pressure increases, the oil can dissolve more CO_2 and more oil components can be vaporized by the CO_2. At some pressure, when the CO_2 and oil are in intimate contact, they will become miscible. When the contact between CO_2 and oil occurs with little or no reservoir mixing, the pressure at which miscibility happen is defined as The Thermodynamic Minimum Miscibility Pressure (Thermodynamic MMP). The effects of small scale reservoir mixing can decrease the displacement efficiency of CO_2 and increase the pressure required for miscibility.

A plot of oil recovery versus CO_2 pressure (assuming 1D displacement, little reservoir mixing and constant reservoir pressure) shows oil recovery increasing rapidly with increasing pressure, then flattening out near 100%, when the thermodynamic MMP is reached (See **Figure 26** in Appendix A). At pressure above the thermodynamic MMP, there is little increase in oil recovery.

The oil recoveries shown in **Figure 26** (Appendix A) were obtained by Yellig and Metcalfe from CO_2 displacement of crude oil in slim tube displacement tests. Note that

the homogeneous sand used in slim tube tests limits reservoir mixing that might disturb the multiple equilibrium contact process required to develop miscibility. In actual reservoir, the effect of small scale heterogeneities can reduce the ideal slim tube oil recovery shown in **Figure 26** (Appendix A).

3.1.3 Diffusion Theory and Definitions

Diffusion is the process by which matter is transported from one part of a system to another as a result of random molecular motions. Diffusion is driven by a gradient in chemical potential [2]. This gradient can be caused by a difference in concentration, temperature, pressure, electrical potential etc. An example of gravitational and thermal diffusion is the process that causes an initial composition gradient in most petroleum reservoirs. Diffusion caused by concentration gradients is considered in the proposed method; i.e., an isothermal, isobaric (i.e., no diffusion caused by pressure gradients) system with no external force field gradients.

3.1.3.1 Diffusion Concept

The development of a theory for miscible liquid displacement requires evaluation of the variables which affect growth of the mixing zone between solvent and displaced oil. Factors which appear to be important are individual fluid viscosities, viscosity ratios, flood rate, fluid densities, and flow characteristics of the porous medium and molecular diffusion coefficients of the fluid components.

In rich gas flooding, injection gases containing intermediate hydrocarbon may develop miscibility with in place oil. Molecular diffusion is responsible for mixing at the pore level and has been shown to be an important rate controlling mechanism in gas flooding (Grogan and Pinczewski, 1987). Also diffusion rates are important for determining the extent of the mixing zones and the amount of solvent to be injected to achieve high recoveries [2].

A good example of molecular diffusion miscibility displacement is the injection of carbon dioxide in oil reservoirs. Carbon dioxide may generate miscibility by successive contacts, causing decreasing of saturation pressure, specific gravities, interfacial tension and viscosities with the corresponding increasing of oil swelling and solution gas content.

The mixing process observed during multi component fluid displacements in porous reservoir is generally of convection diffusion type. Convection arises from medium heterogeneity inducing local bulk velocity differences, while diffusion refers to the random motion of molecules. Combination of the two mechanisms leads to what is called "dispersion", i.e, a mechanism which will tend to even out any spatial concentration differences.

3.1.3.2 Diffusion Process

The molecular diffusion process is mainly governed by three mechanisms [11]. Those mechanisms are:

- ❖ Bulk Diffusion where fluid-fluid molecular interactions dominate
- ❖ Knudsen Diffusion for which fluid molecules collide with pore wells
- ❖ Surface Diffusion which corresponds to molecules transported along an adsorbed film

Unless there is a large amount of adsorption, surface diffusion plays a minor role. Knudsen type of transport is independent of fluid pressure as opposed to bulk diffusion for which the diffusion coefficients are inversely proportional to pressure.

3.1.3.3 Diffusion Coefficient and Diffusion Model

Most conventional method for measuring diffusion coefficients require compositional analysis which are both expensive and time consuming, In addition, significant errors may be associated with reported values of diffusion coefficients for multi component mixtures at high pressure [2]. This is due to various approximations made for the models used in calculation of diffusion coefficients from experimental data,

and it is the main reason for significant differences reported for diffusion coefficient measured for the same system. Extrapolation of available data to high pressure through existing correlations may not be accurate. Most correlations are developed based on data available on binary diffusion coefficient of relatively light compounds at high pressure.

The need for an accurate method to estimate liquid diffusion coefficients has been shown by da Silva and Belery (1989), by Coats (1989) and by Hu, Whitson and Yuanchang (1991). However, there is still a lack of appropriate models for the diffusion process, as well as experimental diffusion coefficients at high pressures in multi components reservoir fluids. Reported high pressure diffusion coefficients sometimes differ by more than 100 % from one source to another.

In this section, the author tries to discuss one method that was used to measure diffusion coefficient in Heidrun fluid properties. That method is Sigmund Correlation. The basic principle of this correlation is diffusion coefficients are approximately inversely proportional to pressure. Both Dawson, Khoury and Kobayashi (1970) and Khoury and Kobayashi (1970) have shown how a temperature independent expression for the ratio of the high pressure and the low pressure density – diffusivity product $\rho_m.D\,/(\rho_m D)^o$ may be developed. They start with a hard sphere model for self diffusion and the simplified kinetic theory of dilute gases. This can be defined with equation:

$$\rho_m = \frac{1}{4}\sigma.\rho_m\sqrt{\frac{\pi.RT}{M}}\left[\frac{pv}{RT}-1\right]^{-1} \quad \text{...(32)}$$

And

$$(\rho_m D)^o \; \propto \; \sqrt{T} \quad \text{...(33)}$$

Then it is possible to write the reduced value of density diffusivity product as:

$$\frac{\rho_m D}{(\rho_m . D)^o} = \beta . \rho_m \left[\frac{pv}{RT} - 1 \right]^{-1} \quad \text{...(34)}$$

Use the virial equation of state for pv/RT gives:

$$\frac{\rho_m D}{(\rho_m D)^o} = \beta \rho_m \left(1 + \frac{B}{v} + \frac{C}{v^2} + ... - 1 \right)^{-1} \quad \text{...(35)}$$

$$= \beta \rho_m (B \rho_m + C \rho_m{}^2 + D \rho_m{}^3 ...)^{-1}$$

The virial coefficients B, C .. are temperature independent for hard spheres. Modifying the polynomial and assuring that the value of $\rho_m D/(\rho_m D)^o$ approaches unity as the density approaches zero, results in the following equation:

$$\frac{\rho_m D}{(\rho_m D)^o} = 1 + B \rho_m + C \rho_m{}^2 + D \rho_m{}^3 + ... \quad \text{...................................(36)}$$

Where :

M	= Molecular weight, g/gmol
P	= Pressure, Pa
R	= Universal gas constant, 8.31438×10^6 Pa Cm^3/(K gmol)
T	= Temperature, K
ρ_m	= Molar density, gmol/cm^3
D	= Diffusion coefficient, cm^2/s
σ	= Interfacial tension, N/m
π	= Constanta, 3.14
v	= Molar volume,cm^3/gmol
β ,B,C,D	= The virial coefficients
o (superscript)	= equilibrium or original

The Sigmund correlation for estimating high pressure binary diffusion coefficients is based on **Equation 36** has been used in reservoir simulators for both vapor and liquid. This correlation is simple and requires only the component critical properties and other parameters available in a compositional simulator. Binary diffusion coefficients are given as a function of the mixture molar density, the low pressure diffusion coefficient, and a correction factor (Sigmund, 1976). It can be defined as:

$$D_{ij} = \frac{\rho_m D_{ij}^{\ o}}{\rho_m} \alpha_D \qquad \dots\dots\dots\dots\dots\dots\dots\dots\dots(37)$$

Where:

D_{ij} = High pressure diffusion coefficient of in in j, cm^2/s

α_D = Diffusivity product correction factor, dimensionless

The correction factor α_D is given by Sigmund as:

$$\alpha_D = 0.99589 + 0.096016\ \rho_{mr} - 0.22035\ \rho_{mr}^2 + 0.032874\ \rho_{mr}^3 \quad \dots\dots\dots(38)$$

Where:

ρ_{mr} = Reduced molar density, $gmol/cm^3$

For a mixture reduced molar $\rho_{mr} > 3.0$, an empirical correlation was recommended by Da Silva and Belery (1989):

$$\alpha_D = 0.18839\ e^{(3-\rho_{mr})} \qquad \dots\dots\dots\dots\dots\dots\dots\dots\dots(39)$$

In Eclipse 300 simulator, there are two diffusion models that can be used. In the first model, diffusion is driven by concentration gradient:

$$J_i = -cD_i \frac{\partial x_i}{\partial d}$$ ....(40)

In the second model, diffusion is driven by the gradient of chemical potential:

$$J_i = -cD_i^a x_i \frac{1}{RT} \frac{\partial}{\partial d} [\mu_i - M_i G(h - h_o) + M_i D_i^T \ln(T)]$$ ....(41)

Where:

J_i is the molar flux of component i per unit area,

c is the total molar concentration given by $c = 1/v_m$,

v_m is the molar volume of the mixture,

D_i is the diffusion coefficient of component i,

D_i^a is the activity-corrected diffusion coefficient of component i,

D_i^T is the thermal diffusion coefficient of component i,

x_i is the mole fraction of component i,

$\frac{\partial}{\partial d}$ is the gradient in the direction of flow,

M_i is the molecular weight of component i,

G is the acceleration due to gravity,

h is the height,

h_0 is the reference height,

T is the temperature,

R is the gas constant, and

μ_i is the chemical potential of component i, given by

$$\mu_i = \mu_{i0} + RT\ln(f_i)$$

where:

μ_{i0} is the reference chemical potential, and

f_i is the component fugacity.

Therefore, there are two ways of specifying diffusion coefficients [9]:

- ➤ Use normal diffusion coefficients, D_i (defined by keyword DIFFCOIL and DIFFCGAS in Eclipse 300)
- ➤ Use activity corrected diffusion coefficients, D_i^a (defined by keyword DIFFAOIL and DIFFAGAS in Eclipse 300)

3.2 CO₂ Displacement Process

Basically CO_2 displacement process in WAG (Water Alternate with Gas) injector can be divided into two phases: Phase Equilibria and Phase Transport [13]. The following notes explain about the observed physical behaviour from each phase.

3.2.1 Phase Equilibria

CO_2 joins with reservoir brine and oil in sometimes highly complex phase behaviour. This can be explained as follow:

A. CO_2 is stripped from the slug through partitioning into the aqueous phase. Aqueous phase density is somewhat reduced.

B. At pressure lower than the minimum miscibility pressure (MMP), CO_2 partitions into the oil possibly salting out methane in exchange

1. If sufficiently swollen with CO_2, the oil may be mobilized and subsequently produced. Another way of looking at this is that a trapped hydrocarbon phase will contain less stock tank oil.

2. Oil viscosity drops with CO_2 solubilization. This may help the water oil ratio as well as the CO_2 displacement mobility ratio. Oil density is often increased bringing water and oil densities closer together.

C. At somewhat higher pressure, but it is still below the MMP, CO_2 extracts deeply from the gas-oil fractions of the oil. Depending on temperature and composition,

this might be a vapour – liquid or a liquid – liquid extraction. Recovery of this CO_2 rich phase constitutes a CO_2 recovery mechanism.

1. The viscosity of the CO_2 rich phase increases with extraction of hydrocarbon components from the oil. This creates a more favourable mobility contrast between the CO_2 and oil or water

2. As the critical point for the mixture is approached, the interfacial tension between the CO_2 rich and the oil rich phase approach zero. Here the non linear phase interference effects as reflected by relative permeabilities are attenuated. This leads to more efficient displacement with possibly lower residual oil saturation.

D. When the MMP is exceeded, a dynamic miscibility condition is generated.

1. CO_2 is generally not miscible with reservoir oil upon first contact at any reasonable pressure. However, component mass transfer between the CO_2 rich phase and the oil rich phase will generate a zone upon multiple contacts which may locally be miscible with the oil. Unfortunately, dispersion causes the dissipation of the required composition and the system falls back into the multiphase region. Mass transfer then resumes with the subsequent re-approach to miscibility. This continuing competition between mass transfer promoted by phase equilibria and dispersion, gives the CO_2 displacement above the MMP characteristics of both miscible and immiscible drives.

2. The MMP is a strong function of reservoir temperature and is related to the pressure where the CO_2 has strong extraction or vaporization characteristics. Methane or flue gas reduces the extractive capability of CO_2 and hence their presence results in higher MMP's. The MMP is postulated to be at least as high as the local oil bubble point pressure. Thus if previous depletion and re-pressurization has led to a special distribution of bubble points, the MMP might likewise be a spacially varying parameter.

3. At higher temperature (for example T > 120 F), phase behaviour tends to be relatively simple. Above the MMP, a CO_2 rich vapour phase is displacing the

oil rich phase under conditions of dynamic miscibility. An oil residual containing some CO_2 may be left behind the transition zone.

4. At lower temperature, phase behaviour may be very complex indeed, with more than two phases observed behind the transition zone. Here, we might find a CO_2 rich liquid phase and an oil rich liquid phase. Phase boundaries have been observed to be ill defined indicating low interfacial tensions. Thus oil recovery due to capillary number effect might play an important part. Additionally, a solid phase has often been observed. This might be composed of asphaltine or paraffin dropout. The effect of multiple phase behaviour on reservoir flow is uncertain; however, one could readily envision a resultant mobility reduction or flow impairment.

3.2.2 Phase Transport

Water, whether present in the oil bank due to injection of water with or subsequent to CO_2 injection, may have significant effects on the displacement process

A. Water in the oil banks lowers oil mobility and hence results in a less favourable CO_2- oil displacement. Much will be dictated by the oil bank formation and water displacement and, hence, the drainage relative permeability curves (for a water wet reservoir)

B. Water in the CO_2-oil transition zone may result in oil filled pores blocked from access from the invading solvent. Again, although there is still some industry debate on the subject, oil recovery by dispersion through the water film seems probable. Rock wettability seems a significant factor.

3.3 Laboratory Tests for CO_2 Flooding in Heidrun Field

Heidrun was identified as one of the fields with potential for increased oil production from CO_2 injection in a screening study. CO_2 injection in Heidrun was evaluated by compositional reservoir simulation in sector model (Upper Tilje Formation

in H and I segments) where CO_2 was injected in down-dip WAG (Water Alternate Gas) injectors. In this section, the author will try to explain some laboratory tests that have been done in Heidrun to support compositional reservoir simulation for CO_2 injection.

3.3.1 Heidrun Minimum Miscibility Pressure (MMP)

The minimum miscibility pressure is the lowest pressure where practically all oil can be recovered after injection of just above a hydrocarbon pore volume of gas from a core with negligible dispersion [1]. MMP for CO_2 is usually lower than for typical hydrocarbon gases used for gas injection. In this study, MMP for the two oils were estimated from EOS simulation. The MMPz program from Zick Technologies was used in the majority of the calculations while MMP calculations will be verified by slimtube masurements (PVT5) and slimtube simulations with Eclipse 300 (PVT2).

The MMP for PVT2 with the Heidrun EOS is just below 250 bar, while the estimates for the heavier PVT5 oil is close to 380 bar [6]. Typical reservoir pressure for Heidrun is in the range 220 to 250 bar, indicating that near miscibility can be achieved if CO_2 is injected in the lighter Heidrun oils. MMPz predicted miscibility to be developed by the condensing / vaporizing mechanism which is typical for CO_2 injection.

All Heidrun fluid characterization [5] used a critical temperature for CO_2 of 298 ^{o}Kelvin, i.e lower than literature value of 304.2 ^{o}Kelvin. It is not clear why the literature value was not used. The change in critical temperature for CO_2 has practically no effect of the EOS predictions of oil properties because typical Heidrun reservoir oil contains just above 1 mol % CO_2. Using the Heidrun critical temperatures gives higher MMP than by using the literature value. MMP estimates are about 220 bar for light oil and 350 bar for heavy oil when the literature value is used.

MMPs were calculated both with the original 30 components EOS and the 9 components pseudoized EOS to check that pseudoization did not have a major impact on the MMP estimates. **Table 6** below shows that MMPs estimated from full and pseudoized EOS are reasonably close, with a maximum deviation of 8 bars. It was therefore assumed

---

that the 9 components EOS gave an accurate enough description of the fluids to be used in the reservoir simulations.

Number of components	CO_2 critical temperature	PVT2 MMP	PVT5 MMP
30	Heidrun	247.6	377.0
9	Heidrun	246.3	379.5
30	Literature	221.6	352.4
9	Literature	219.7	344.3

Tabel 6: Estimated Minimum Miscibility Pressure for Heidrun Oil with Different Number of Components and Critical Temperature of CO_2. MMPs were estimated by using 200 cells in MMPz Software [6]

Mixing CO_2 and reservoir fluids can sometimes give three phases especially at low reservoir temperature. This may create severe problems for the reservoir simulation model, where maximum two hydrocarbon phases are assumed. MMPz searched for mixtures that should give three phases during MMP calculations, but did not find such compositions.

Then these MMP calculations will be verified by slim tube test experiments (for PVT5 Heidrun oil) and slim-tube simulations (for PVT2 Heidrun oil) with Eclipse 300. In the next section, the author will try to explain more detail about slim tube test and slim tube simulation

3.3.1.1 Measurement MMP by Slim-Tube Test Experiment

The basic laboratory to determine thermodynamic MMP is slim tube test, shown in **Figure 27** (Appendix A), which produces 1D displacement with a very low level of mixing. The slim tube is constructed of stainless steel, typically ¼ in outside diameter and 40 ft long. Commonly sand packing is 160 to 200 mesh Ottawa Sand.

The test begins with a sand pack saturated with oil at a constant temperature. Carbon dioxide is introduced at a given pressure (controlled by a back pressure regulator) and oil displacement is measured as oil is recovered. No water is involved.

A high pressure sight glass shows the number of phases exiting the slim tube. Below the thermodynamic MMP, the sight glass shows oil with bubbles of CO_2. When the CO_2 has become miscible with the oil, there should be essentially only one phase flowing.

The CO_2 displacements are carried out for a range of pressures, holding the temperature constant at the reservoir temperature. For each pressure, typically, the oil recovery at 1.2 HCPV (Hydrocarbon Pore Volume) of CO_2 injected is plotted. An oil recovery factor of at least 90% is often used as a rule of thumb for estimating the thermodynamic MMP.

Uncertainties can arise in identifying the thermodynamic MMP precisely from slim-tube displacement test data. Oil recovery above 90% does not necessarily prove that miscibility has developed because one might occasionally see a few gas bubbles in the sight glass where the fluid exits the slim-tube. Such as displacement might be the result of a highly efficient immiscible gas displacement. From a practical point of view, however, achieving an oil recovery of close to 100% is more important than understanding whether or not miscibility truly was developed.

In spite of experimental uncertainties, slim tube tests provide valuable data that can contribute to the design of a CO_2 flood. Slim-tube data give the upper limit for oil displacement efficieny, which is defined as the oil recovery for 1D flow (ignoring the effects of areal and vertical sweep). Slim-tube data are also used in tuning an Equation of State (EOS) model to better predict both the development and loss of miscibility.

Regarding of slim-tube test, SINTEF had done slim-tube experiments with CO_2 for Heidrun heavy oil (for PVT5) in year 1999. High pressure slim tube displacement tests were performed for ten different pressures at 85 °C. The slim tube was charged with reservoir fluid at the required experimental conditions, and CO_2 was injected into the tube at constant flow rate. Based upon the visual observation and on the experimental results,

the miscibility pressure for Heidrun Oil (PVT5) is estimated to **362 bar +/- 4 bar** [7] (Please See **Figure 28** in Appendix A)

3.3.1.2 Measurement MMP by Slim-Tube Simulation (E300)

Because no MMP measurements were available for Heidrun light oils, so for verifying MMP calculation for Heidrun PVT2 oil (light crude oil), slim-tube simulations were run with different grid block size (500, 1000, 2000 and 10000 grid block size) and different pressure (220, 240, 260 and 280 bar). The length of slim-tube that was used in this simulation is 10 m (1000 cm). In this simulation, we assumed: porosity=10% and Permx=1000 mD. Twenty three (23) components (from PVT2 oil sample) were used in this simulation. CO_2 rate was injected into slim tube is about 0.1 HCPV (Hydrocarbon Pore Volume) / year. For running this slim tube simulation, we need CPU time around 2-7 days depend on how many grid block sizes that we used. More grid block sizes, more CPU time. The result from slim tube simulation can be seen in **Table 7** below:

Grid Block Size	Oil RF (P=220 bara)	Oil RF (P=240 bara)	Oil RF (P=260 bara)	Oil RF (P=280 bara)
500	82.51%	87.00%	90.65%	93.67%
1000	85.70%	89.82%	93.10%	95.62%
2000	88.86%	92.50%	95.23%	97.09%
10000	94.53%	96.93%	98.01% (Linear Extrapolation)	98.701% (Linear Extrapolation)

Tabel 7: Slim-Tube Simulation Result for Heidrun Oil (23 components) with different grid block size and different pressure

From those result, the next step, we try to do some extrapolation to get Oil Recovery Factor value for infinite grid block. We used extrapolation equation as follow:

$$RF_{i+1} = \left[\frac{RF_{i-2} - RF_i}{\frac{1}{\sqrt{Nx_{i-2}}} - \frac{1}{\sqrt{Nx_i}}} \ x\left(0 - \frac{1}{\sqrt{Nx_i}}\right) \right] + RF_i \qquad \dots\dots\dots\dots\dots\dots\dots(42)$$

Where: RF   = Oil Recovery Factor

                 Nx   = Grid Block Size

                 i, i+1 ..   = Sequence number of data

Based on extrapolations of slim-tube results (plot oil RF vs pressure) with different grids, indicated that the MMP is around **240 bar** . We estimate this MMP value when infinite grid block achieve oil recovery close to100% (See **Figure 29** in Appendix A). This estimation based on a practical point of view that achieving an oil recovery close to 100 % is more important than understanding whether or not miscibility truly was developed. In the other side, this result is also consistent with MMPz predictions.

3.3.2 Heidrun CO_2 Swelling Test

The measurement with the Heidrun oil swelled with CO_2 and HC gas was done by transferring oil from the recombination bottle to PVT cell [7], performing a PV measurement to measure the bubble point of the reservoir oil, adding gas to the oil and measuring the bubble point of the swelled oil in the PVT cell. The oil density data at the bubble point is plotted in **Figure 30** (Appendix A). From that plot, the density was found to increase with the addition of CO_2. Some of the density increase is related to the fact that the pressure at which the density is measured increases with the addition of CO_2. The grey line in **Figure 30** (Appendix A) shows the density of the pure Heidrun oil calculated at the bubble point pressures of the different CO_2-oil mixtures. For the lowest pressure, the density of the oil-CO_2 mixtures and pure Heidrun oil are close to equal, but at higher pressure, the density of the oil-CO_2 mixtures increases more than the pure oil. This can indicate that the partial molar density of CO_2 increases more with pressure than the molar density of the oil.

3.3.3 Diffusivity Coefficient for Heidrun Fluid Properties

Diffusivity coefficients for Heidrun light oil and gas were developed by using Sigmund correlation. This correlation was used to measure diffusivity coefficient for 23 components in Heidrun fluid properties. The value of diffusivity coefficient for each component in oil and gas Heidrun field can be seen in **Table 8** below.

Component Name	Oil Diffusion Coefficients (m^2/day)	Gas Diffusion Coefficients (m^2/day)
N2-C1	2.4609906476283D-05	4.4371121835183D-03
CO2	1.2666020337944D-05	3.5030221685031D-03
C2	1.7119150888023D-05	3.2187503826274D-03
C3	1.3085935800564D-05	2.5006912467352D-03
C4	1.0779909876953D-05	2.0941824372211D-03
C5	9.2032774704120D-06	1.7916120579619D-03
C6	7.9942081695250D-06	1.5547508972910D-03
C7	7.9629521943887D-06	1.6769330362902D-03
C8-C9	7.0646461654222D-06	1.4572486040753D-03
C10-C11	5.9695941572839D-06	1.1783855247369D-03
C12-C13	5.3656668557606D-06	1.0604573773544D-03
C14-C15	4.9703134307414D-06	9.9197600674106D-04
C16-C17	4.6153442904636D-06	9.3795684204982D-04
C18-C19	4.2911917042661D-06	8.8656726741367D-04
C20-C21	3.9866417302651D-06	8.4565046838506D-04
C22-C23	3.8092635118707D-06	8.2018114846996D-04
C24-C25	3.6710910624244D-06	8.0118304278914D-04
C26-C29	3.5466760580003D-06	7.7510336424642D-04
C30-C33	3.3348656333832D-06	7.4603099984614D-04
C34-C38	3.1692272942775D-06	7.1990253347896D-04
C39-C44	3.0069576222102D-06	6.9456340859289D-04
C45-C54	2.8595196378949D-06	6.6881644143058D-04
C55-C80	2.6958119584311D-06	6.4238786506382D-04

Tabel 8: Effective Diffusion Coefficients (23 components) for Oil and Gas in Heidrun Field based on Sigmund Correlation

From table above, it looks that diffusion coefficient value will increase for lighter components and it will decrease for heavier components. It means if we inject CO_2 into Heidrun reservoir, CO_2 will be easier to diffuse with lighter components. In the other side, we can see that diffusion coefficient value for gas is higher than diffusion coefficient value for oil. This occurred because gas consists of lighter components.

4. RESERVOIR MODELING HEIDRUN FIELD

In the current study, CO_2 injection was evaluated by compositional reservoir simulation on a sector model. For getting this compositional model, original black oil simulation model was converted. In this project, we used Eclipse 100 and Eclipse 300 simulator to run simulation study. The example of Eclipse 300 input file (Base Case

Compositional Model) which completely describes the developed reservoir model is presented in **APPENDIX B**

4.1 Reservoir Gridding

Basically, the original Heidrun simulation model is generated from a stochastic integrated 3D Geological model built in Petrel and RMS. For this project thesis, we used simulation grid from Base Case Black Oil Model (2B_BHP_CON_ISWR_TOLCRIT). This model covers all segments in Upper Tilje Formation - Heidrun Field (See **Figure 31** in Appendix A). The key numbers for the simulation grid are given in **Table 9** below.

Nx	Ny	Nz	Active Cells	Non Active Cells
97	138	27	91378	270044

Tabel 9: Key Number for Simulation Grid in Heidrun Base Case Black Oil Model (2C_PD_IMB_PC0_WI_2B_BHP_CON_ISWR_TOLCRIT)

For making simulation model for Upper Tilje H and I segment, we try to cut base case simulation grid above by using Floviz software. We used programming script in Floviz to create new property (MULTPV). Then this new property will be used as 'Include File' in Eclipse Data Input (in grid property section). When we cut the model, we used Equilibrium Number (EQLNUM) 14, 15 and 43 as reference because these numbers represent equilibrium number for H and I Segments plus Aquifer segment. After we cut the model, the number of active cells for simulation grid H and I Segment become **24272 cells**. This model includes three seal layers between each main layer. The final gridding model of Heidrun Field for Upper Tilje formation – H and I segment is presented in **Figure 32** (Appendix A).

4.2   Uncertainty in Heidrun Reservoir Model

Regarding uncertainties in reservoir model, the author tries to use uncertainty modelling tool (We called as "**CIRCE**" – Complexity Indices for Reservoir Characterization and Evaluation) for understanding about subsurface complexity and the key subsurface uncertainties for a particular reservoir model. Basically, there are 2 types of Circe Tool:

1. The static complexity tool (CIRCE –S, related to earth science / geological model issues like fault data, permeability heterogeneity etc)
2. The dynamic complexity tool (CIRCE – D, related to petroleum engineering issues like: Production / Injection wells, reservoir mechanism etc).

For Heidrun simulation study, the author tries to review uncertainties in geologic model (fault sealing, vertical heterogeneity etc) and simulation model (productivity reduction, multi-lateral wells etc). The objective of this uncertainty assessment is to identify major gaps in simulation processes and fundamental work that needed finished. The weakness of this review is that minimal time was spent understanding the details of "how" the analysis was done to create the geological model.

The static uncertainty (CIRCE –S) of Heidrun model can be seen in **Figure 33** (Appendix A) and the dynamic uncertainty (CIRCE – D) of Heidrun model can be seen in **Figure 34** (Appendix A)**.** In those figures, we can see all uncertainties that we have in static (geologic) and dynamic (simulation) model. Overall, the uncertainties in our static (geological) model can be divided into 3 main parts: Petrophysical Uncertainty, Reservoir Architecture Uncertainty and Compartment Uncertainty. For dynamic model, the uncertainties can be divided into 5 main parts: Production Well, Injection Well, Reservoir Mechanism, Unwanted Fluid and IOR (Improved Oil Recovery) method. From those parts of uncertainties, we try to select which factors that have the biggest uncertainties in our geologic and simulation model. Based on author's review, we can come up with 4 factors that have the biggest uncertainties.

Those factors are:

- ✓ Vertical Heterogeneity
- ✓ Fault Sealing
- ✓ Kv/Kh Ratio
- ✓ Productivity Reduction

4.2.1 Vertical Heterogeneity

In reservoir characterization, rock properties which receive most attention from variability standpoint are porosity and permeability. These two properties exhibit both heterogeneity and non uniformity but from now on will be referred to as heterogeneity. When the measured permeabilities and porosities at different areal locations within the reservoir, the reservoir is said to have areal heterogeneity. If the variations are from one layer to another layer, this is referred to as layer/vertical heterogeneity. Anisotropy means property variations with direction. Some reservoir rocks have different permeability in different directions. Recognizing the presence of heterogeneity in a given reservoir is important in determining well spacing, completion intervals and number of new infill wells. They also affect the performance of oil recovery process especially from a volumetric sweep efficiency stand point. Reservoir heterogeneity can be accessed at least qualitatively from the scales, geometries and distributions of various strata units in the reservoir.

Vertical heterogeneity is one of uncertainty factor in geological model Heidrun field because if we evaluated permeability data distribution, these data show variability from one to another layer within the vertical section of reservoir. The variability is between 200 - 6000 md. If there is vertical communication, this will create the biggest uncertainties for us when we try to determine infill well location and perforation interval regarding water displacement from aquifer and CO_2 flooding direction. This condition can be seen in **Figure 35** (Appendix A).

For reducing uncertainties and avoiding vertical communication between layers, geologist put three shale barriers in Heidrun geological model. This justification is based

on well log analysis. Then the uncertainty will depend on shale barrier continuity and the degree of sealing from shale barrier. Regarding shale barrier, we need detail evaluation to make sure shale barriers continue from one well to another well in Upper Tile formation, not disappear in some parts of reservoir.

4.2.2 Fault Sealing

In geological model Heidrun field, there are a lot of faults that create compartments for each segment. Each fault in geological model Heidrun field has sealing numbers. These numbers vary from one point to another point in fault plane. This created the biggest uncertainty in history matching because this related with cross flow fluid production from one segment to another segment. The fault seal model itself has a large number of parameters and these parameters have been used as the main variables in history matching for base case simulation model in Heidrun field. Based on this reason, we put fault sealing as one of the biggest uncertainties in our geological model. This uncertainty will affect areal sweep efficiency in reservoir regarding water – CO_2 displacement from one segment to another segment in Heidrun field.

4.2.3 Kv/Kh Ratio

Reservoir anisotropy (difference between Kv and Kh) can also be deduced from comparing permeability data in horizontal and vertical directions or in two different horizontal directions. Clastic reservoirs are characterized by more permeability variations in the vertical compared to horizontal directions (we called as "**Kv/Kh Ratio**"). Usually available cores and probe permeability measurements are used to develop average values of vertical/horizontal permeability ratio (Kv / Kh). The concept utilized here is that arithmetic average yield horizontal permeability and harmonic average yields vertical value. In applying this concept, the scale of measurement and reservoir stratifications should be taken into account in order to arrive at representative values of the permeability ratio

Basically vertical / horizontal permeability ratio depends on the stratification scale. Larger stratification scales (such as bed set and parasequences) would most likely exhibit lower vertical / horizontal permeability ratio (in range 0.01 to 0.5). On the other hand, smaller stratification scales (such as lamina and lamina sets) would tend to have higher values in the range 0.5 to 1.0

In term of this anisotropy and heterogeneity, these uncertainties are represented by the following parameters:

- ❖ Variations in reservoir facies and quality from both thickness and lateral extent standpoints
- ❖ Variations in stratification characteristic such as layers, laminae, cross bedding etc
- ❖ Variations in physical properties (porosity, permeability, relative permeability, capillary pressure etc)

For Heidrun H and I Segment case, we try to compare permeability variation between PERMX and PERMZ in grid block cells. Based on this comparison, we found that in H and I segment – Heidrun field, more permeability variation occurred in vertical direction compared with horizontal direction (See **Figure 36** in Appendix A). This condition is not good for sweep efficiency because it can create vertical communication between layers. For Heidrun model, Kv/Kh ratio will be represented by MULTZ value in 3 shale barriers. This parameter will be one parameter that needs to be considered/ adjusted when we try to do history matching in Heidrun field especially to get match with water production. The visualization of transmissibility value in Z direction for Heidrun model can be seen in **Figure 37** (Appendix A). This parameter is one uncertainty in our simulation model.

4.2.4 Productivity Reduction

The productivity reduction and uptime reduction factor cover two operational effects:

1. Fines migration reduces well productivity after water break through.

2. Scale deposition after sea water break through plug wells and the wells must be treated.

The first effect is modelled in the simulator by applying a PI multiplier (keyword: PIMULTAB in Eclipse 100) as a function of water cut where well productivity is reduced as a function of water cut due to fines migration. The reduction is based on experience data. The second effect is in addition modelled by a reduced uptime (keyword: WEFAC) for wells after sea water break through where wells are assumed to have a regularity of 0.95. Due to the need for scale treatment the regularity is reduced to 0.75 near the time of predicted seawater break through in the base case. We choose this parameter as one uncertainty in Heidrun H and I segment simulation model because there are a lot uncertainty ranges in multiplier value that we input in those keywords (refer to the statement that these multiplier values were created based on assumption and experience). In the other side, when we convert Eclipse 100 model to Eclipse 300 model, we should remove PIMULTAB keyword in Eclipse 300 schedule file because this keyword only valid for Eclipse 100. This parameter will contribute little bit uncertainty when we compare the simulation result of Eclipse 100 black oil with the simulation result of Eclipse 300 black oil.

5. SIMULATION STUDY

After data characterization and data inputting, the next step is running of simulation data using Eclipse 100 and Eclipse 300. The author puts the following 4 steps into consideration when running simulation data for Upper Tilje H and I Segment Heidrun Field:

1. History matching Heidrun Production Data (H and I segment) in Eclipse 100.
2. Convert Eclipse 100 model to Eclipse 300 Black Oil, and compare the result.
3. If the result of comparison between E100 and E300 Black oil is good enough, Run Eclipse 300 compositional case.
4. Doing prediction (sensitivities) in Eclipse 300 compositional with different cases and different parameter adjustment.

5.1   Simulation Basic Concept

Simulating multiphase fluid flow in porous media involves solving a system of coupled non-linear partial differential equations. Similar to the case of single-phase flow models, developing a computer model for these types of systems requires the use of finite-difference approximation to discretize these equations. The various solution techniques differ with respect to how we manipulate the governing partial differential equations. In this section, we try to summarize the most prominent methods used for handling multiphase flow equations.

5.1.1   Black Oil Model

Components: Oil, gas and water

Phases: Oil, Gas and Water

Oil density:

$$\rho = \frac{\rho_{os} + \rho_{gs}.R_{so}}{Bo} \quad \text{...(43)}$$

Where: **Bo, Bg, Rs, rs ~ ƒ(Po, Pb)**

The above parameters can be determined from PVT Experiments

We may write Black Oil Model equations as:

$$\frac{\partial}{\partial x}\left(\frac{kk_{ro}}{B_o\mu_o}\frac{\partial P_o}{\partial x}\right) - qo' = \frac{\partial}{\partial t}\left(\frac{\phi S_o}{B_o}\right) \quad \text{..(44)}$$

$$\frac{\partial}{\partial x}\left(\frac{kk_{rg}}{B_g\mu_g}\frac{\partial P_g}{\partial x} + \frac{kk_{ro}R_{so}}{B_o\mu_o}\frac{\partial P_o}{\partial x}\right) - q_g' - Rs_o.qo' = \frac{\partial}{\partial t}\left[\phi\left(\frac{S_g}{B_g} + \frac{S_oR_{so}}{B_g}\right)\right] \quad \text{.......(45)}$$

5.1.2 Compositional Model

Components: Methane, ethane, propane … N

Phases: Oil, Gas and Water

- In reservoir containing light oil, the hydrocarbon composition as well as pressure affects fluid properties
- Equilibrium flash calculation using K values or and equation of state (EOS) must be used to determine hydrocarbon phase compositions
- In a compositional model, we in principle make mass balance for each hydrocarbon component, such as methane, ethane, propane etc. In practice, we limit the number of components included and group components into pseudo components

Then, we define:

C_{kg} = mass fraction of component k present in the gas phase

C_{ko} = mass fraction of component k present in the oil phase

Thus, we have conditions that for a system of Nc components:

$$\sum_{k=1}^{N_c} C_{kg} = 1 \qquad \qquad \sum_{k=1}^{N_c} C_{ko} = 1$$

Then, a mass balance of component k may be written (in one dimension for simplicity):

$$-\frac{\partial}{\partial x}\left(C_{kg}\rho_g u_g + C_{ko}\rho_o u_o\right) = \frac{\partial}{\partial t}\left[\phi\left(C_{kg}\rho_g S_g + C_{ko}\rho_o S_o\right)\right]$$

..............(46)

Darcy's equations for each flowing phase are identical to the Black Oil equations:

$$u_o = -\frac{kk_{ro}}{\mu_o}\frac{\partial P_o}{\partial x}$$

$$u_g = -\frac{kk_{rg}}{\mu_g}\frac{\partial P_g}{\partial x}.$$

....(47)

Where:

Pc_{og} $= P_g - P_o$

Pc_{ow} $= P_o - P_w$

And

$So + Sg = 1$

Thus, we may write flow equations for Nc components as:

$$\frac{\partial}{\partial x}\left(C_{kg}\rho_g\frac{kk_{rg}}{\mu_g}\frac{\partial P_g}{\partial x} + C_{ko}\rho_o\frac{kk_{ro}}{\mu_o}\frac{\partial P_o}{\partial x}\right) = \frac{\partial}{\partial t}\left[\phi\left(C_{kg}\rho_g S_g + C_{ko}\rho_o S_o\right)\right], \quad k = 1, N_c$$

........(48)

- **The properties of oil and gas phases** depend on **pressure and composition**, so that the functional dependencies may be written:

$$\rho_g \,(P_g, C_{1g}, C_{2g}, ..)$$
$$\rho_o \,(P_o, C_{1o}, C_{2o}, ..)$$
$$\mu_g \,(P_g, C_{1g}, C_{2g}, ..)$$
$$\mu_o \,(P_o, C_{1o}, C_{2o}, ..)$$

- The equilibrium K values may be used to determine component ratios:

$$\frac{C_{ig}}{C_{io}} = K_{igo}(T, P, C_{ig}, C_{io})$$

....(49)

Where:

K	= Absolute Permeability [mD]
Kro,Krw,Krg	= Relative permeability oil,water and gas [fraction]
K_{igo}	= Equilibrium K values
C_{kg}	= Mass fraction of component k present in the gas phase
C_{ko}	= Mass fraction of component k present in the oil phase
Po,Pw,Pg	= Pressure in oil, water and gas phase [psi]
Pcow,Pcgo	= Capillary pressure in oil-water and gas oil phase [psi]
Δx,	= Delta in x direction [ft]
μo,μw, μg	= Oil, water and gas viscosity [cp]
ρo,ρw,ρg	= Oil, water and gas density [lb/cuft]
Bo,Bw	= Oil and water formation volume factor [bbl/STB]
Bg	= Gas formation volume factor [bbl/SCF]
qo',qw'	= Oil and water rate in reservoir condition [bbl/day]
qg'	= Gas rate in reservoir condition [cuft/day]
So, Sw,Sg	= Oil, water and gas saturation [fraction]
Rso	= Solution gas in oil [SCF/STB]
Ø	= Porosity [dimensionless]
T	= Time[day]
P	= Pressure [psi]

The numbers of equations that must be solved in compositional simulation depend on the number of components modeled. Often, we model the lighter components individually and group heavier components into a pseudo component. If non hydrocarbons are involved, these may have to also be modeled separately [8].

5.1.3 Fully Implicit Method

For Heidrun H and I segment simulation project, we will use Fully Implicit method as formulation in simulation study for history matching in Eclipse 100 simulator. In this section, we will try to discuss about this method. Basically, in the *Fully Implicit*

Solution with Newtonian iteration method, we reduce the six principal unknowns of the three-phase flow equations to three linearly independent principal unknowns (most often one phase pressure and two saturations) by using the capillary pressure and saturation relationships. We then use finite-differences to approximate the three partial differential equations that result. By treating the coefficients implicitly (at the same level as the principal unknowns) we generate a system of non-linear algebraic equations. We can linearize these equations using the generalized Newton-Raphson procedure, such that we can implement a Newtonian iteration. In the solution process, a residual function is formed and its derivative calculated with respect to each principal unknown to construct the Jacobian. We then use a numerical differentiation scheme to obtain the elements of the Jacobian matrix. The salient points of the Newton-Raphson method are highlighted below.

Consider a set of non-linear equations in two unknowns, x and y:

$$f(x, y) = 0 \quad \text{..} (50)$$

$$g(x, y) = 0 \quad \text{..} (51)$$

With (x_o, y_o) as an initial guess to the solution. Suppose that $(x_o + \Delta x, y_o + \Delta y)$ is the exact solution. Then, a Taylor series expansion can be written in the neighborhood of (x_o, y_o), i.e.,

$$f(x_0 + \Delta x, y_0 + \Delta y) = f(x_0, y_0) + \Delta x \left.\frac{\partial f}{\partial x}\right|_{x_0, y_0} + \Delta y \left.\frac{\partial f}{\partial y}\right|_{x_0, y_0} + \ldots = 0$$
$$\text{....................} (52)$$

$$g(x_0 + \Delta x, y_0 + \Delta y) = g(x_0, y_0) + \Delta x \left.\frac{\partial g}{\partial x}\right|_{x_0, y_0} + \Delta y \left.\frac{\partial g}{\partial y}\right|_{x_0, y_0} + \ldots = 0$$
$$\text{....................} (53)$$

Truncating the above series after the first-order terms, we obtain a system of linear equations in two unknowns, Δx and Δy.

$$\Delta x \left.\frac{\partial f}{\partial x}\right|_{xoyo} + \Delta y \frac{\partial f}{\partial y} = -f(xoyo)$$

....(54)

$$\Delta x \left.\frac{\partial g}{\partial x}\right|_{xoyo} + \Delta y \frac{\partial g}{\partial y} = -g(xoyo)$$

....(55)

The solution of these two equations for Δx and Δy leads to better estimates of the solution of the original non-linear equations. We repeat this process in an iterative manner until the improvements in Δx and Δy become small enough to satisfy the pre-set convergence criterion. We can express the iterative process in the matrix form as follows:

$$x^{(k+1)} = x^{(k)} + \Delta x^{(k+1)}$$ ....(56)

$$y^{(k+1)} = y^{(k)} + \Delta y^{(k+1)}$$ ....(57)

In the above matrix equation, the coefficient matrix is referred to as the *Jacobian* (J).

5.1.4 Adaptive Implicit Method

For Heidrun H and I segment compositional simulation project, we will use Adaptive Implicit Method in Eclipse 300 (keyword: AIM) as formulation in simulation study. The advantage of this method to avoid time step restrictions imposed by small block particularly those containing wells [9]. Basically, The Adaptive Implicit Method is a compromise between the fully implicit and IMPES procedures. Cells with a high throughput ratio are chosen to be implicit for stability and obtain large time-steps, while the majority of cells can still be treated as IMPES where the solution may be changing little. All completions are treated implicitly with target fraction of implicit cells in a compositional run is 1%.

5.2 Heidrun Black Oil Simulation Model

The original base case simulation model from Heidrun field was an Eclipse 100 model. This model includes all segments in Upper Tilje formation. Both small scale heterogeneities and faults below seismic resolution are included. The number of active grid block in this base case model is 91378 cells, with a typical spatial grid block size just below 100 m. The thickness of numerical layers typically varies from 2 to 15 meters. A top view from oil water contact and gas oil contact in the base case model is shown in **Figure 13** (Appendix A).

For simulating Upper Tilje in H and I segment Heidrun field, just like the author mentioned before in previous section, we try to cut original base case simulation model by using programming script in Floviz software. When we cut the model, we used Equilibrium Number (EQLNUM) as reference to choose H, I and aquifer segment (EQLNUM= 14, 15 and 43). After we cut the model, the number of active cells for simulation grid H and I segment become **24272 cells**. This model includes six producer wells, two WAG injectors and one virtual gas injector. The location of these wells can be seen in **Figure 38** (Appendix A). The initial volume and number of active grid block in Heidrun Black Oil Simulation Model can be seen in **Table 10** below.

Model Name	STOIIP MSm3	WIIP MSm3	GIIP MRm3	Pore Volume MRm3	Number of Active Grid Blocks
Heidrun Black Oil Model (H an I Segment)	29.962	2506.23	7943.13	2626.125	24272

Tabel 10: Initial Volume and Number of Active Grid Block Heidrun Black Oil Model for H and I Segment

In this section, the author tries to explain some assumptions [6] that were used in Heidrun Black Oil Simulation Model (for H and I segment) to get better description about this model.

Those assumptions are as follow:

❖ Heidrun Black Oil model used a virtual gas injector (Wellname: GIA-UT-I) to model the flow of gas from the gas cap in Garn/Ile down to Tilje 3.2.-4.

❖ Heidrun Black Oil model allows connection factors for producers to be a function of the water cut, and this option was used in the sector model to include the effect of fines.

❖ Heidrun Black Oil Model did not allow swelling of the oil (DRSDT=0), even for gas injected in the under-saturated part of the oil column.

❖ Heidrun Black Oil Model used threshold pressures to ensure stable initialisation in Eclipse 100

❖ Heidrun Black Oil Model used the VFP curves that were generated from Prosper software to tabulate the pressure drop in the tubing as a function of the GOR (and other variables like rate and water cut). This assumption is only valid when the composition of the produced gas not changes dramatically during the production period.

5.3 History Matching Heidrun Production Data

History Matching, the most practical method for testing a reservoir model's validity and accuracy, is a process of parameter adjustment. Its goal is to procure a set of parameters that yields the best prediction of the reservoir's performance history. Simulating the reservoir's past performance is central to history matching, and the process should ideally help to identify weaknesses in and ways of improving reservoir and model description data.

The main parameters usually adjusted in history matching are

➢ Reservoir and aquifer transport capacities, $(kh)_{res}$ and $(kh)_{aq}$

➢ Reservoir and aquifer storage, $(fhc_t)_{res}$ and $(fhc_t)_{aq}$

➢ Relative permeability and Capillary Pressure function

➢ Original saturation distribution

Other parameters (like: PVT data, reservoir boundary, well skin etc) are adjusted only if we observe a poor match or new information becomes available. The two broad parameters considered in determining a match are *pressure history* and *fluid movement*. These translate to pressure, flow rates, water-oil ratios, and gas-oil ratios.

Regarding History matching in H and I Segment, we will use original base case simulation model from Upper Tilje Heidrun field as reference. In this case, we assumed that the simulation result from original base case Heidrun model was correct because it was official and reference model from Statoil when doing simulation study in Heidrun field. Before doing history matching in H and I segment, we try to compare simulation result trend from cut model (H and I segment) with production data trend from original base case. This comparison can be seen in **Figure 39** (Appendix A).

For doing history matching in H and I Segment Heidrun field, the first step that we try to do is reviewing production data segment by segment and well by well to identify the main contributor wells for fluid production and fluid injection. From this, we try to understand key parameters that we should adjust to get well history matching in main contributor wells. For H and I segment case, we identified well A-28 and A-40 as main contributor producer wells and well WIA-37T3/GIA-37T3 as main contributor injector wells during production / injection history period.

Based on that assessment, we try to do adjustment in some parameters like:
- ❖ Water Injection Rate: we choose water injection rate as one parameter that we should adjust with consideration to decrease reservoir pressure in H and I segment, because based on production review chart in **Figure 39,** it looks that reservoir pressure increase drastically starting year 2000. This because after we cut the model, areal sweep from injector wells is limited because cross flow communication from one segment to another segment is not occurred in this case. That's why reservoir pressure in this model increases drastically. In this case, we try to do sensitivities by reducing water injection rate 25%, 50% and 75%. From the history matching result, it looks we have good history matching after we cut

water injection rate +/- 50%. The history matching result for this case can be seen in **Figure 40, Figure 41** and **Figure 42** (Appendix A)

❖ MULTZ in shale barrier: we choose Multiplier Z direction (for 3 shale barriers in H and I segment case) as another parameter that we should adjust with consideration to increase vertical communication from aquifer and water injector wells to well A-28. The justification for this because in H Segment, we have big gap in water production between simulation result and actual production data (See **Figure 40** in Appendix A). The main contributor for this gap is well A-28 due to this well produced high water production since the beginning of production (See **Figure 42** in Appendix A). In this case, we try to do sensitivities by increasing MULTZ 10x and 100x to see the effect of vertical communication, see **Figure 43** in Appendix A. From the history matching result when we increased MULTZ 100x (See **Figure 44** in Appendix A), it looks we can get good match in water production but we didn't get good match in oil and gas production. If we visualized water flow by using Floviz software, it looks that we need time to get water breakthrough from injector/aquifer to A-28 producer because the location of well A-28 is in the middle of segment H. We also tried to visualize full field simulation model to identify the possibility water flow from another segment. From this visualization, it looks that the possibility early water breakthrough production in well A-28 comes from cross flow from another segment. But we need detail evaluation to prove this theory. This phenomenon can be seen in **Figure 45** (Appendix A).

Overall based on history matching result above, we can say that the simulation result from cut model (H and I Segment) has quite good match with production data from Heidrun original base case model. But for water production in H Segment, we cannot get good match because we still have uncertainty where water production come from. We tried to increase MULTZ in shale barrier for increasing vertical communication from aquifer and water injector to well A-28, but the result is not good. We need detail evaluation to answer this uncertainty.

5.4 Simulation Study for H and I Segment Heidrun Field

After we got history matching between cut model and Heidrun original base case model, the next step is we try to convert this cut model from Eclipse 100 Black Oil to Eclipse 300 Black Oil and compare the result to identify the difference. In the next section, the author tries to discuss more detail about this model conversion.

5.4.1 Conversion Eclipse 100 to Eclipse 300 Black Oil

Basically, there are some procedures that we should do when we converted Heidrun Eclipse 100 black oil model to Eclipse 300 black oil model because some keywords in Eclipse 100 are not available in Eclipse 300. Those procedures are:

- ✓ Disable keyword for API Tracking Option (Keyword: API)
- ✓ Disable keyword for Threshold pressure option (Keyword: THPRESS)
- ✓ Disable keyword for Fault Dimension (Keyword: FAULTDIM) and Dimension for Tracer Option (Keyword: TRACERS)
- ✓ Disable keyword for not allowing the swelling of the oil (Keyword: DRSDT), because in Eclispe 300, gas swelling will be infinite
- ✓ Disable keyword for well productivity reduction as a function of water cut due to fines migration (Keyword : PIMULTAB, WPITAB)
- ✓ Disable keyword for automatic retubing (THP) and lift switching option (Keyword : WLIFT, GLIFTLIM)

After we disabled keywords above, we ran simulation in Eclipse 300 black oil for Upper Tilje H and I segment case. In this simulation case, we still use Eclipse 100 production / injection schedule and PVT Data. The comparison result between Eclipse 100 and Eclipse 300 Black Oil Simulation can be seen in **Figure 46 and Figure 47** (Appendix A). Based on this comparison, we can say that we can get good match between Eclipse 100 and Eclipse 300 Black oil simulation result for H and I Segment case study. There are a little bit minor differences due to the effect of disabled keywords, but these differences can be ignored.

5.4.2 Eclipse 300 Compositional Study

After we converted E100 model to E300 black oil model, then the next step, we try to run base case E300 compositional simulation study for Upper Tilje H and I segment. There are some steps that we should do first before we can run Eclipse 300 compositional case. Those steps are as follow:

➢ Add keyword for enabling Adaptive Implicit Method as formulation in compositional simulation study (Keyword : AIM)

➢ Add keyword for enabling horizontal well completion option (Keyword: HWELLS)

➢ Add keyword for enabling K Values to be entered to control liquid vapour phase (Keyword: KVTABLE)

➢ Add keyword for enabling field separator option to define separation oil and gas in place (Keyword: FIELDSEP)

➢ Add keyword for specifying the nature of gas to be injected by a group (Keyword: GINJGAS)

➢ Use fluid properties for 23 components. These components properties were generated by EOS SRK-Peneloux.

➢ Disable keyword for dissolved gas in live oil (Keyword: DISGAS)

When we run base case Eclipse 300 compositional simulation for H and I segment, we faced convergence problem where E300 simulator get difficult to compute flow equations in some iterations. For fixing these problems, we try to do some steps below:

❖ Shut all connections in WAG Injector (WIA-37T3/GIA-37T3) in periods where the twin injectors are injecting water and vice versa. The main problem that we identified in this case: during water injection period, there was vertical cross flow from gas that we injected before, even though we already shut in all connections in gas injector before we start water injection in water injector. There was debug problem in Eclipse 300 (Keyword: WELOPEN). For fixing

this problem, we should write twice 'SHUT' keyword and input 0 values in connection grid (see example below).

Example:

```
WELOPEN
'WIA-37T3'    'OPEN' 5* /
'WIA-37T3'     'OPEN' 0 0 0 /
'GIA-37T3'    'SHUT' 5* /
'GIA-37T3'    'SHUT' 0 0 0 /
```

❖ Change critical water saturation in water zone from value 0.6 to value 0.2 because compositional simulator gets difficult to calculate big saturation changing in end point relative permeability curve between water zone and oil zone. This changing won't affect to oil and gas production rate in simulation calculation because this was done in water zone.

For getting faster performance in running Eclipse 300 compositional, we tried to do some adjustments in Tuning keyword and add some keywords in schedule and data files. Some adjustments to improve CPU performance in Eclipse 300 compositional are as follow:

✓ Adjust Tuning Keyword in input data file with decreasing maximum length of time steps (TSMAXZ) from 30 to 5 and maximum time step increase factor (TSFMAX) from 3 to 1.1

✓ Add keyword to specify the size of integer table used for fast property lookups (Keyword: VECTABLE)

✓ Add keyword to modify convergence criteria (Keyword: CVCRIT). In this case, we try to increase gradually maximum pressure change over iteration. If the largest pressure change (for any cell) for a non linear iteration is less than this value, the solution is accepted.

Overall, we need two or four days to get result for Heidrun Eclipse 300 compositional simulation, it depends on cases that we run. When we ran Eclipse 300 compositional simulation for H and I segment, we used the same production / injection schedule with previous Eclipse 300 black oil model. In that schedule, we produced oil

and gas from six producer wells and inject water & gas to two WAG injector wells and one virtual gas injector (GIA-UT-I). This simulation case was run until year 2020 without including a blow-down of the reservoir during the last years of production. The comparison result between E300 compositional and E300 black oil for H and I Segment case can be seen in **Figure 48** (Appendix A). From that figure, we can see that oil and gas production from Eclipse 300 compositional has the same trend with oil and gas production from Eclipse 300 black oil, but the oil production from Eclipse 300 compositional simulation is little bit lower than oil production from Eclipse 300 black oil. In the opposite, gas production from Eclipse 300 compositional simulation is little bit higher than gas production from Eclipse 300 black oil. This difference probably was caused by the effect of components behaviour in fluid properties.

5.4.2.1 Compositional Simulation Scenarios

The main purpose of this project was to identify a potential problem with CO_2 Injection in oil reservoirs with gas caps is that gas cap may be contaminated by CO_2. This could be an issue on the Heidrun Field where down-dip using CO_2-WAG is considered. Compositional reservoir simulations will be used to investigate if the injected CO_2 will form a stable CO_2 layer below the hydrocarbon gas cap or if the CO_2 will be mixed with the hydrocarbon gas before or during the production of the gas cap.

Production from the Heidrun field is currently limited by platform gas processing and full field simulation predicts that the field will operate at a gas plateau for the next 20 years. In this study, CO_2 will be injected for 5 years, started in year 2015 and gas cap will be produced, started in year 2020.

In Eclipse 300 compositional simulation study for H and I Segment, both CO_2 and Hydrocarbon gas were injected in down-dip WAG injectors. The injection schedule is based on four months water injection and two months gas injection. Two wells were used as WAG injectors (WIA/GIA-37T3 and UTWI/UTGI-H2). The injectors were divided in two groups, where one group injected gas when the other group injected water. In prediction period, all producer wells were controlled by bottom hole pressure constraints

(it was set to 200-210 bars). Gas injection and water injection were controlled by reservoir volume rate target. For gas injection volume rate target, it was set to 5000 RM^3/day and for water injection volume rate target, it was varied from 500 – 6000 RM^3/day.

Basically there are two cases that will be run in this study, those cases are:

- Case I: Blow down gas with gas rate production 2 M m^3/day and BHP constraint: 100 bar from gas cap (I Segment) in year 2020 without CO_2 Injection. During year 1997 -2019, we injected hydrocarbon gas through virtual gas injector (GIA-UT-I)

- Case II: Inject water and CO_2 in two WAG Injectors (H Segment) for 5 years, started in year 2015 where both injection rates were controlled by reservoir volume rate target: 3500 m^3/day and BHP constraint: 500 bar. After that, blow down gas from gas cap in year 2020 with gas rate production 2 M m^3/day and BHP constraint: 100 bar. During year 1997 -2014, we injected hydrocarbon gas through virtual gas injector (GIA-UT-I)

All results in the following section are based on compositional simulations with twenty three (23) components EOS. In this CO_2 Injection simulation study, we also used some assumptions. Those assumptions are:

- Dissolution of CO_2 in water was not included in the simulations.

- The original VFP curves (from black oil model) will be used in all cases. Basically, the VFP curves should also be changed as a function of CO_2 content. But in this study, we did simplification. This simplification should not have a major effect because most producers with High CO_2 content are not limited by tubing head pressure constraint.

- Economic limit data for group and field (Keyword; GECON, GCONPROD) will be ignored

- The effect of fracturing at injector wells (Keyword: WINJMULT) will be used in this case to increase injectivity index of the injector well. For this case, we assumed Pf (fracturing pressure) =300 bar and a=0.1 as multiplier gradient

- o Turn off interpolation oil and gas relative permeability near the critical point to prevent un-physical discontinuities which may cause problem in solving the flow equations, for example oil saturation can be zero in oil zone after flooding. The keyword in Eclipse 300 that we used for this case: NOMIX.

- o Include gas lift during part of the simulation. The keyword that we use to include gas lift in Eclipse 300 simulation study is ACTIONW. In this case, we used assumption if well water cut >0.5, we will inject gas lift into well is around 50000 Sm3/day with BHP constraint 210 bar.

5.4.2.2 Compositional Simulation Results

The comparison of simulation result for two cases above can be seen in **Figure 49** to **Figure 54** (Appendix A). **Figure 49** shows that total oil production in Heidrun CO_2 injection case (Case 2) is about 0.37 M Sm^3 higher (1.17 % of STOOIP) than Heidrun Gas Cap Blow-Down case without CO_2 injection (Case 1). This was expected because CO_2 injection gives better microscopic displacement efficiency and sweep in most cases with down-dip injection. For water production (See **Figure 50** and **Figure 51**), it looks that water production trend in case 2 was affected by CO_2 Injection period in two WAG Injectors because in that period, we injected water based on schedule (4 months water injection and 2 months CO_2 injection), so this affects water production trend during that period. In the other side, the gas production trend in two cases look little bit different when gas was produced from gas cap in I segment. In **Figure 51**, it looks that plateau period in case 1 ended 8 months earlier compared with plateau period in case 2. This was caused field pressure in case 2 is little bit higher around 5 – 6 bar (due to CO_2 injection) than field pressure in case1.

The produced gas at Heidrun contains about 1.7 mol % CO_2 where water and produced gas is injected. Typical sales specifications for gas allows 2.5 mol % CO_2. CO_2 contamination after CO_2 breakthrough can become serious problem in Heidrun field. From comparison chart in **Figure 52** (Appendix A), it looks that in case 1, CO_2 contents in gas production is relatively stable (around 1.7 mol % CO_2) until the end of production

in year 2034. This condition was different for case 2 where in case 2, CO_2 contents increase rapidly after CO_2 breakthrough in year 2027 (12 years after first CO_2 injection). The peak of CO_2 contamination in case 2 occurred in year 2031, where CO_2 contents can reach 10 mol %.

Based on visualization flow in **Figure 53** (Appendix A), it looks that during gas hydrocarbon injection period (1997-2019) through virtual gas injector (GIA-UT-I), CO_2 created special layer below hydrocarbon gas. When we blow down the gas from gas cap, this CO_2 will be produced, together with hydrocarbon gas. But because there is no CO_2 injection in this case, the content of CO_2 that will be produced is relatively constant and stable (around 1.7 mol % CO_2). From **Figure 54** (Appendix A), we can conclude that after we injected water and CO_2 in year 2015 (Case 2), the injected fluid thus moves rapidly across the bottom of formation than it does across the top. This was caused by the pressure difference between the injections well and the production well is greater at the bottom of the formation than at the top, with proportional pressure difference in between. When the mobility ratio is greater than one, the fluid accelerates as it moves, because it occupies an increasingly high proportion of the distance between injector and producer. During this flow, gravity segregation will occur where the gas phase then travels through a layer at the top and the water through a layer at the bottom. Because limited vertical communication, the thickness of these segregated layers will be different. In the other side, if we looked CO_2 contents visualization flow, after we inject CO_2 in WAG injector, CO_2 will be dissolved in water and crude oil for awhile. After that, because the density difference between an injected fluid and the water/oil, it will cause a vertical separation of the fluids (gravity stabilization). Then CO_2 will flow upward (to gas producer direction) and contaminate hydrocarbon gas. In year 2027, CO_2 will reach gas producer and CO_2 breakthrough will be occurred.

Overall, the oil recovery factors by case 1 and case 2 until year 2034 are 48.635% and 49.805% respectively (See **Figure 49** in Appendix A). A main factor in explaining why a recovery factor is moderate (not high), probably due to Heidrun field has large permeability contrast between layers. Moderate gravity segregation even for gas and CO_2 injection is observed in simulation because the effect of three shale barriers between

layers in Upper Tilje formation Heidrun field. These barriers cause vertical communication between layers limited. The increases in vertical sweep by WAG injection for both cases are therefore relatively not high.

For Upper Tilje Heidrun case, while the permeability of intervening shale layers may be low (it is not zero), the vertical distance between a layer that pinches out and the ones above and below it that do not pinch out is small. The horizontal area is much larger than the vertical area perpendicular to the direction of horizontal flow. Typically the area ratio is 100 to 1000 and the vertical distance is 0.01 to 0.001 times the horizontal inter-well distance [10]. When the adjacent layers are both connected from well to well, the inter layer pressure gradients are small typically much smaller than the horizontal pressure gradient, except for possible capillary pressure difference. Hence, interlayer cross flow is moderate or may be prevented entirely by high capillary pressure difference between the permeable layers and the shales between the permeable layers. If, on the other hand, the flow in a given layer is stopped due to pinch out, the pressure in that layer build up to approach the injection well pressure (See **Figure 55** in Appendix A). This results in a large pressure difference between that layer and the adjacent layers above and below. Even with very low permeability shale barriers, if the capillary pressure difference between the shale layer and the oil bearing sand layers is not too great to overcome by the pressure difference mentioned, leakage of oil through the shale layers from the pinched out layer to the adjacent connecting layer can occur at a significant rate (Uncertainty in MULTZ shale barrier). A pinched out sand layer of medium to high permeability may therefore be equivalent to a connected layer of considerably lower permeability.

5.4.3 Sensitivity Analysis

In this simulation, we also did some sensitivities analysis to know the effect of some parameters to CO_2 contamination in Gas Cap. Those sensitivities are:

❖ Sensitivities to gas production rate when we blow down gas cap. In this case, we run sensitivity simulation with changing gas production rate to 1 M Sm^3/day, 2M Sm^3/day and 4M Sm^3/day.

❖ Sensitivities to gas producer well location. In this case, we try to run sensitivity simulation with moving gas producer well from old location to new location (in the upper part of gas cap reservoir). Gas production rate that we used in this case is 2 M SM^3/day.

❖ Sensitivities to perforation interval. In this case, we try to run sensitivity simulation with closing some perforation intervals if we faced CO_2 breakthrough problem in some layers. Gas production rate that we used in this case is 2 M Sm^3/day.

❖ Sensitivities to diffusion effect. In this case, we try to run sensitivity simulation without or with including diffusion coefficient in fluid flow calculation. We also increase diffusion coefficient 10 times to see the real effect of diffusivity to CO_2 contents in gas cap.

In the next section, we will try to discuss the result of sensitivities more detail.

5.4.3.1 Sensitivity Study to Gas Production Rate

The comparison of simulation result for sensitivity study to gas production rate can be seen in **Figure 56** to **Figure 58** (Appendix A). From **Figure 56,** it looks there are no differences in field oil, water and gas production plot for three cases until year 2020. The difference was started when we start blowing-down gas from gas cap in year 2020. Based on field oil production plot, oil production from case 3 (gas production rate = 4M Sm^3/day) has higher rate than oil production from case 1 (gas production rate = 1M Sm^3/day) and case 2 (gas production rate = 2M Sm^3/day), but oil rate in case 3 decreased faster compared with two cases. In this case, oil rate in case 3 start decreasing in year 2023 and oil rate in case 2 start decreasing in year 2027. The same case occurred in gas production where gas production plateau from case 3 ended earlier compared gas production plateau from case 1 and case 2. The main reason for this related to field pressure where in case 3, we produced gas with higher rate rather than case 1 and case 2, so this caused field pressure in case 3 decreased earlier and drastically compared field pressure in another 2 cases.

Regarding CO_2 contamination in produced hydrocarbon gas, **Figure 57** shows that CO_2 breakthrough occurred faster in case 3 (in year 2025), compared with another two cases. After CO_2 breakthrough occurred in case 3, CO_2 contents increase rapidly. The peak of CO_2 contamination in case 3 occurred in year 2028 where CO_2 contents reach 10 mol %. CO_2 breakthrough in case 2 occurred two years later (in year 2027). Compared CO_2 contamination in case 3, the highest percentage value of CO_2 contamination occurred in case 2 where CO_2 contents can reach 10.6%. This happens because CO_2 breakthrough time in case 2 occurred slower, so more CO_2 will be accumulated in gas caps (See **Figure 58** in Appendix A). For case 1, CO_2 breakthrough occurred in year 2031, 4 years after CO_2 breakthrough in case 2. The peak of CO2 contamination from case 1 cannot be monitor because simulation time was ended in year 2034.

Overall for this sensitivity case, we can conclude that:

> ➢ The time of CO_2 breakthrough occurred was affected by gas production rate. Higher gas production rate will cause CO_2 Breakthrough time occurred faster.

> ➢ The percentage value of CO_2 contamination in hydrocarbon gas was affected by the time of CO_2 breakthrough occurred. If CO_2 breakthrough occurred slower, the percentage value of CO_2 contamination in hydrocarbon gas will be higher due to more CO_2 contents will be accumulated in gas cap.

5.4.3.2 *Sensitivity Study to Gas Producer Location*

The comparison of simulation result for sensitivity study to gas producer location can be seen in **Figure 59** to **Figure 61** (Appendix A). From **Figure 59,** it looks there are no differences in field pressure, water and gas production plot for both cases. The slightly difference occurred in field oil production rate when we start blowing-down gas from gas cap in year 2020. Based on field oil production plot, oil production from case 2 (new gas producer location) has higher rate than oil production from case 1 (old gas producer location) because we put this new gas producer location in un-swept area. Case 2 produced oil condensate in initial rate 175 Sm^3/day, then after 4 month production, oil production decreased drastically. Case 2 has the same production rate (around 60

Sm^3/day) with case 1 in year 2023. In this sensitivity, we blow down gas with the same gas production rate (2 M Sm^3/day) for both cases.

Regarding CO_2 contamination in produced hydrocarbon gas, **Figure 60** shows that CO_2 breakthrough in both cases occurred in the same time (in year 2027). After CO_2 breakthrough occurred, CO_2 contents in both cases increase rapidly. The peak of CO_2 contamination in case 2 occurred in year 2030 where CO_2 contents reach 5.79 mol %. Compared CO_2 contamination in case 2, the highest percentage value of CO_2 contamination occurred in case 1 where CO_2 contents can reach 10.6%. This happens because gas producer well in case 1 located closer to CO_2 swept area. The location of old and new gas producer wells and the visualization three phase flow from CO_2 contents can be seen in **Figure 61** (Appendix A).

For this sensitivity case, we can conclude that:

➢ The time of CO_2 breakthrough occurred was not affected by the location of gas producer wells. From simulation result in **Figure 60**, CO_2 breakthrough time for both cases occurred in the same time

➢ The percentage value of CO_2 contamination in hydrocarbon gas was affected by the location of gas producer wells. The well location is closer to CO_2 swept area will cause high contamination CO_2 to hydrocarbon gas.

5.4.3.3 Sensitivity Study to Perforation Interval

For sensitivity study to perforation interval, the comparison of simulation result can be seen in **Figure 62** to **Figure 64** (Appendix A). **Figure 62** shows that production plot for oil, water and gas in case 1 (no perforation interval in gas producer wells changed during CO_2 breakthrough period) and case 2 (some perforation intervals in gas producer well were shut off during CO_2 breakthrough period) are totally the same during CO_2 Injection and gas blow down period. Field pressure trend is also the same for both cases. This means when we shut off some perforation intervals in gas producer well (GIA-UT-I) during CO_2 breakthrough period, it won't affect to oil/gas production in that well. In this sensitivity, we blow down gas with the same gas production rate (2 M Sm^3/day) for both

cases. During CO_2 breakthrough period, we shut off perforation interval two times, first time in year 2028 and second time in year 2030. The justification to shut off some perforation interval based on CO_2 contents visualization review in Floviz software. We try to shut off some layers that have high CO_2 contents to reduce CO_2 contamination in produced hydrocarbon gas. In year 2028, we shut off perforation interval in grid cell 18 to 24 and in year 2030, we shut off perforation in grid cell 10 to 24.

Regarding CO_2 contamination in produced hydrocarbon gas, **Figure 63** shows that CO_2 breakthrough in both cases occurred in the same time (in year 2027). After CO_2 breakthrough occurred, CO_2 contents in both cases increase rapidly. The peak of CO_2 contamination both cases occurred in the same year (year 2030) where CO_2 contents in case 1 reach 10.6 mol % and CO_2 contents in case 2 reach 10.46 % mol. Little bit difference was shown in chart after the percentage value of CO_2 contents reached peak in year 2030. CO_2 contents in case 2 decreased 1% lower than CO_2 contents in case 1. Overall, there is no significance difference in the percentage value of CO_2 Contents for both cases. The main reason for this because when CO_2 breakthrough occurred, CO_2 didn't create stable layer like water breakthrough, so we got difficult to determine which layer that we should shut off. In this case, CO_2 mixed with the hydrocarbon gas during the production of the gas cap (See **Figure 64** in Appendix A). As long as we still produce gas in CO_2 swept area, CO_2 contamination in hydrocarbon gas will still occur.

For this sensitivity case, we can conclude that:
- ➤ Perforation interval management is not effective to reduce CO_2 contamination in hydrocarbon gas because CO_2 didn't create stable layer in gas cap. CO_2 will be mixed with hydrocarbon gas during the production of the gas cap.

5.4.3.4 Sensitivity Study to Diffusion Effect

The last sensitivity study in Heidrun compositional simulation (for H and I segment) is sensitivity study to diffusion effect. Just like we explained before in the previous chapter that diffusion is the process by which matter is transported from one part of a system to another as a result of random molecular motions. Diffusion is driven by a

gradient in chemical potential. There are 3 cases that we evaluate in sensitivity simulation to diffusion effect. Those three cases are as follow:

1. Case 1: Compositional simulation was run without including diffusion coefficient
2. Case 2: Compositional simulation was run with including diffusion coefficient from Sigmund Correlation
3. Case 3: Compositional simulation was run with including and increasing diffusion coefficient 10 times.

Those three compositional simulations will be run in the same condition like previous simulations: Injecting water and CO_2 in two WAG Injectors (H Segment) for 5 years, started in year 2015 where both injection rates were controlled by reservoir volume rate target: 3500 m^3/day and BHP constraint: 500 bar. After that, blow down gas from gas cap in year 2020 with gas rate production 2 M m^3/day and BHP constraint: 100 bar.

The comparison of simulation result for this case can be seen in **Figure 65** to **Figure 67** (Appendix A). **Figure 65** shows that overall production plot for oil, water and gas in case 1, case 2 and case 3 are relatively the same during CO_2 Injection and gas blow down period. There are little differences in water and gas fluctuation trend during water and CO_2 injection from year 2015 -2020. Probably this is caused by diffusion effect where CO_2 try to be soluble through a water barrier to a trapped oil phase and the subsequent swelling of the oil phase. CO_2 diffusion may generate miscibility by successive contacts, causing decreasing of saturation pressure, specific gravities, interfacial tensions and viscosities with the corresponding increasing of oil swelling and solution gas content. For the case in WAG injector where there are differences on compositional gradients between vapour (CO_2) and liquid phase (Water), molecular diffusion is processed through successive liquid fringe which is contacted directly by CO_2. In this process, the composition of liquid tends to be equalized. Molecular diffusion will stop when final chemical equilibrium is attained throughout the liquid. For Heidrun simulation, we did not see any significance difference in oil production between case with diffusion and case without diffusion. Probably this was caused by time required for diffusion to swell the oil is short. We only injected CO_2 for 5

years and after that we shut down oil production to blow down gas from gas cap. For gas production, the diffusion effect will be known related to CO_2 contents in hydrocarbon gas during gas blow down period.

Regarding CO_2 contents in produced hydrocarbon gas, **Figure 66** shows that CO_2 breakthrough in three cases occurred in the same time (in year 2027). After CO_2 breakthrough occurred, just like the previous cases, the percentage value of CO_2 contents in three cases will increase rapidly. The peak of CO_2 contamination in case 1 and case 2 occurred in year 2031 where case 1 reach 10.6 mol % and CO_2 contents in case 2 reach 10.3 % mol. The significance difference occurred in case 3 when we increased diffusivity coefficients 10 times, the peak of CO_2 contamination in hydrocarbon gas decreased to 6.06 mol %. The main reason for this, if diffusion coefficients are high, mostly CO_2 molecular will spread out below gas hydrocarbon layer due to CO_2 tries to diffuse into and through the water phase towards the oil. This phenomenon can be seen in visualization picture for CO_2 contents and three phase flow in **Figure 67** (in Appendix A)

Overall for this sensitivity case, we can conclude that:

➢ The time of CO_2 breakthrough occurred was not affected by diffusion effect because CO_2 breakthrough in three cases above occurred in the same time.

➢ The percentage value of CO_2 contamination in hydrocarbon gas was affected by diffusion effect. Higher diffusion coefficient will reduce CO_2 contamination in hydrocarbon gas because higher diffusion coefficient will cause more CO_2 spread out below gas hydrocarbon and oil layer.

6. RESULTS AND DISCUSSION

Basically CO_2 flooding is currently a popular form of multiple contact miscible flooding. Factors which appear to be important in multiple contact miscible flooding are individual fluid viscosities, injection rate, fluid densities, formation permeability, reservoir geometry, flow characteristic of the porous medium and molecular diffusion coefficients of the fluid components. Reservoir management for CO_2 flooding should

focus on predicting these parameters and planning wells accordingly. Use of reservoir modeling in this case is to design a miscible CO_2 flood with maximum economic potential. Key issues for project design include the amount and location of remaining oil, reservoir sweep efficiency, flood rate, gas injection volume and strategy for handling produced gas (related to CO_2 contamination to hydrocarbon gas). For this thesis project, we used compositional simulation to find the answer whether CO_2 that we injected in WAG injector can cause contamination to hydrocarbon gas during gas blow down period.

A sensitivity analysis to investigate the effect of well placement, gas production rate, perforation interval and diffusion coefficients to CO_2 contamination in hydrocarbon gas during gas blow down period was performed. Using reservoir simulation, the effect of those parameters can be examined.

From reservoir characterization and all simulation study cases that we have run in H and I segment Heidrun field, we can conclude:

A. CO₂ Displacement Process in WAG Injector

Basically water and CO_2 injection in WAG injector is very sensitive to reservoir heterogeneity. Unfavourable mobility miscible displacement can lead to cross flow from the low permeability layer to an adjacent higher permeability layer and tend to reduce frontal advancement in the lower permeability layer. Vertical conformance of WAG displacement is strongly influence by conformance between zones. For Heidrun cases where we have 3 shale barriers in H and I segment, vertical distribution of CO_2 is dominated by permeability contrast. Flow into each layer is essentially proportional to the fraction of the overall system kh (flow capacity where k=permeability, md and h= height of layer zone, ft). There is tendency for more CO_2 to enter high permeability zone because the most permeable layer respond more quickly and takes more fluid than is relative to its permeability height contribution. When water is injected, it quickly displaces the highly mobile CO_2 and all the layers attain an effective mobility nearly equal to the initial value. The higher permeability layers always respond first. WAG will reduce mobility not only in the high permeability layer but also in the low permeability layer, resulting in a larger amount

of CO_2 entering the highest permeability. In the other side, the ratio of viscous to gravity forces is the prime variable for determining the efficiency of WAG injection and it controls vertical conformance and displacement efficiency of the flood. Cross-flow or convective mixing can substantially increase injection even in the presence of low vertical to horizontal permeability ratios. Transport of CO_2 is enhanced significantly by the high permeability layers establishing a highly conductive path parallel to the low permeability layer. With cross-flow, CO_2 is transported through the highly permeable layer and reaches down stream locations in the low permeability layer. Without cross-flow, CO_2 would have to flow through the low permeability layer to reach the down-streams locations. Basically different growth rates in the mixing zone in region of low oil saturation (for CO_2 swept regions) were caused by permeability contrast and mobility ratio contrast. This phenomenon can be seen in visualization flow in **Figure 53** to **Figure 54** (Appendix A)

B. CO₂ Recovery Mechanism

When we injected CO_2 and water in Heidrun field through WAG injector, CO_2 is significantly soluble in reservoir brine or injected flood water, whereas hydrocarbons are not. At typical reservoir conditions, CO_2 has a density near that of reservoir crude oils, while the density of the light hydrocarbon miscible drive agents is considerably lower. In some cases, carbon dioxide is slightly more dense than the crude oil; however, it is always considerably less dense than liquid water. Hence, there is much less gravity segregation of carbon dioxide, though it still occurs relative to a mobile water phase. At any given pressure, more carbon dioxide than methane will dissolve in crude oil. Multiple contact miscibility between CO_2 starts with dense phase CO_2 and hydrocarbon liquid. The CO_2 first condenses into the oil, making it lighter and often driving methane out ahead of the "oil bank" [1]. The lighter components of the oil then vaporize into the CO_2 rich phase, making it denser, more like the oil, and thus more easily soluble in the oil. Mass transfer continues between the CO_2 and oil until the resulting two mixtures become indistinguishable in term of fluid properties. At that point, there is no interface between the CO_2 and oil and one hydrocarbon phase

results. During oil displacement, there is gradation in composition from pure CO_2 to virgin oil. The vaporizing region occurs upstream of the condensing region. Every contact in the process involves a miscible displacement, even though pure CO_2 is not miscible with original oil. For Heidrun field, injected CO_2 may develop miscibility with the lighter Heidrun oils. Estimated minimum miscibility pressure for Heidrun oil ranges from 220 bar (for light oil) to 380 bar (for heavy oil). Overall, for CO_2 flooding in Heidrun field, multiple contact miscibility is only one of the recovery mechanism and enhancement which should be considered. Others include: oil swelling with CO_2 and reduction of oil viscosity for improved mobility ratio.

C. Parameters to control and reduce CO_2 Contamination in hydrocarbon gas.

As mentioned previously, for this thesis project, we used compositional simulation to find the answer whether CO_2 that we injected in WAG injector can cause contamination to hydrocarbon gas during gas blow down period. Based on sensitivities simulation that we have run, we found some important parameter that can control CO_2 contamination to hydrocarbon gas in Heidrun field.

Those parameters are:

1. Gas production rate

    Gas production is one parameter that can affect CO_2 contamination in hydrocarbon gas. Based on simulation result, it shows that gas production rate will affect the time of CO_2 breakthrough occurred. Higher gas production rate will cause CO_2 breakthrough time occurred faster. Then the timing of CO_2 breakthrough will affect the percentage value of CO_2 contamination in produced hydrocarbon gas. If CO_2 breakthrough time occurred slower, the percentage value of CO_2 contamination in hydrocarbon gas will be higher due to more CO_2 contents will be accumulated in gas cap (The effect of pressure drawdown during gas blow down in gas cap).

2. Well placement

Well placement is another important parameter that we should consider to control CO_2 contamination in hydrocarbon gas. The gas producer location is closer to CO_2 swept area will cause high contamination CO_2 to hydrocarbon gas.

3. Diffusion effect.

Diffusion effect is the last parameter that we should consider to control CO_2 contamination in hydrocarbon gas. Diffusion effect causes the concentration of CO_2 in water and oil phases, increase with time. Diffusion also causes increasing oil and water swelling with CO_2. Higher diffusion coefficient will reduce the percentage value of CO_2 contamination in hydrocarbon gas because more CO_2 molecular will spread out below gas hydrocarbon layer due to CO_2 diffuses into and through the water phases towards the oil.

Based on results obtained from the simulation model, suggest that a practical reservoir management strategy for Heidrun field to reduce CO_2 contamination in hydrocarbon gas may consider the following:

1. Maintain gas production rate to retard CO_2 breakthrough time

From simulation result in sensitivity study, it shows that gas production rate=1 M Sm3/day is the better option to retard CO_2 breakthrough time during gas blow down period in Heidrun field. We need to retard CO_2 breakthrough time in case building gas processing facility is not economic for CO_2 injection project in Heidrun field.

2. Drilling Infill Well

Drilling infill well can be another alternative to reduce CO_2 contamination, bypass un-swept oil and achieve gas production target. Some key parameters should be considered when we decide to drill infill well, like the amount and location of remaining oil/gas and reservoir sweep efficiency (vertical and areal sweep). In case, we want to reduce CO_2 contamination in hydrocarbon gas during gas blow down, we should put the infill well far away from CO_2 swept area. Regarding this, probably gas producer horizontal well can be evaluated as one infill well strategy

in Heidrun field because horizontals wells can: (1) enlarge contacts and drainage areas, (2) allow less drawdown hence avoid fines movement and delay coning, (3) provide additional benefit from gravity drainage. Unfortunately, in this thesis project, we did not do sensitivity simulation to prove this theory.

7. CONCLUSION

Reservoir characterization and simulation model have been developed for H and I segment Heidrun field and based on these works, there are some conclusions can be drawn as follows:

1) A deep understanding of the geological and reservoir uncertainties is required for optimal development of a CO_2 injection project in H and I segment Heidrun field especially regarding shale barrier continuity and fault transmissibility. High water production in well A-28 since the beginning of production is the biggest uncertainty in H and I segment simulation model

2) Injected CO_2 may develop miscibility with the lighter Heidrun oil. Estimated minimum miscibility pressure ranges from 220 bar (for Heidrun light oil) to 380 bar (for Heidrun heavy oil)

3) Based on compositional simulation result, the injected CO_2 in WAG injectors did not form a stable CO_2 layer below the hydrocarbon gas cap. This CO_2 will be mixed with the hydrocarbon gas before or during the production of the gas cap. On the contrary, for the case of dry hydrocarbon gas injection, natural CO_2 from that hydrocarbon gas will create a stable layer below the hydrocarbon gas cap.

4) Based on sensitivities simulation result, there are some parameters that can control CO_2 contamination during gas blow-down period. Those parameters are gas production rate, well placement and diffusion effect. Higher gas production will cause CO_2 breakthrough time occurred faster. In the other side, the well location is closer to CO_2 swept area will cause high contamination CO_2 to hydrocarbon gas. For diffusion effect, higher diffusion coefficient will reduce the percentage value of CO_2 contamination in hydrocarbon gas because more CO_2

molecular will spread out below gas hydrocarbon layer due to CO_2 diffuses into and through the water phases towards the oil.

5) Contamination of produced gas by CO_2 is a problem if CO_2 is injected in Heidrun, where the remaining gas reserves are significant. The compositional sector model predicts that the produced gas will contain too much CO_2 after a few years of CO_2 injection, even if CO_2 is injected in a part of reservoir. The Heidrun CO2 project therefore requires separation of CO_2 from produced gas or the possibility to sell CO_2 contaminated gas in order to be an economic success

NOMENCLATURE

WOC	= Water Oil Contact
GOC	= Gas Oil Contact
OOIP	= Original Oil in Place
OGIP	= Original Gas in Place
BHP	= Bottom Hole Pressure, Psia
Kv	= Vertical Permeability
Kh	= Horizontal Permeability
3D	= 3 Dimension
PVT	= Pressure Volume Temperature
Bw	= Water Volume Factor
Bg	= Gas Volume Factor
Bo	= Oil Volume Factor
Cw	= Water Compressibility
μw	= Water Viscosity
μo	= Oil Viscosity
μg	= Gas Viscosity
ρw	= Water Density
Swi	= Irreducible Water Saturation
Sorw	= Residual Oil Saturation in o-w system
Sgc	= Connate Gas saturation
Sorg	= Residual Oil Saturation in o-g system
E100, E300	= Eclipse 100, Eclipse 300
MMP	= Minimum Miscibility Pressure
WAG	= Water Alternate Gas
FOPR	= Field Oil Production Rate
FWPR	= Field Water Production Rate
FGPR	= Field Gas Production Rate
FPR	= Field Pressure
FOIP	= Field Oil in Place
FGPT	= Field Gas Production Total
FOPT	= Field Oil Production Total
FYMF_2	= Field CO_2 Contents in Field Production
RPR 46	= Reservoir Pressure Region 46 (H Segment)
RPR 47	= Reservoir Pressure region 47 (I Segment)
WYMF_2	= CO_2 Contents in Well Production
WGPT	= Well Gas Production Total
WWCT	= Well Water Cut Total
WOPR	= Well Oil Production Rate
WBHP	= Well Bottom Hole Pressure
GOPR	= Group Oil Production Total (Segment Production)
GWPR	= Group Water Production (Segment Production)
GGPR	= Group Gas Production (Segment Production)

REFERENCES

1. Jarrell, Perry.M., Fox, Charles.E., Stein, Michael.H., and Web, Steven.L: "Practical Aspects of CO_2 Flooding", SPE Monograph volume 22, Henry L. Doherty Series, Richardson, Texas, USA, 2002.

2. Christoffersen, Kjell.R.: "High Pressure Experiments with Application to Naturally Fractured Chalk Reservoirs 1.Constant Volume Diffusion, 2. Gas Oil Capillary Pressure", A Dissertation for the Partial Fulfillment of Requirements for the Degree of Doktor Ingeniør, NTNU, Trondheim, 1992.

3. Stalkup, Fred.I.: "Miscible Displacement", SPE Text Book Third Printing, Henry L. Doherty Memorial Fund of AIME , Richardson, Texas, USA, 1992

4. Gomma, Ezzat E.: "Practical Aspects and Reliability of Simulation Studies of EOR Processes", Handout Course for ChevronTexaco Indonesia, Rumbai, Pekanbaru, July 21 – 25, 2003.

5. Tjomsland, T: "Improved Fluid Model for the Heidrun Oil Reservoir", Doc No 99S9700013764, Statoil, PETEK, September 1999.

6. Haugse, V., Stensen, J.A.: "Evaluation of CO_2 Injection in Heidrun", Project No: P.MET.1.1.16, Statoil, September 2002.

7. Vassenden F., Holt, T., Hustad, O.S., and Lindeberg, E.: "Swelling of Heidrun Oil with CO_2 and Hydrocarbon Gas", Report no: 54.5146.00/01/99, SINTEF Petroleum Research, Trondheim, Norway, March 19, 1999.

8. Kleppe, J: "Introduction to Compositional Simulation", Reservoir Simulation Handout Course, NTNU, 2001.

9. Schlumberger: "Eclipse 2004A Reference and Technical Manual (2004)", Schlumberger Technology Center, Abingdon, UK, 2004.

10. Yaghoobi, H., Tsau, J.S., and Heller, J.P.,: "Improving CO2 Floods in Heterogeneous Media", paper SPE 35403 presented at the SPE/DOE Tenth Symposium on Improved Oil Recovery held in Tulsa, Oklahoma, USA, April 21 – 24, 1996.

11. Silva, F.V., and Belery, J.P.,: "Molecular Diffusion in Naturally Fractured Reservoir: A Decisive Recovery Mechanism", paper SPE 19672 presented at the SPE 64th Annual Technical Conference and Exhibition held in San Antonio, Texas, USA, October 8 – 11, 1989.

12. Grogan, A.T., and Pinczewski, W.V,: "The Role of Molecullar Diffusion Processes in Tertiary CO_2 Flooding", paper SPE 12706, Article from Journal Petroleum Technology, May, 1997.

13. Todd, M.R.,: "Modelling Requirement For Numerical Simulation of CO2 Recovery Process", paper SPE 7998 presented at the SPE AIME California Regional Meeting held in Ventura, California, USA, April 13 – 20, 1979.

14. Kleppe, J: "Review of Relative Permeabilities and Capillary Pressures", Reservoir Recovery Handout Course, NTNU, 2001.

15. Rogers, J.D., and Grigg, R.B,: "A Literature Analysis of the WAG Injectivity Abnormalities in the CO_2 Process", paper SPE 73830 presented at the SPE/DOE Improved Oil Recovery Simposium held in Tulsa, Oklahoma, USA, April 3 – 5, 2001.

16. Alstadsæter, I., Næss, A., McCann, A.J.,: "Heidrun Plan Of Development", presented by Heidrun Team, Statoil, Norway, January 2005.

17. Bakken, E., Kjønsvik, D., Slotte, P.A., Knai, T.A.,: "Heidrun Field, 2003 Full Field Reservoir Simulation Model", Technical Report, HNO HD PTEK ØU,Statoil, Stjørdal, Norway, 2003.

18. Jørgenvåg, S., Christoffersen, K., Munkvold, F.R., Hansen, O., Omdal, L., Flormælen, R., Wennberg, K.E., Håvard, N., Boge, R., Skjellanger, A., Høier, L.,: " Reservoir Management Plan Heidrun Field", Document No: HD PETEK - U00095, Statoil, Stjørdal, Norway, November, 23, 2000.

19. Øren, P.E.,   Bakke, S.,   Boassen, T.,: "Pore Scale Predictions of Relative Permeability and Capillary Pressure Heidrun Fangst and Båt Groups", Technical Report, Statoil, Norway, March 10, 2004.

APPENDIX A

Figure 1: Heidrun Field Location in Haltenbanken Area [17]
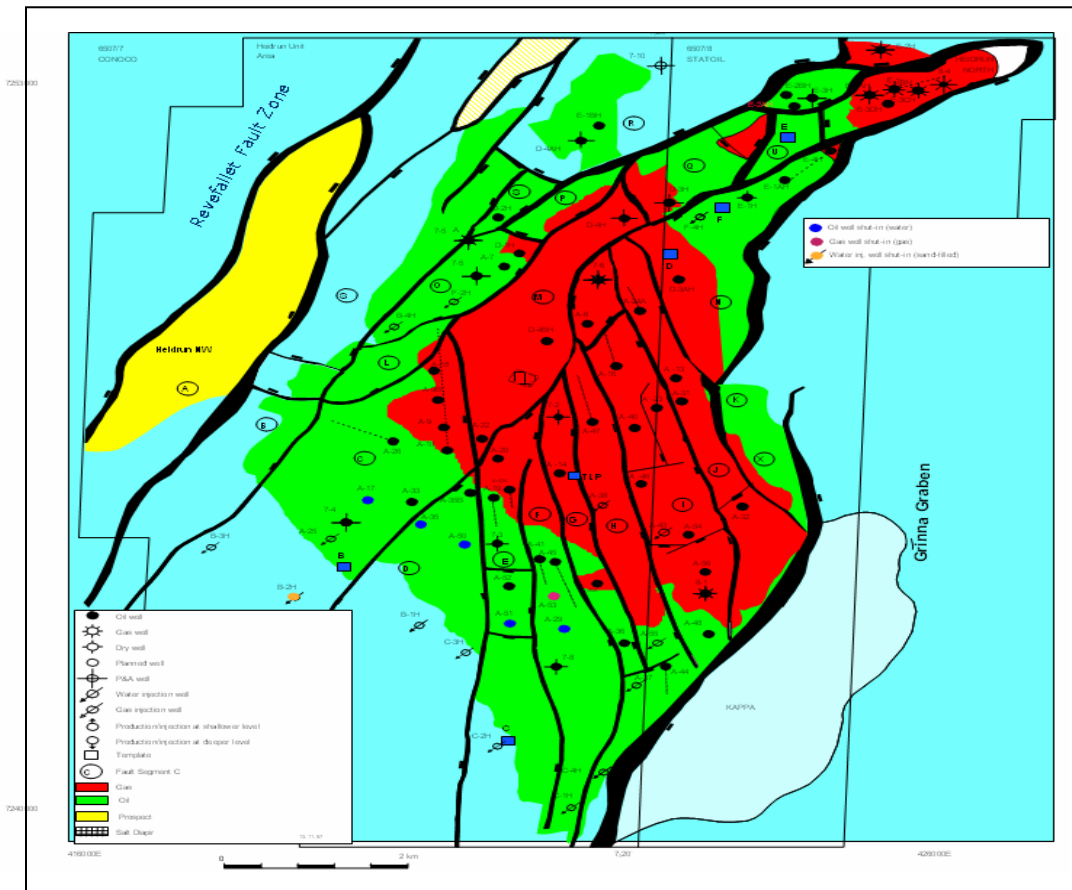
Figure 2: Fault Segments in Heidrun Field [15]
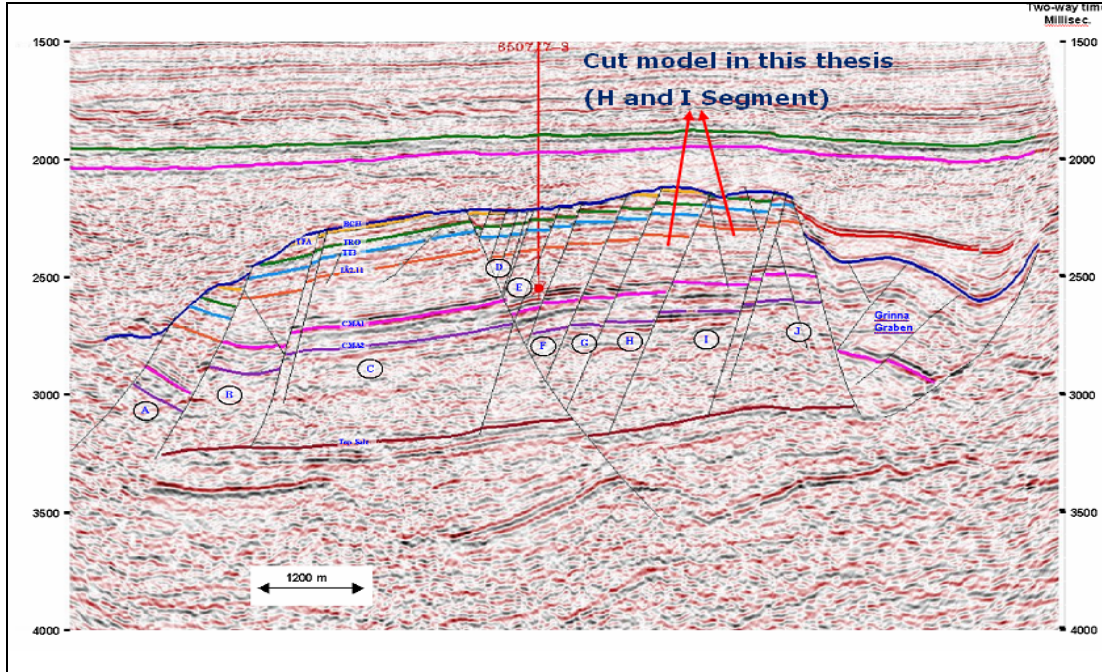
Figure 3: Seismic X Section in Heidrun Field [15]
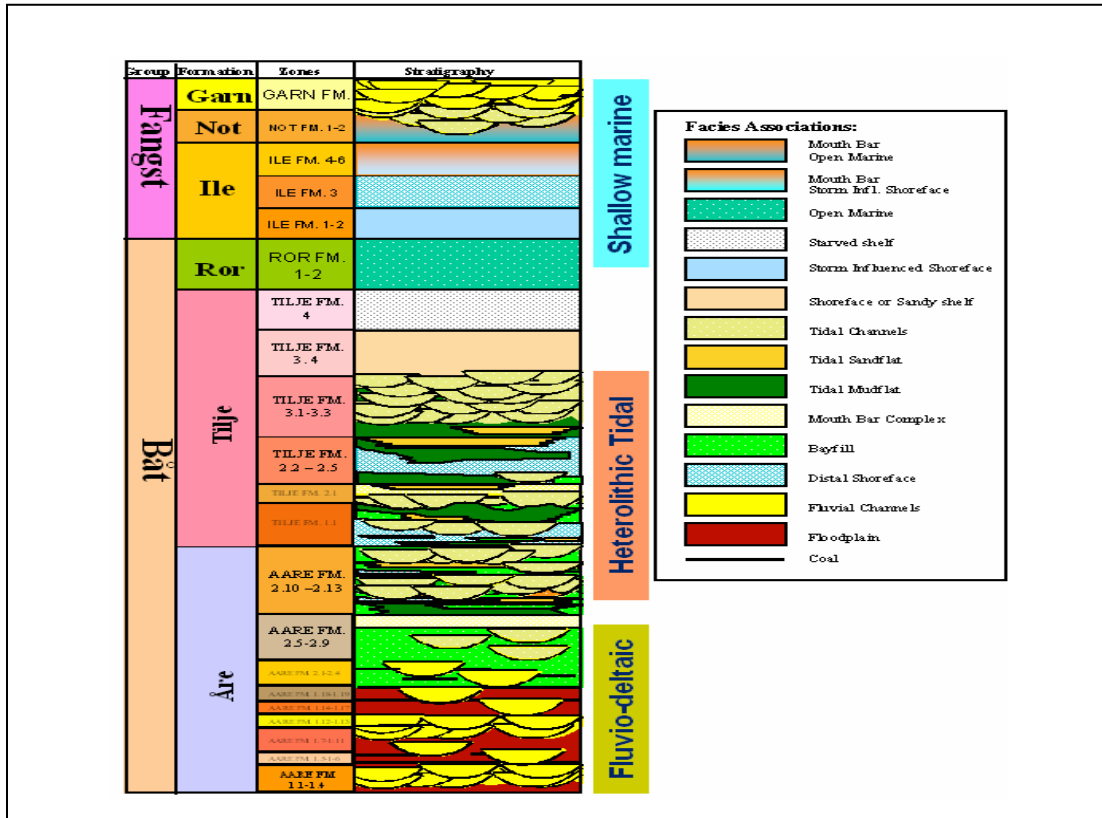
Figure 4: Stratigraphy and Sedimentary Facies from Heidrun Field [15]
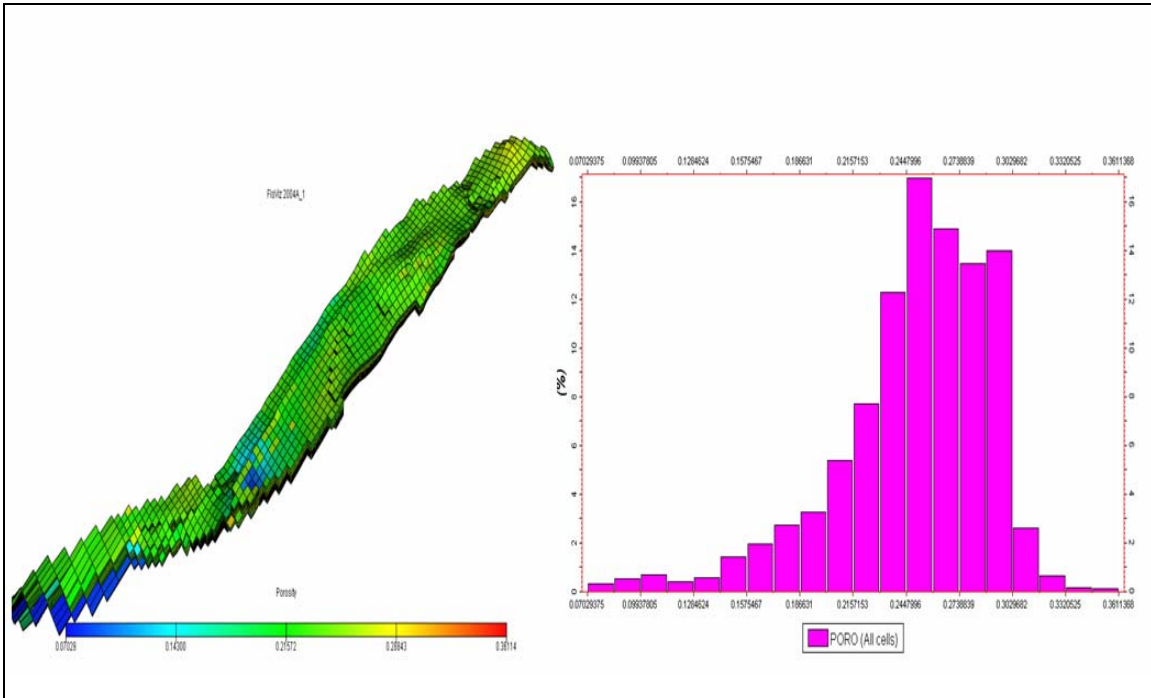
Figure 5: Porosity Data Distribution for H and I Segment Heidrun Field
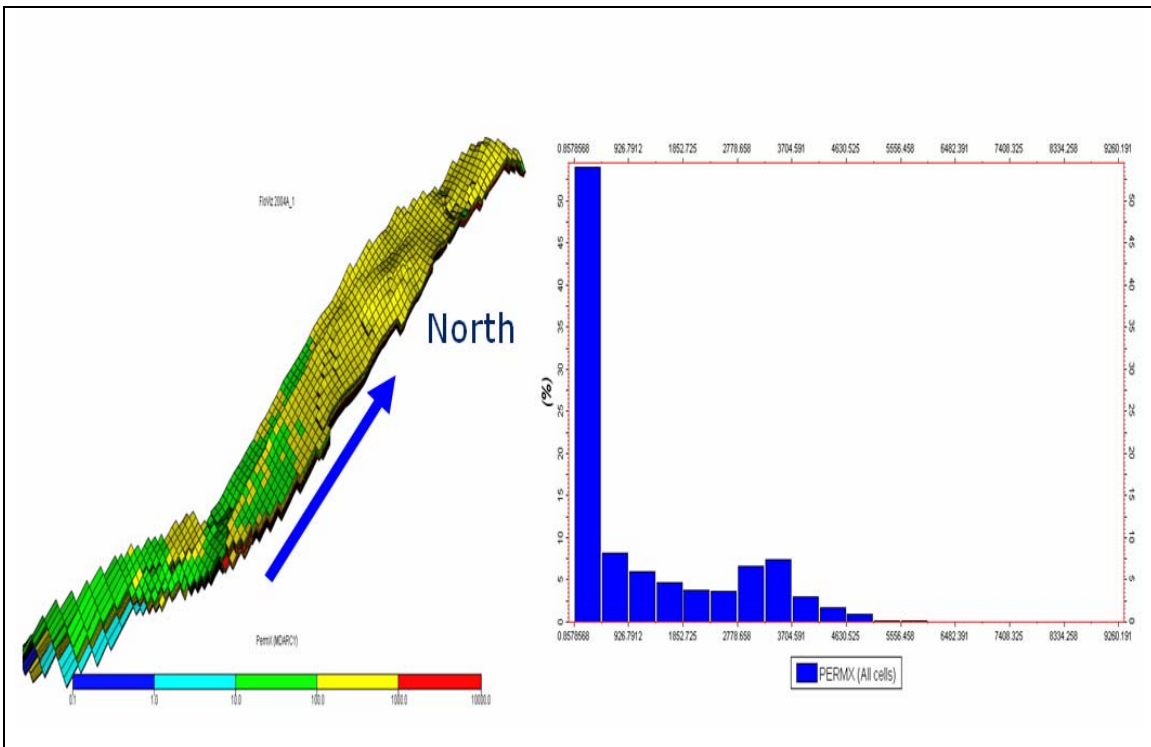
Figure 6: Permeability Data Distribution for H and I Segment Heidrun Field
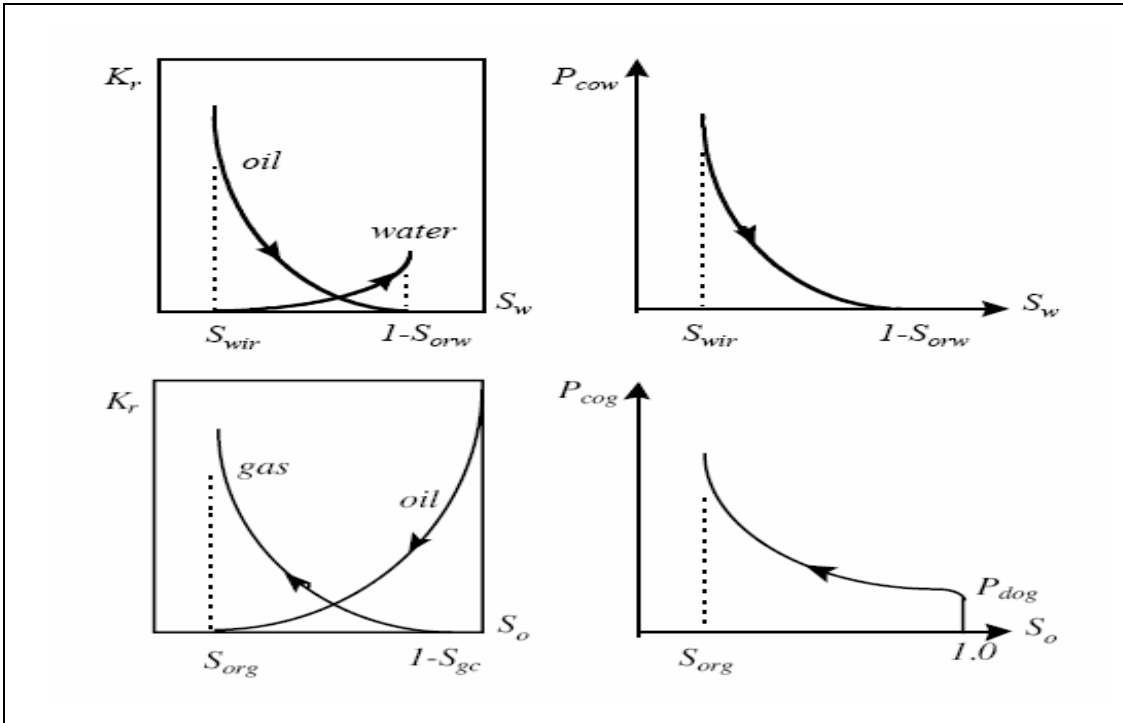
Figure 7: The Sets of Relative Permeability Curve for Oil-Water and Gas-Oil [13]
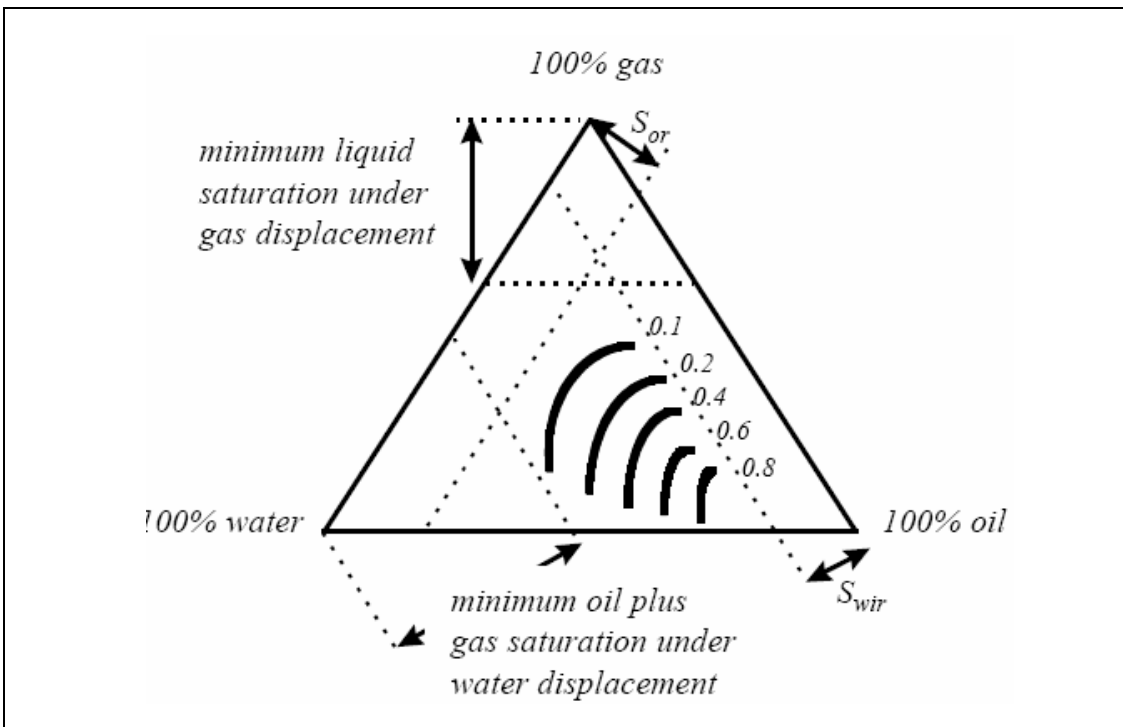
Figure 8: Triangular Diagram of Three Phases Saturation (Oil, Water, Gas) [13]
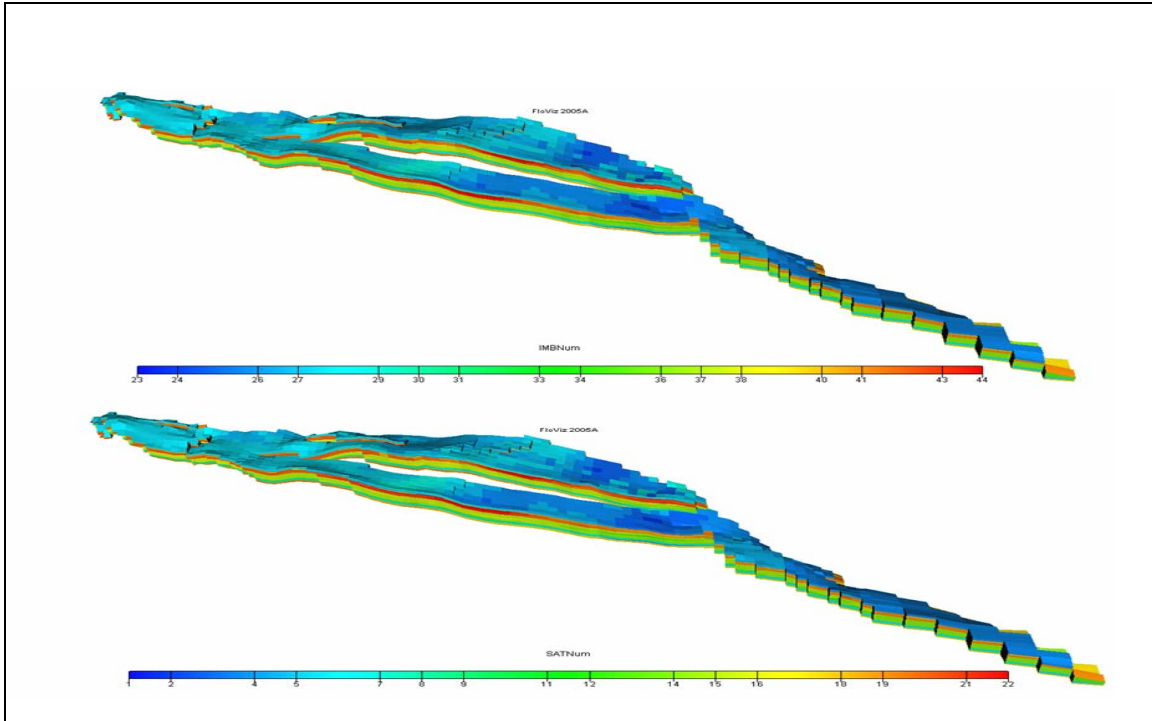
Figure 9: Imbibition and Saturation Function Number (IMBUM, SATNUM) in Heidrun Geologic Model
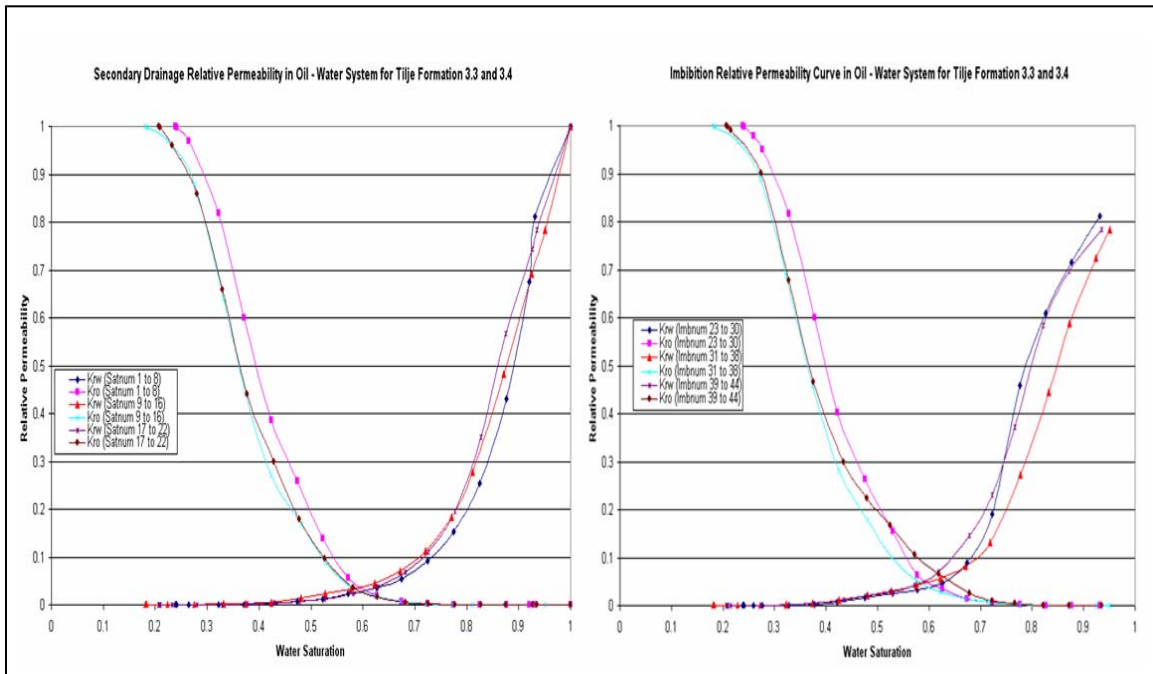
Figure 10: Heidrun Relative Permeability Curve for Oil-Water System
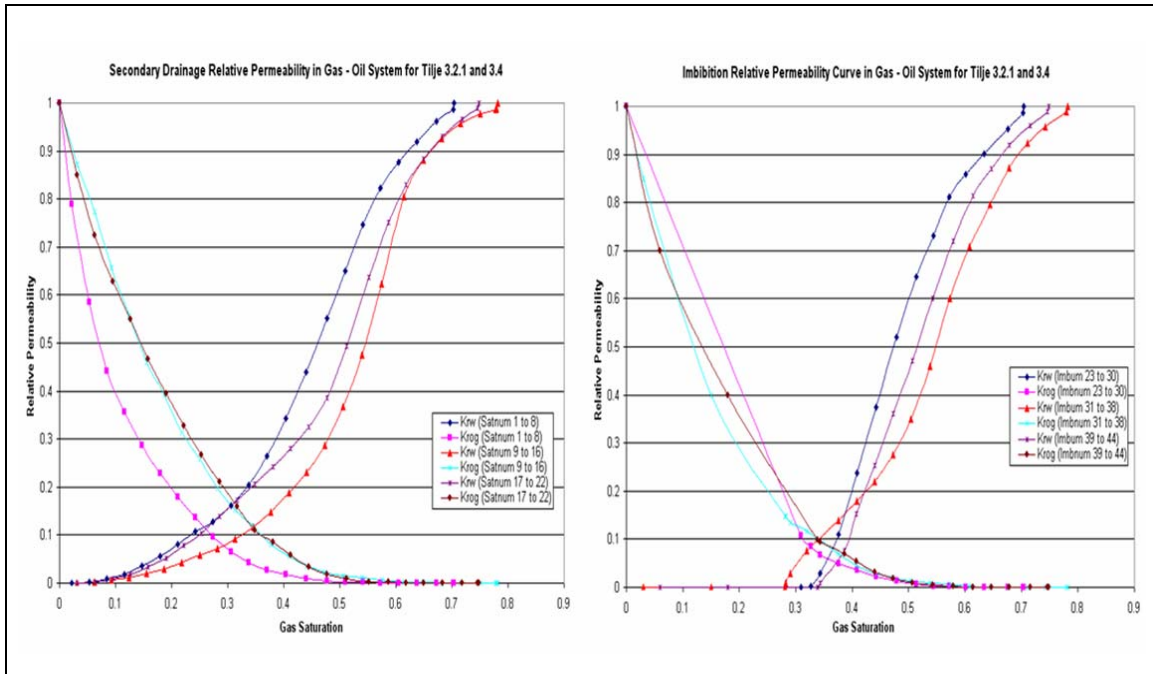
Figure 11: Heidrun Relative Permeability Curve for Gas-Oil System
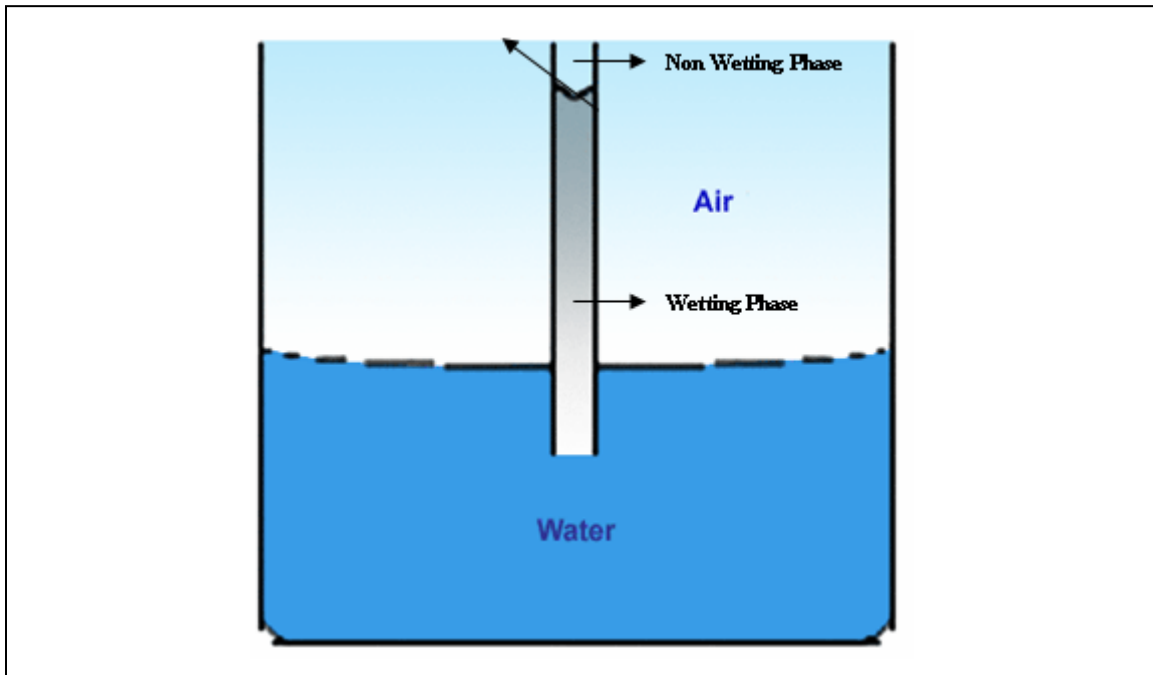
Figure 12: Capillary Mechanism in Tube [(4)]
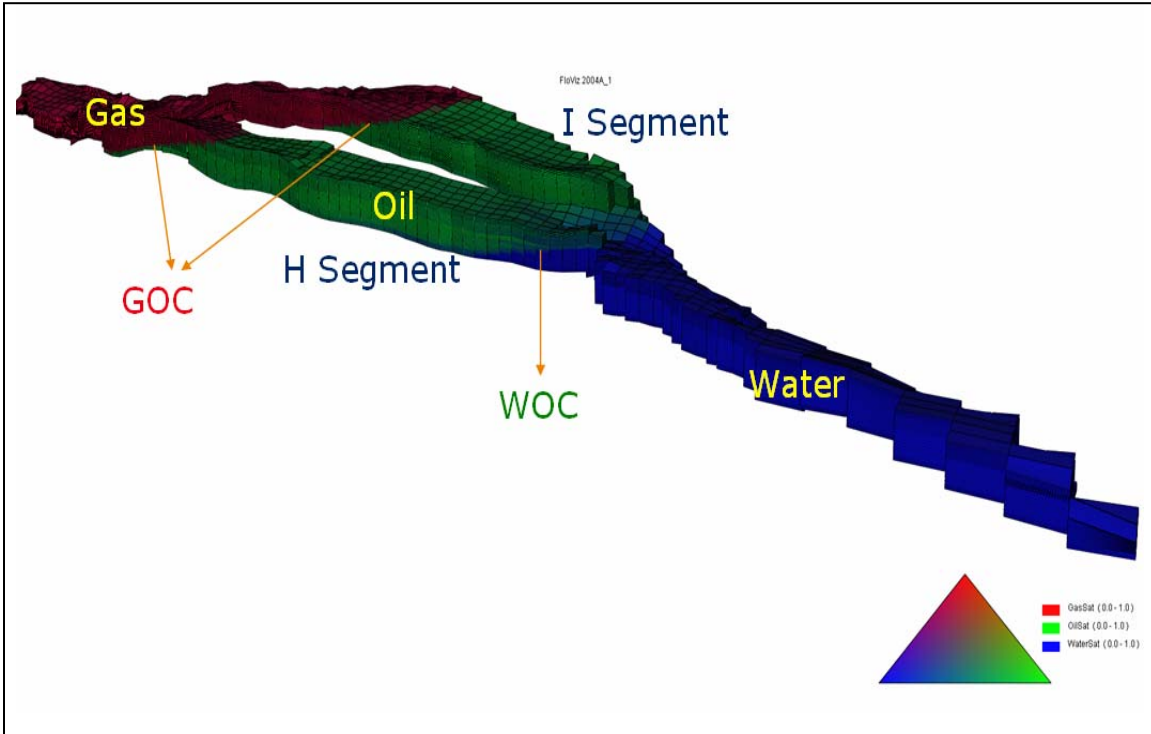
Figure 13: Location Fluid Contact in H and I Segment Heidrun Field
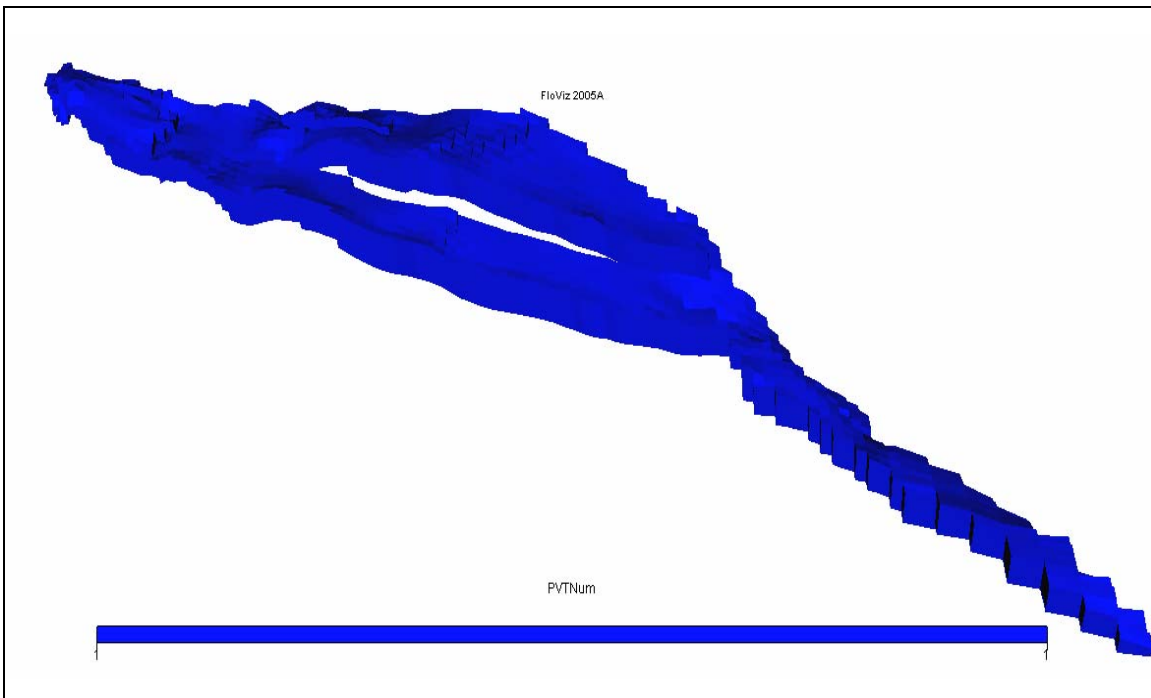
Figure 14: PVT Number (PVTNUM=1) for Group 1 in H and I Segment Heidrun Geological Model
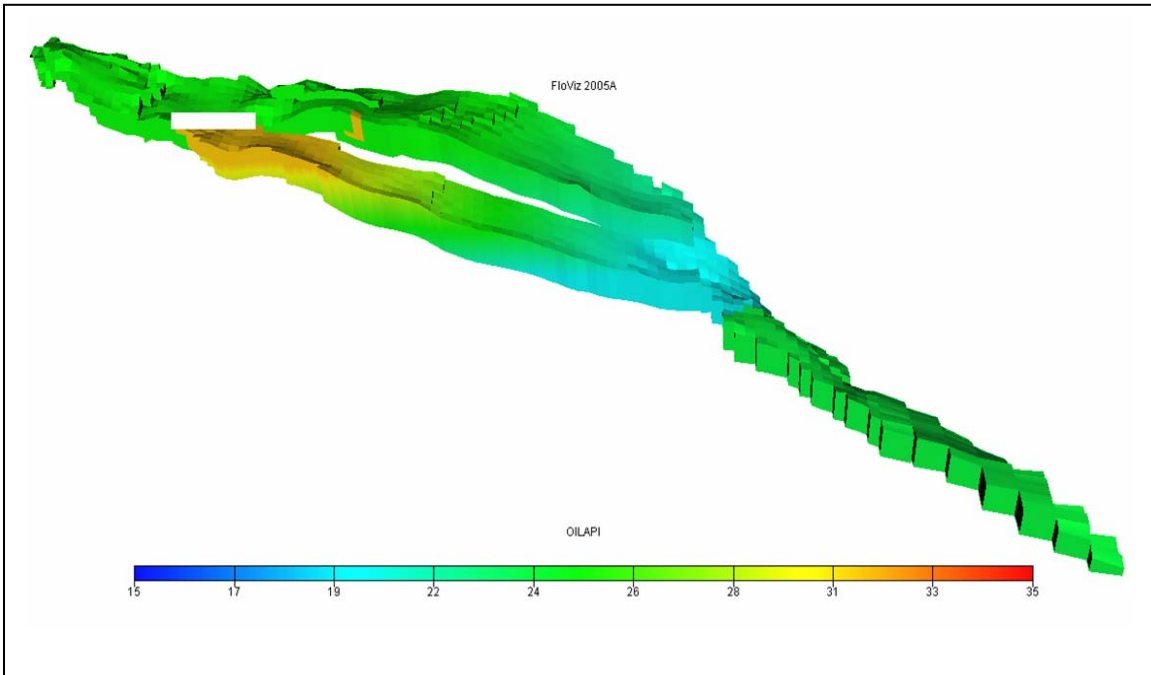
Figure 15: API Region in Upper Tilje H and I Segment Heidrun Simulation Model
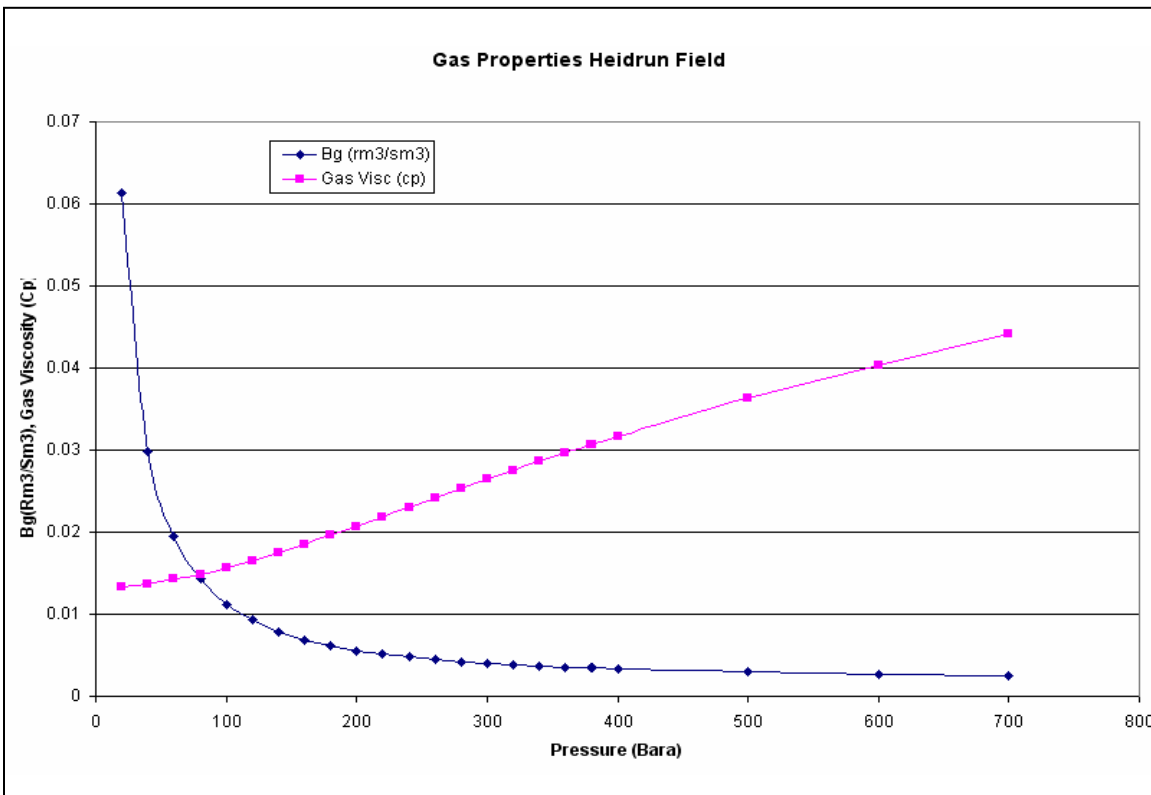
Figure 16: Plot Gas Properties (Bg, µg vs. Pressure) Heidrun Field
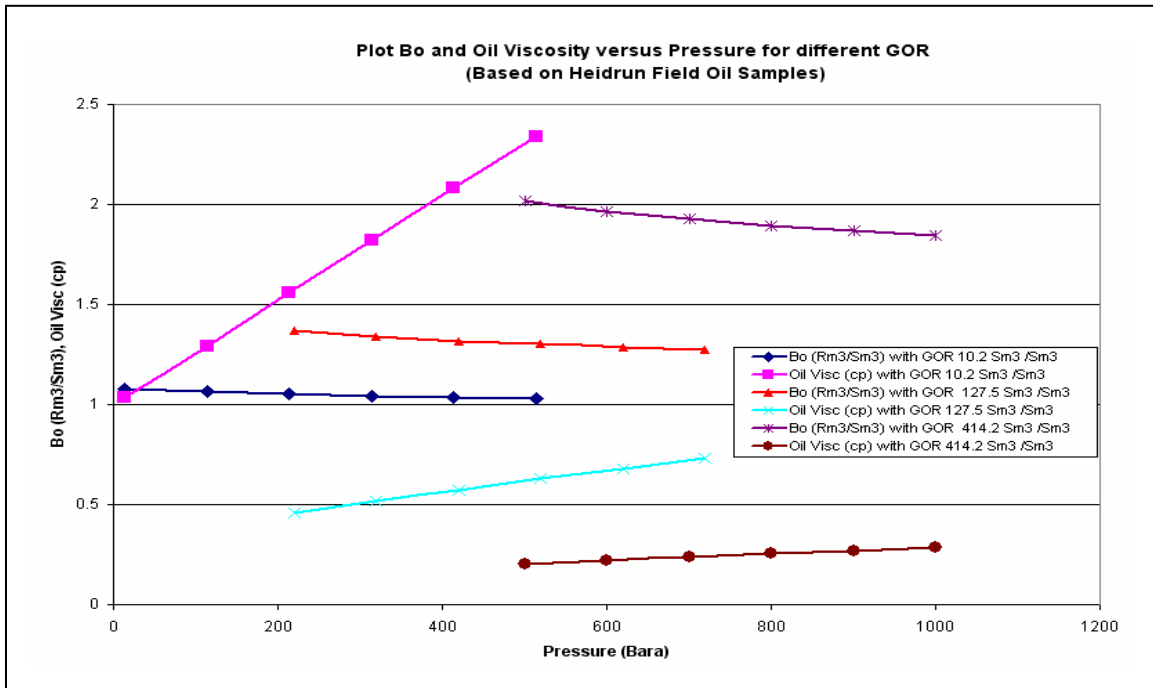
**Figure 17: Plot Oil Properties (Bo, μo vs. Pressure) Heidrun Field
With Different GOR**
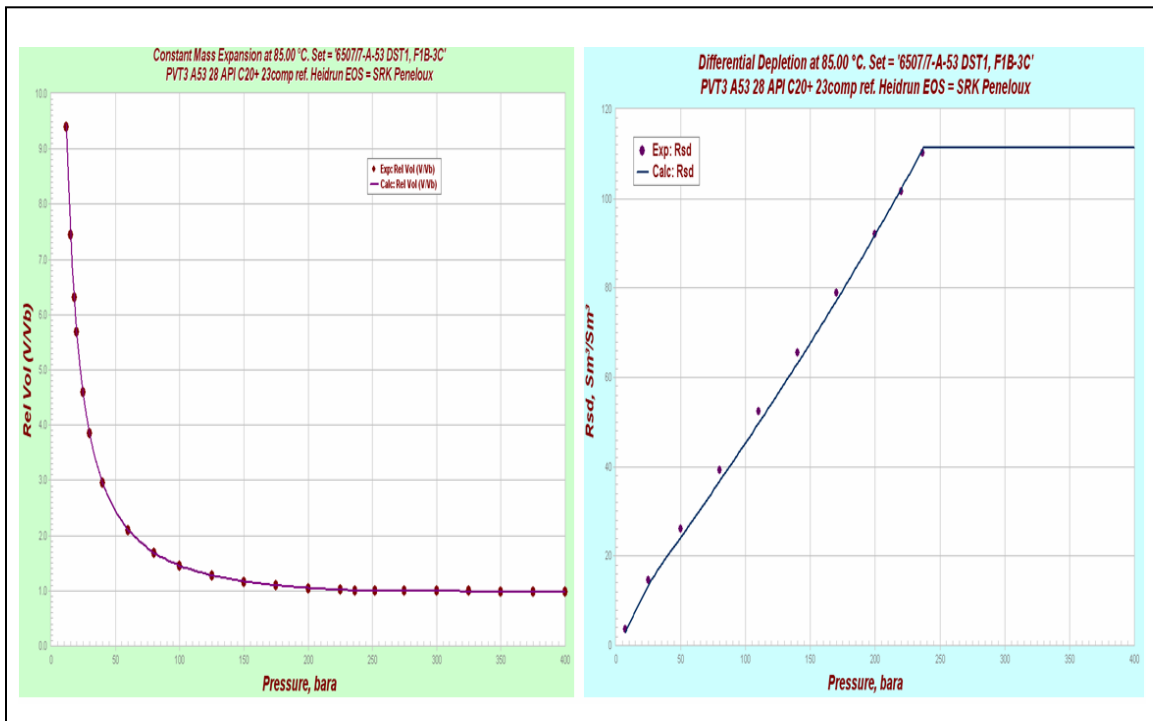
**Figure 18: Matching Heidrun EOS Model with Experimental Data
(For Constant Mass Expansion and Solution Gas)**
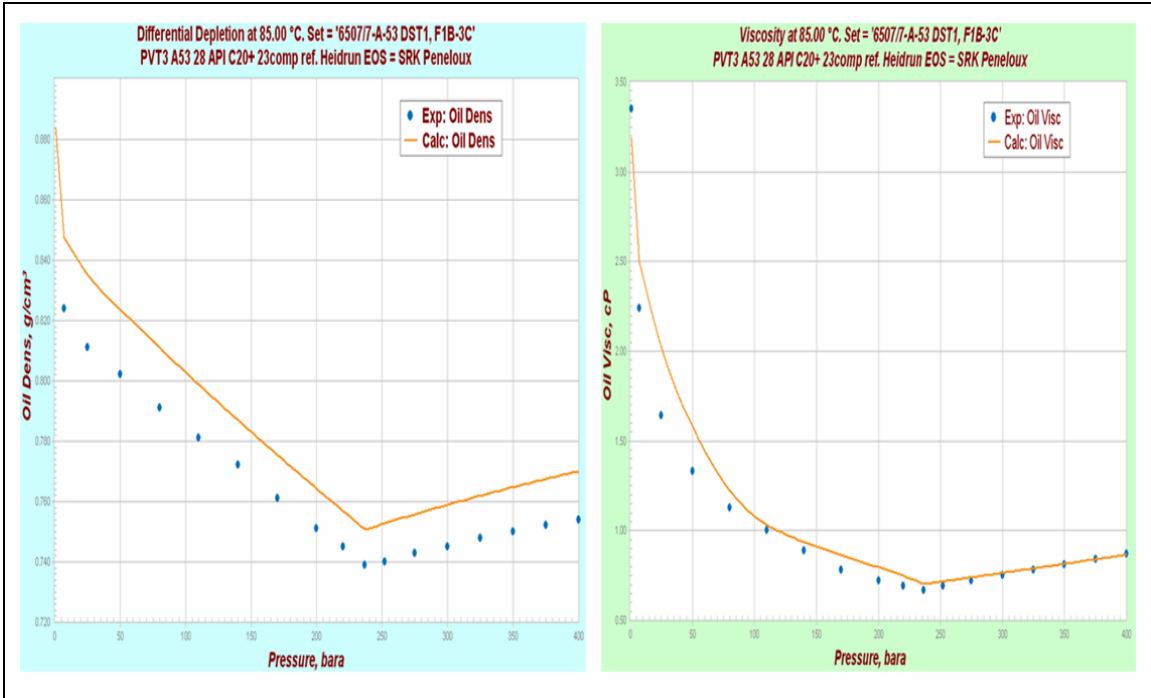
Figure 19: Matching Heidrun EOS Model with Experimental Data
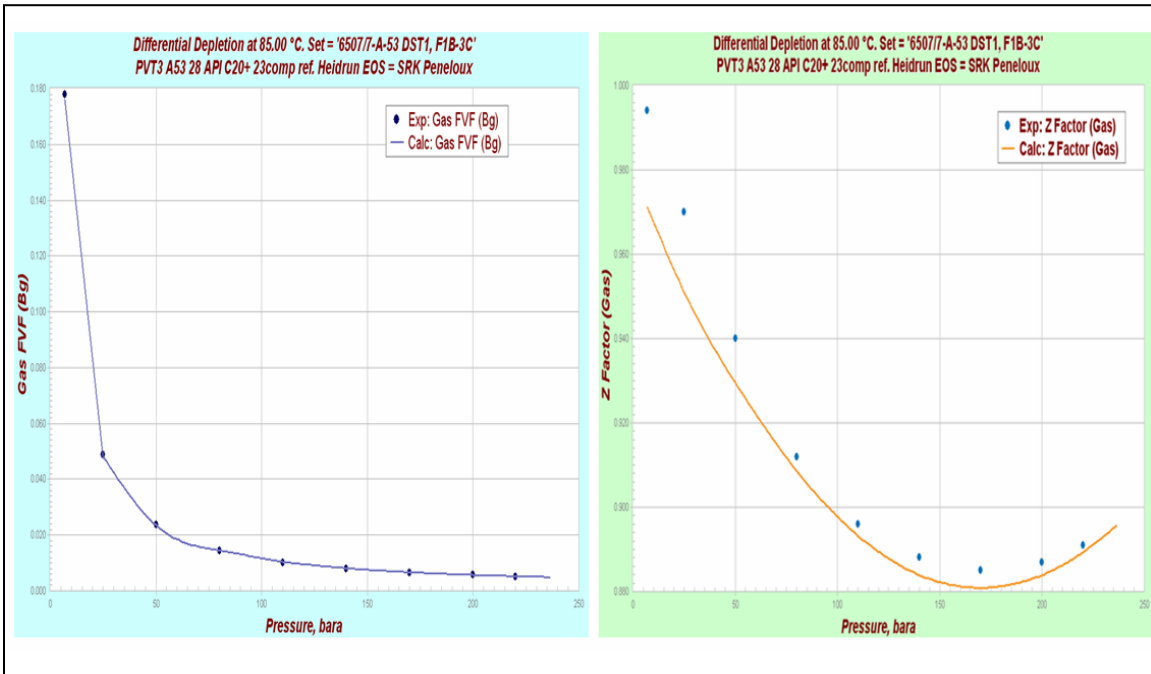**(For Oil Density and Oil Viscosity)**

Figure 20: Matching Heidrun EOS Model with Experimental Data
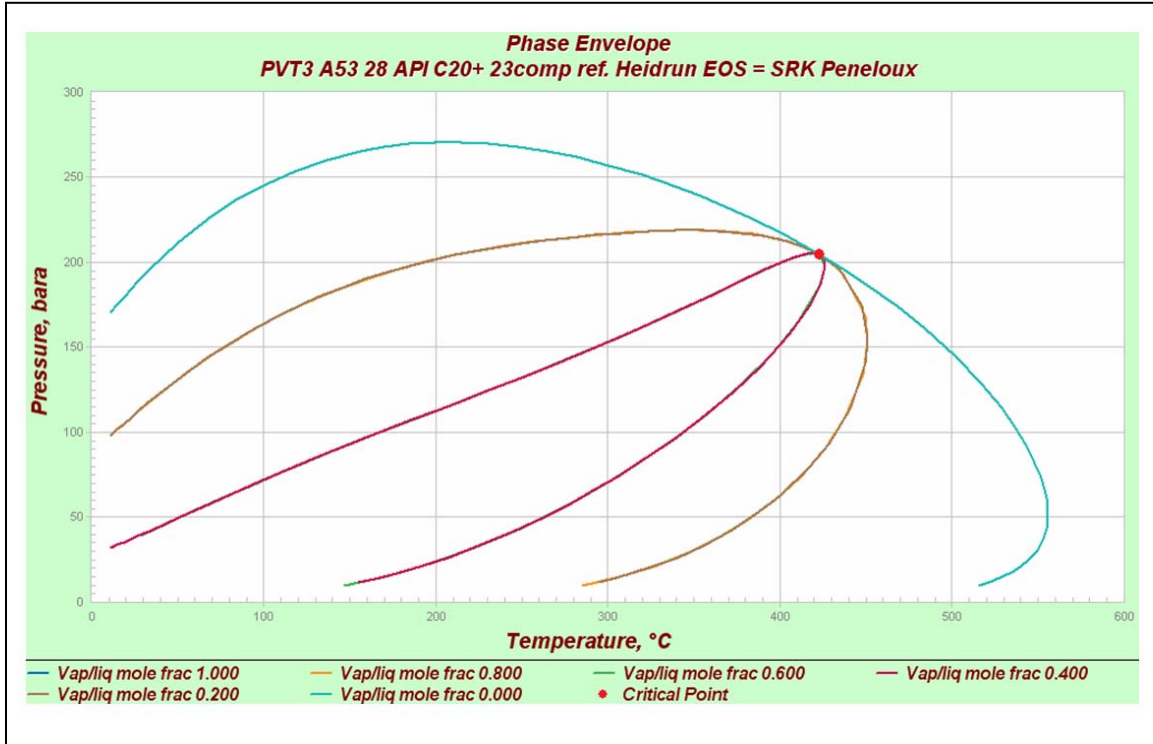**(For Z Factor and Gas Formation Volume Factor)**

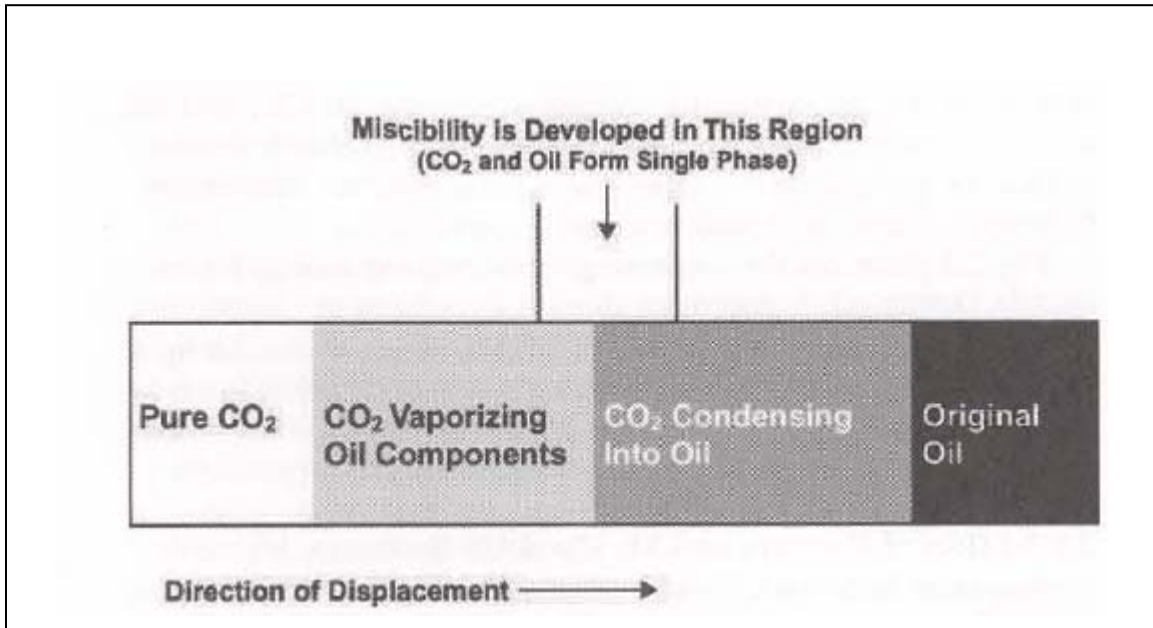**Figure 21: Heidrun Oil Phase Behaviour Chart (23 Components)**

Figure 22: Condensing and Vaporizing Mechanism Illustration [1]
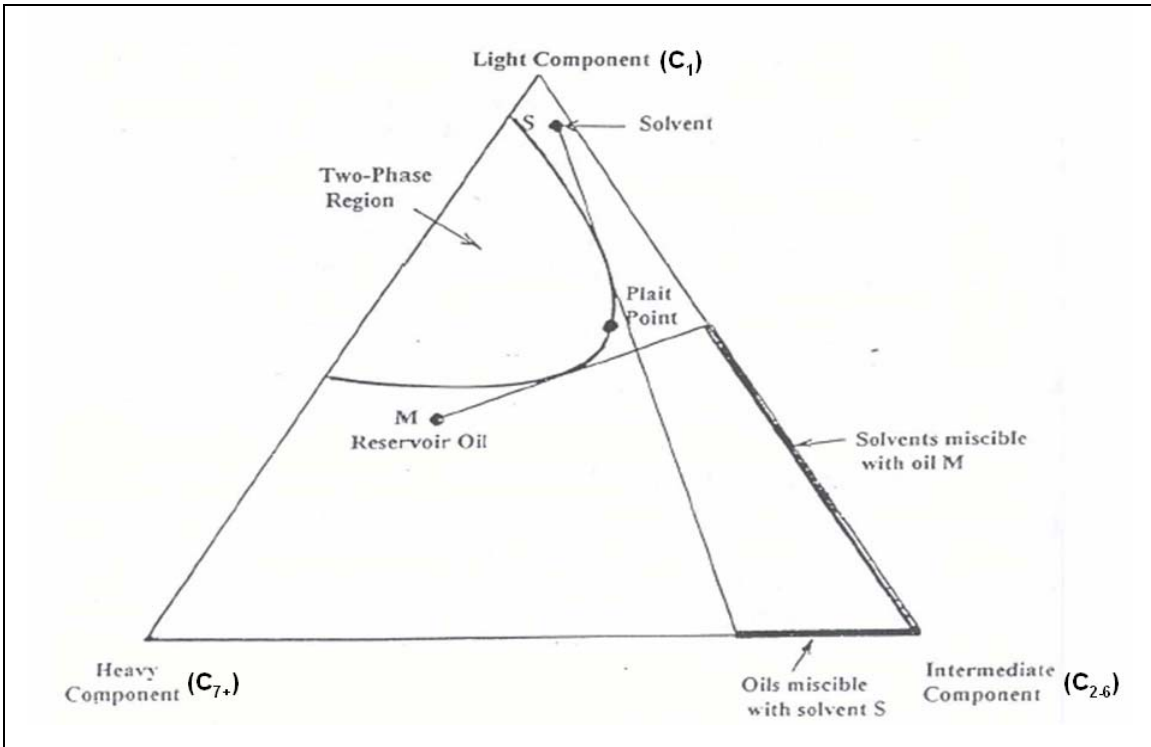
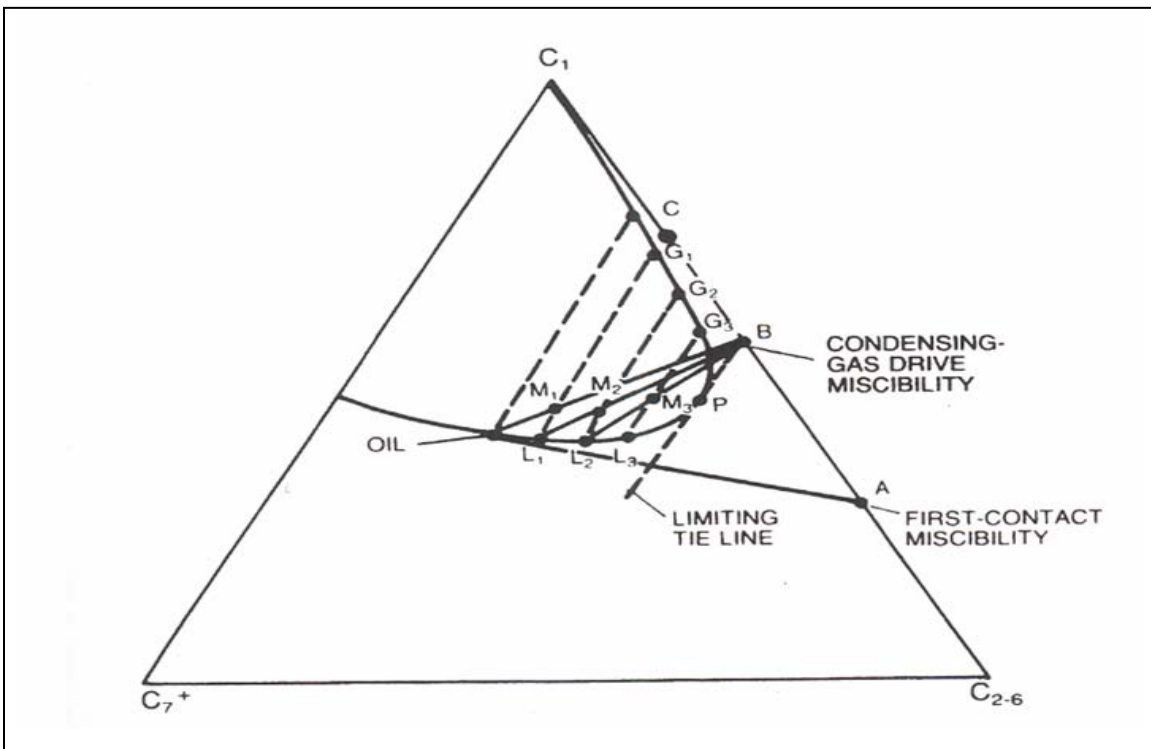**Figure 23: Ternary Diagram to Illustrate First Contact Miscibility Process** [4]

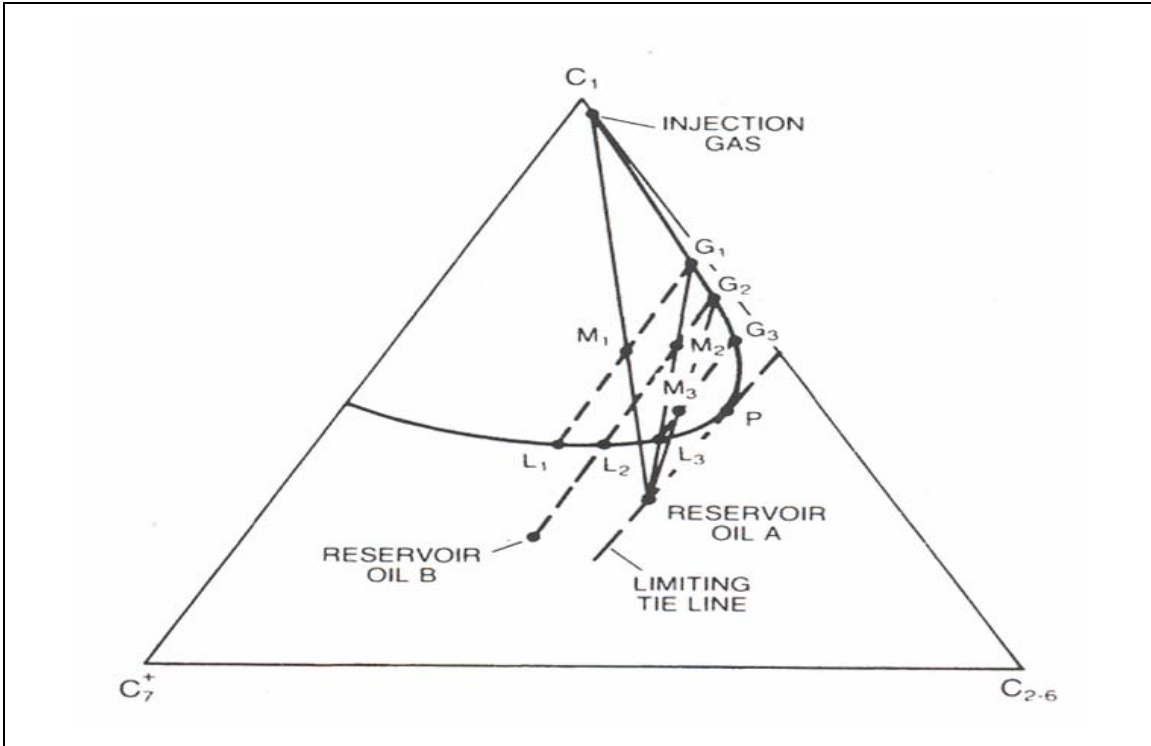**Figure 24: Ternary Diagram to Illustrate Condensing Gas Drive Miscibility** [3]

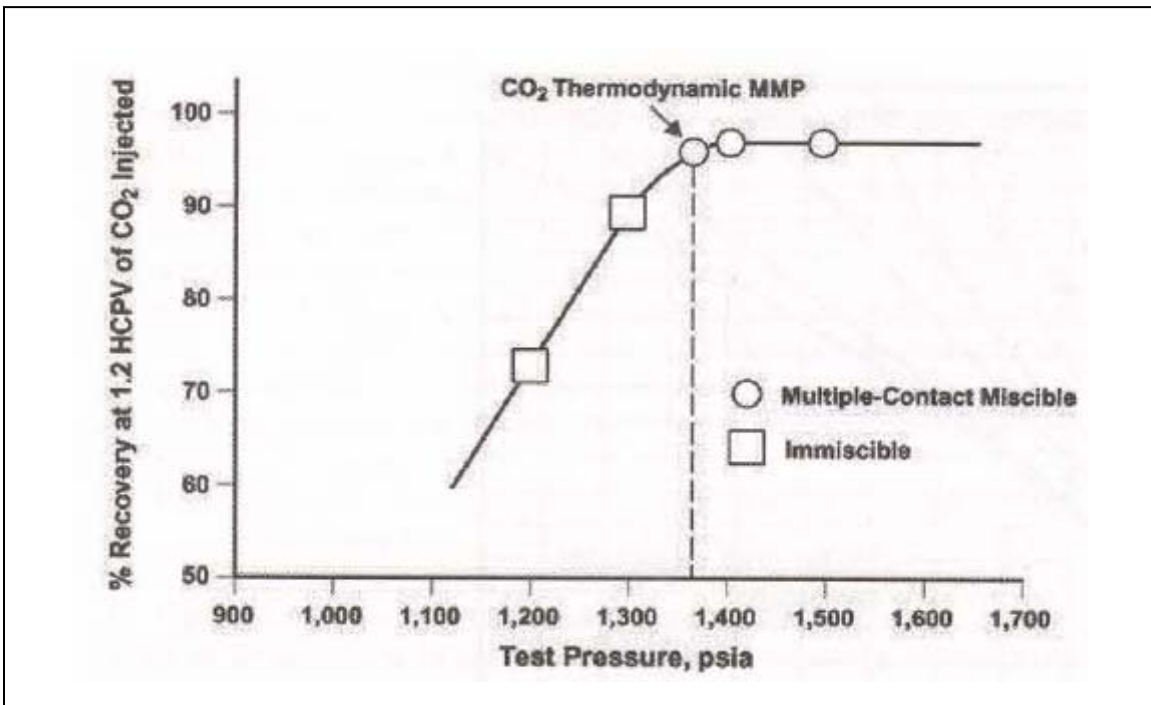**Figure 25: Ternary Diagram to Illustrate Vaporizing Gas Drive Miscibility** [3]

Figure 26: Plot Oil Recovery Factor vs. CO_2 Pressure in 1D CO_2 Displacement [1]
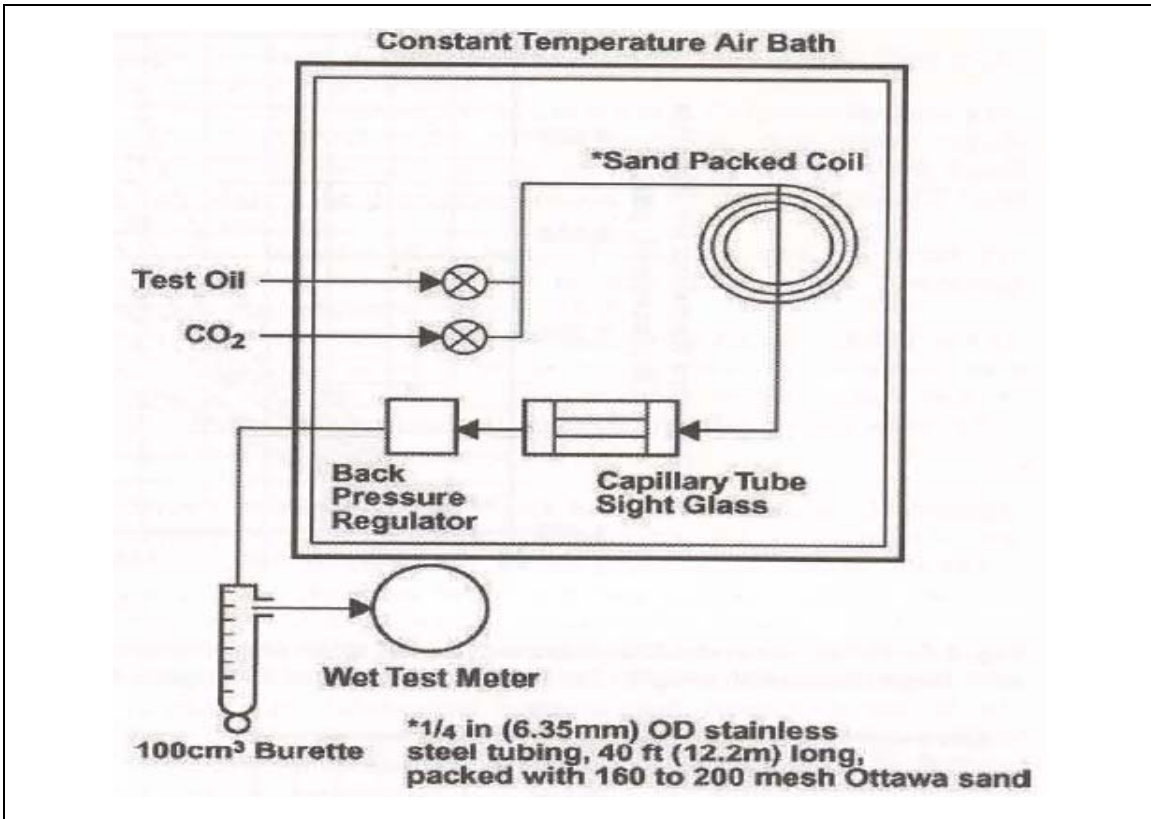
Figure 27: Basic Laboratory Equipment for Slim Tube Test [1]
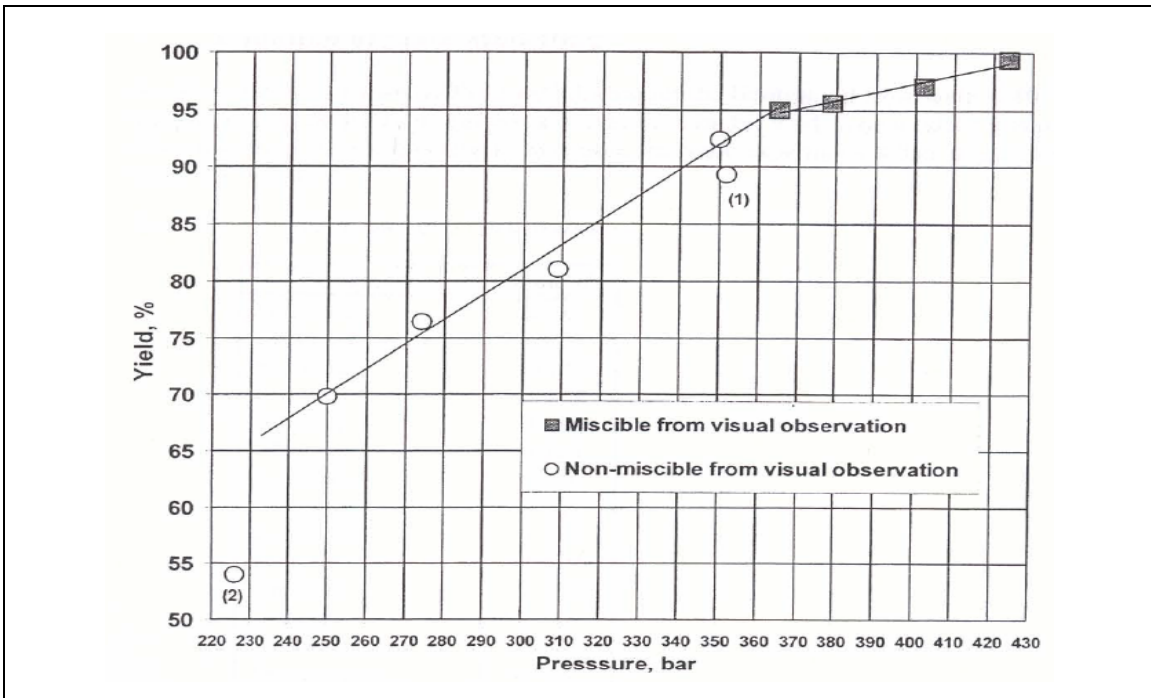
Figure 28: Plot Yield vs. Pressure from Slim Tube Experiment
For Heidrun Heavy Oil [7]
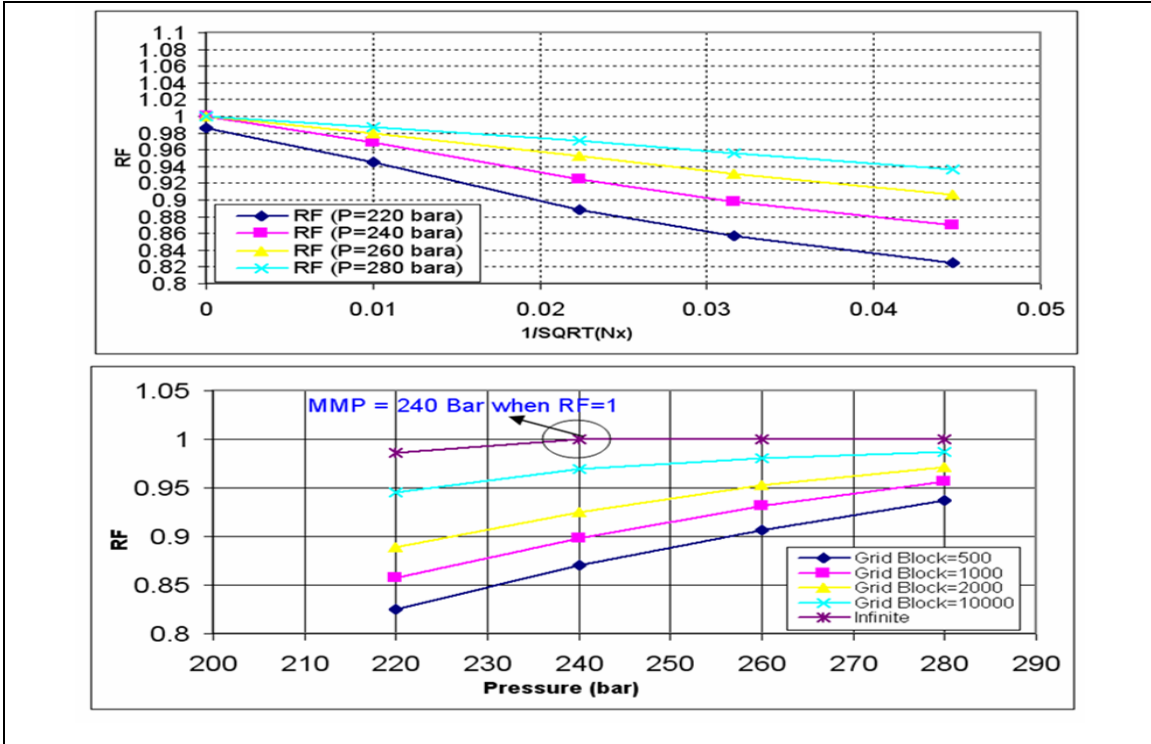
Figure 29: Plot Estimation Minimum Miscibility Pressure Based on Slim Tube Simulation for Heidrun Light Oil (23 Components)
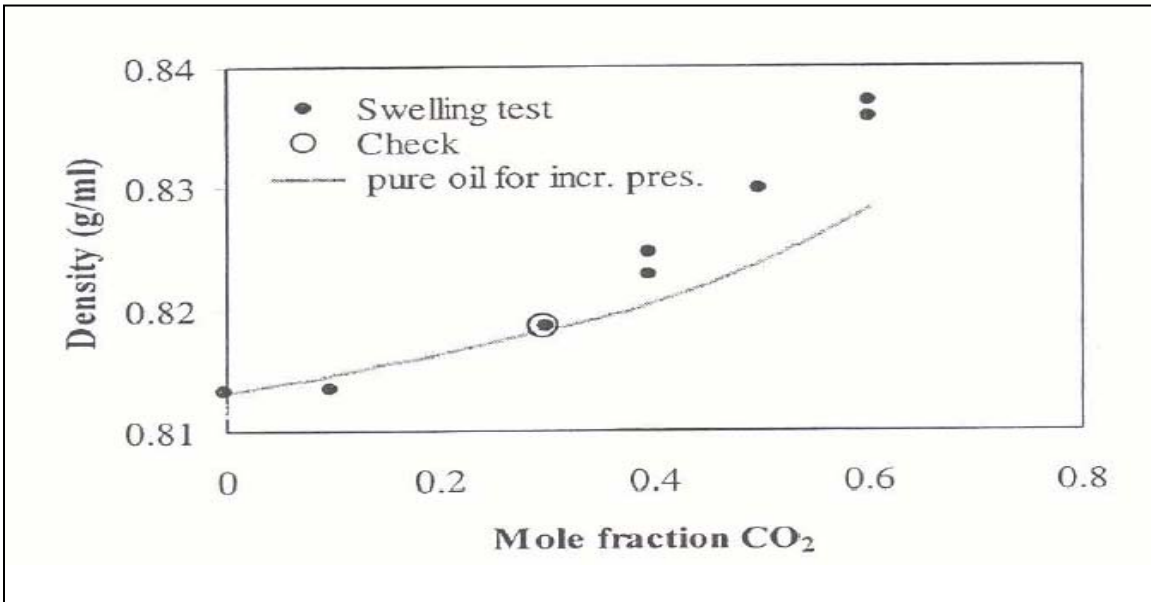
Figure 30: Oil Density at the Bubble Point of Oil-CO_2 Mixtures and Density of Recombined Heidrun Oil at Pressure that corresponds to the Saturation Pressures of the Oil-CO_2 Mixtures [7]
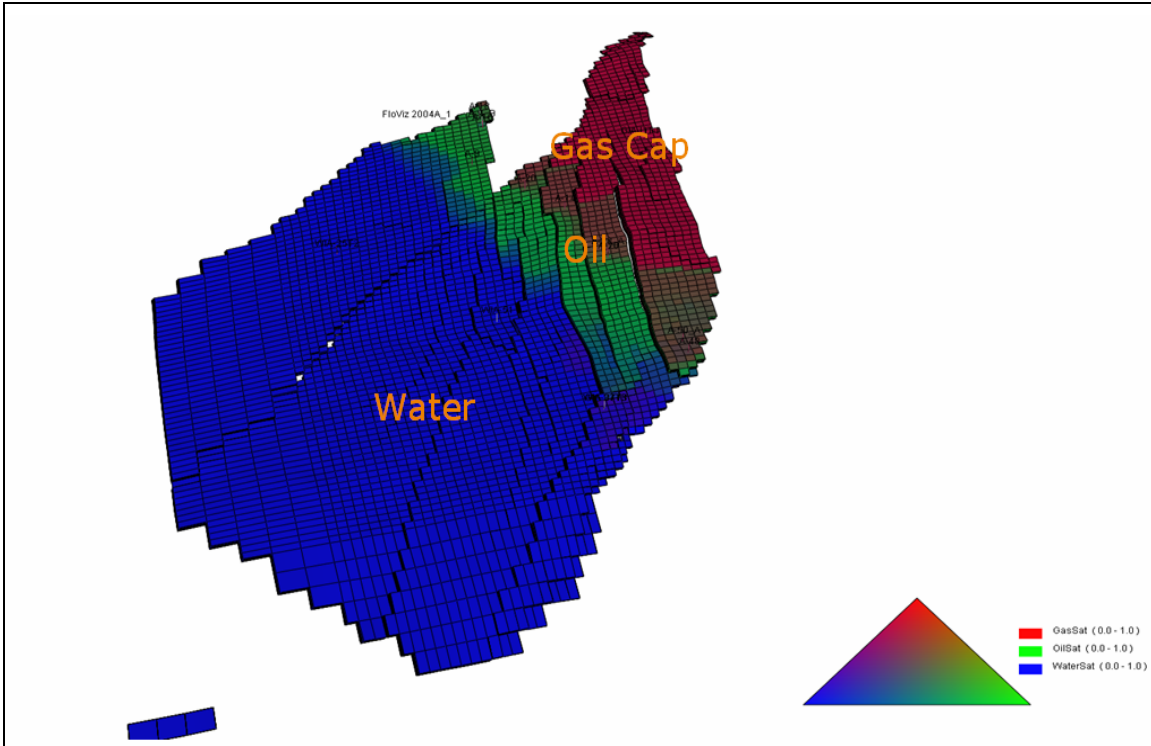
Figure 31: Full Field Heidrun Simulation Model
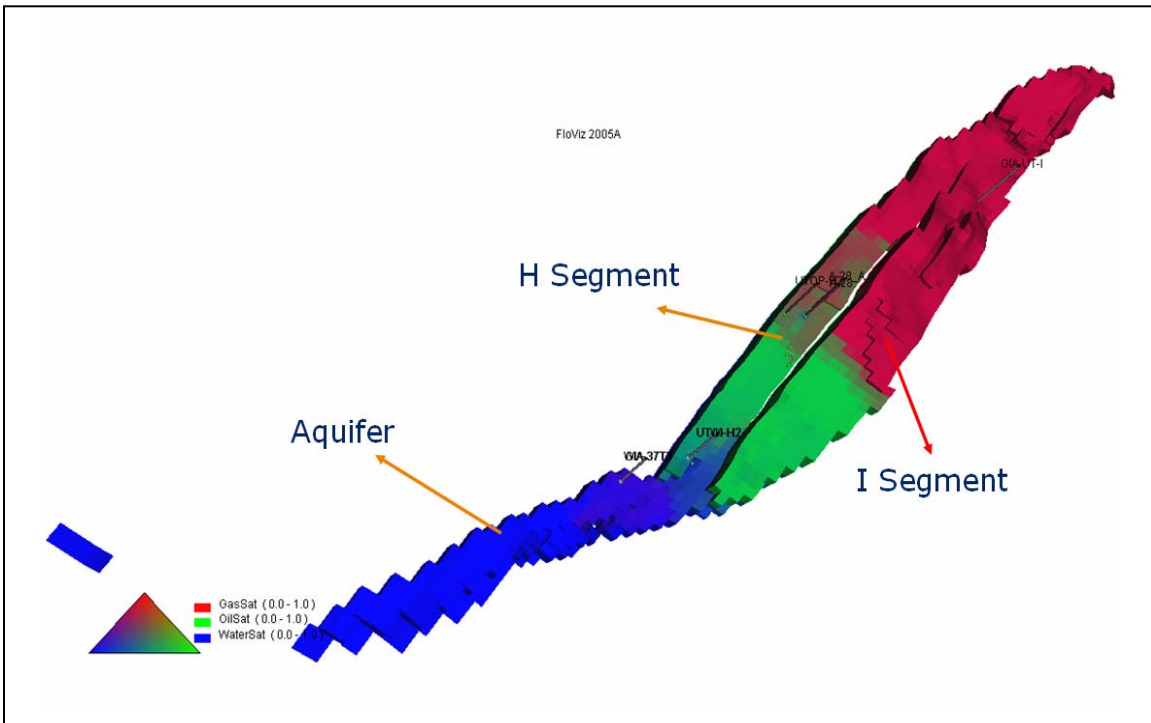
Figure 32: Simulation Model for Upper Tilje H and I Segment Heidrun Field
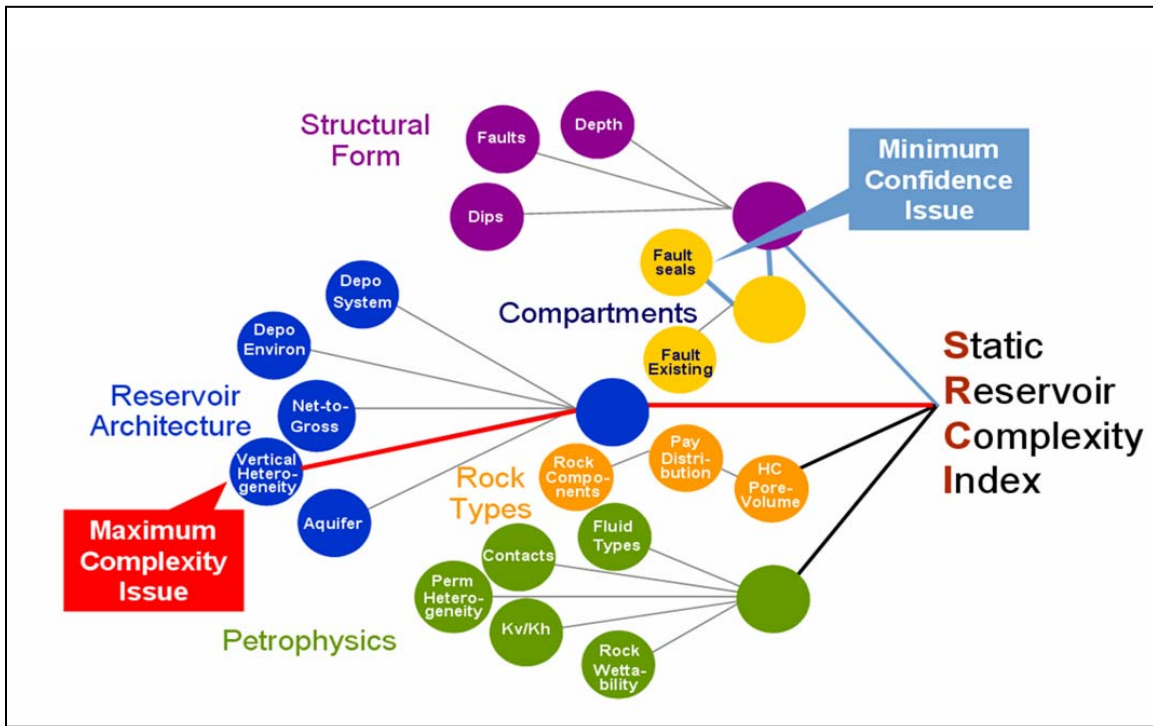
Figure 33: The Static of Reservoir Uncertainties in Heidrun Model
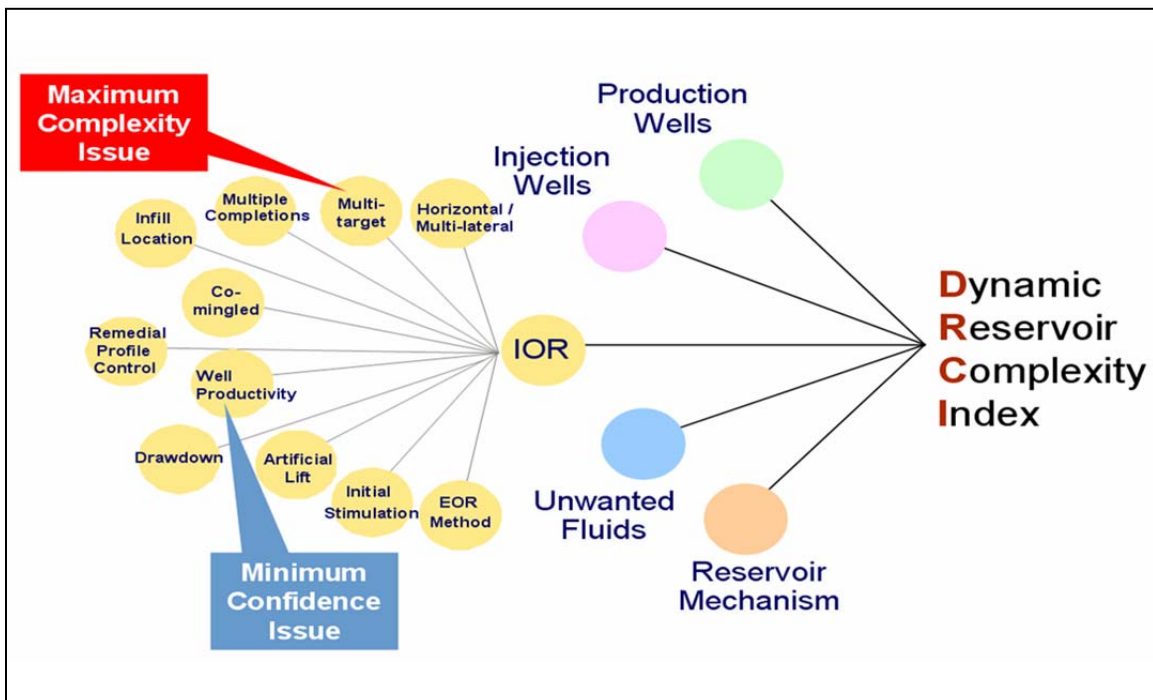
Figure 34: The Dynamic of Reservoir Uncertainties in Heidrun Model
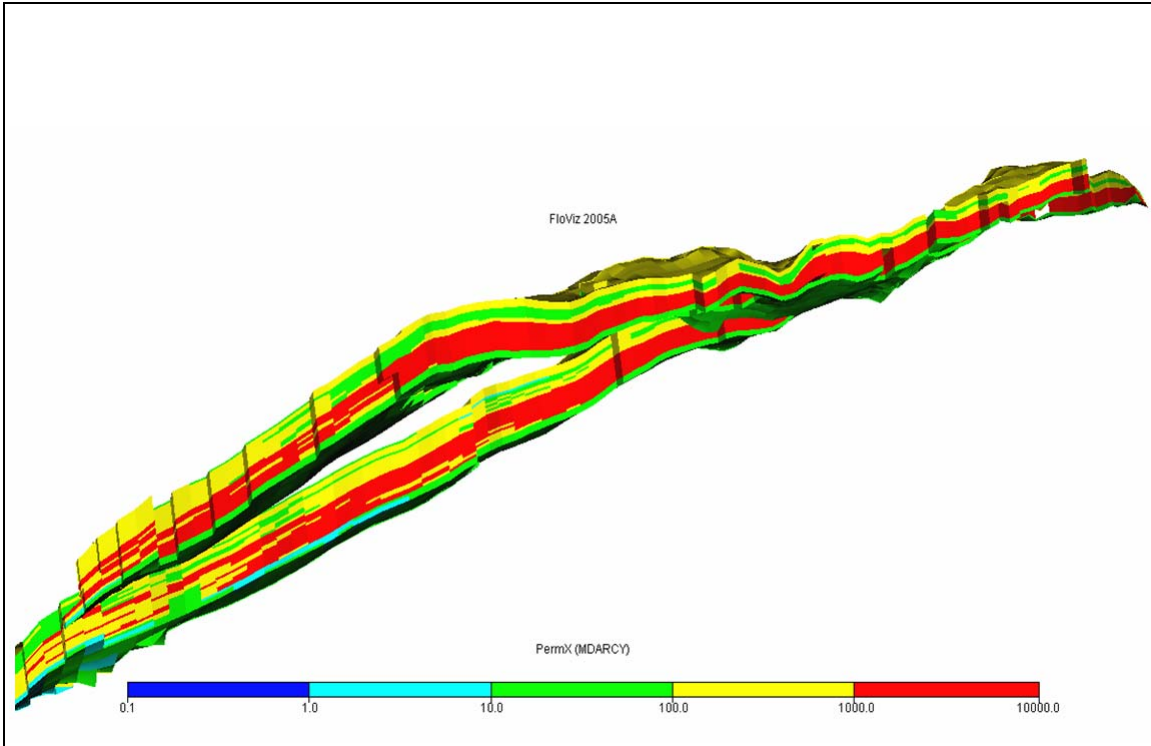
Figure 35: The Visualization of Vertical Heterogeneity in Heidrun Model
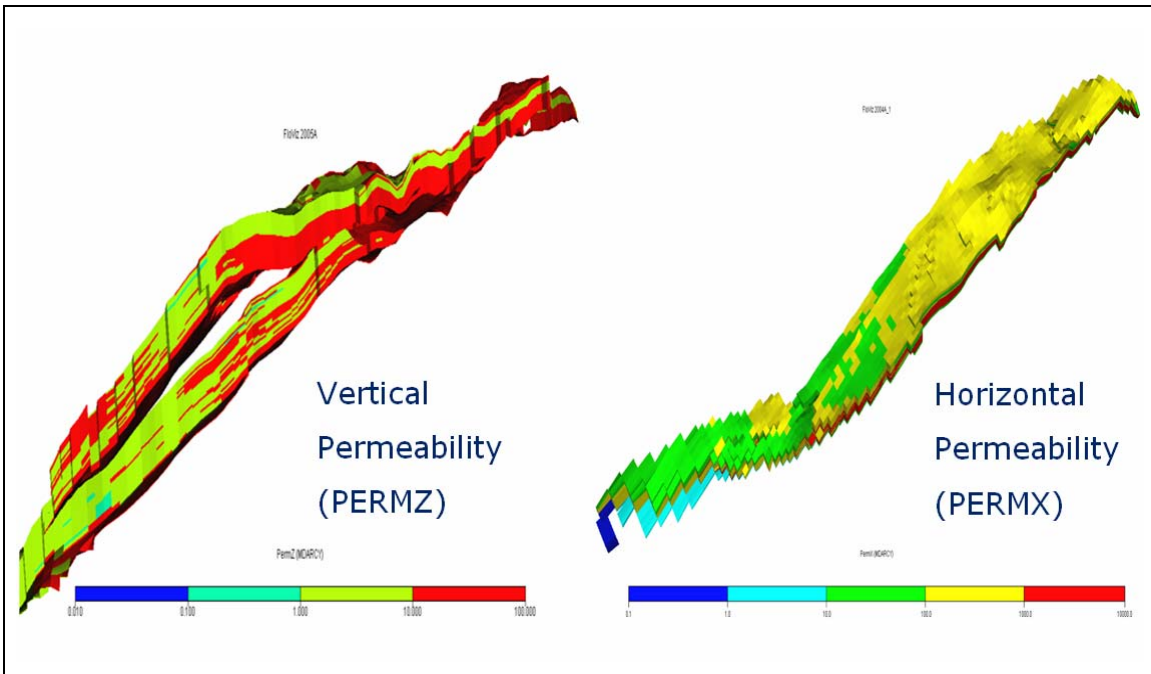
Figure 36: Comparison Permeability Variation in Vertical and Horizontal Direction in Heidrun Simulation Model
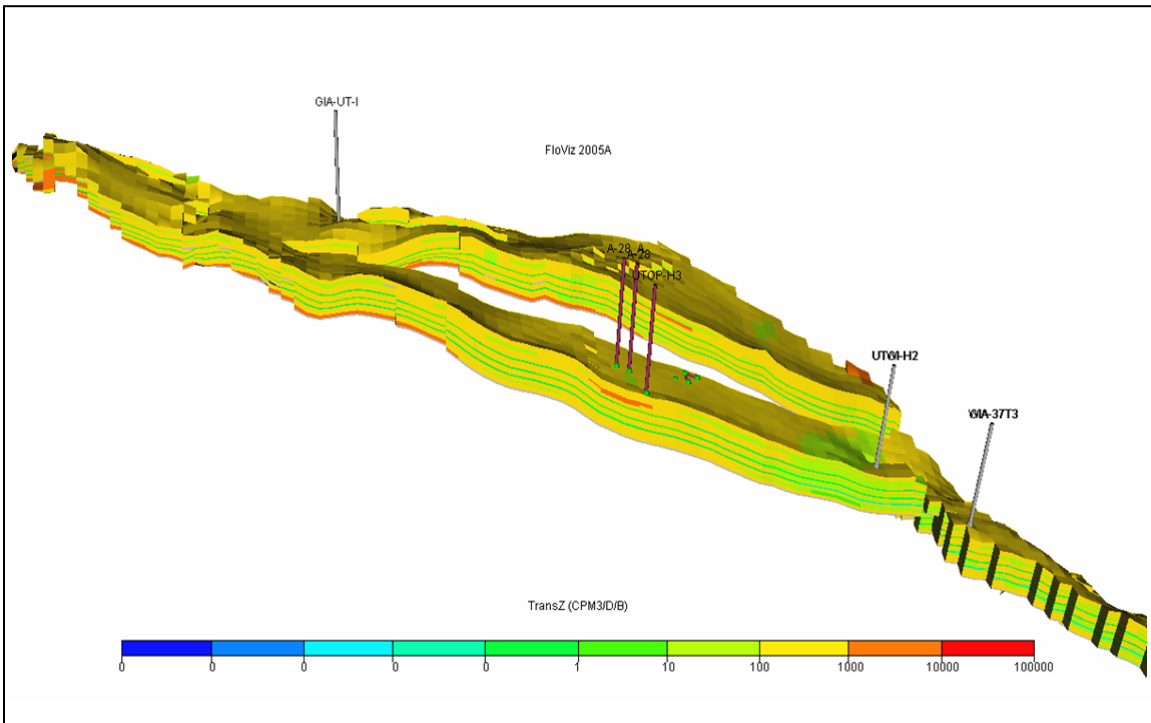
Figure 37: The Visualization of Transmissibility Value in Z Direction from Heidrun Simulation Model
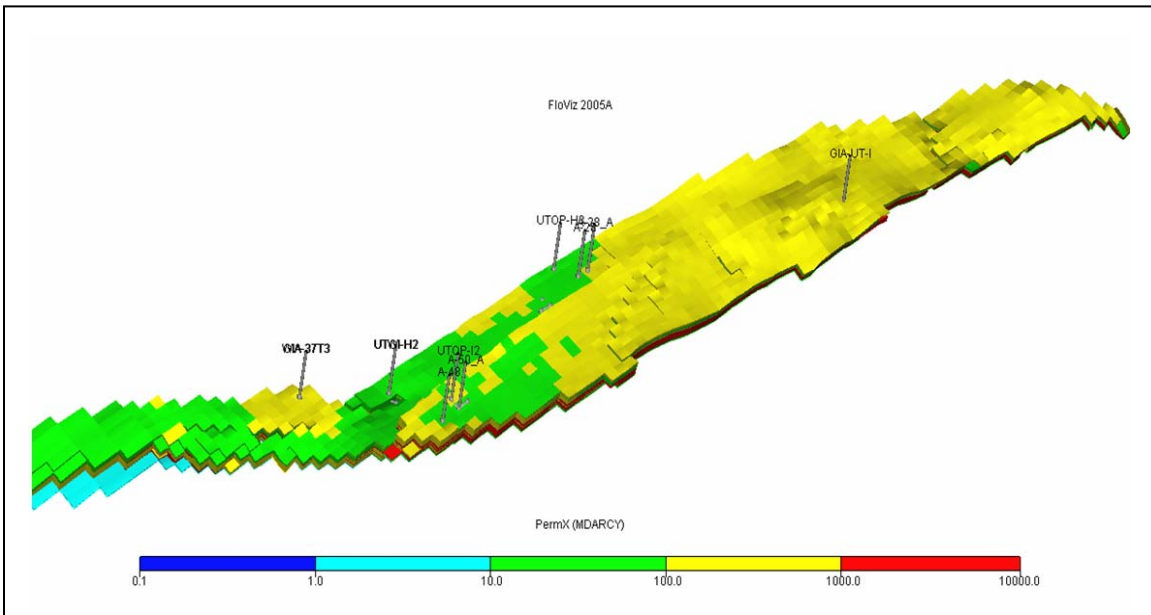
Figure 38: The Location of Six Producer Wells, Two WAG Injectors and One Virtual Gas Injector in Heidrun Simulation Model
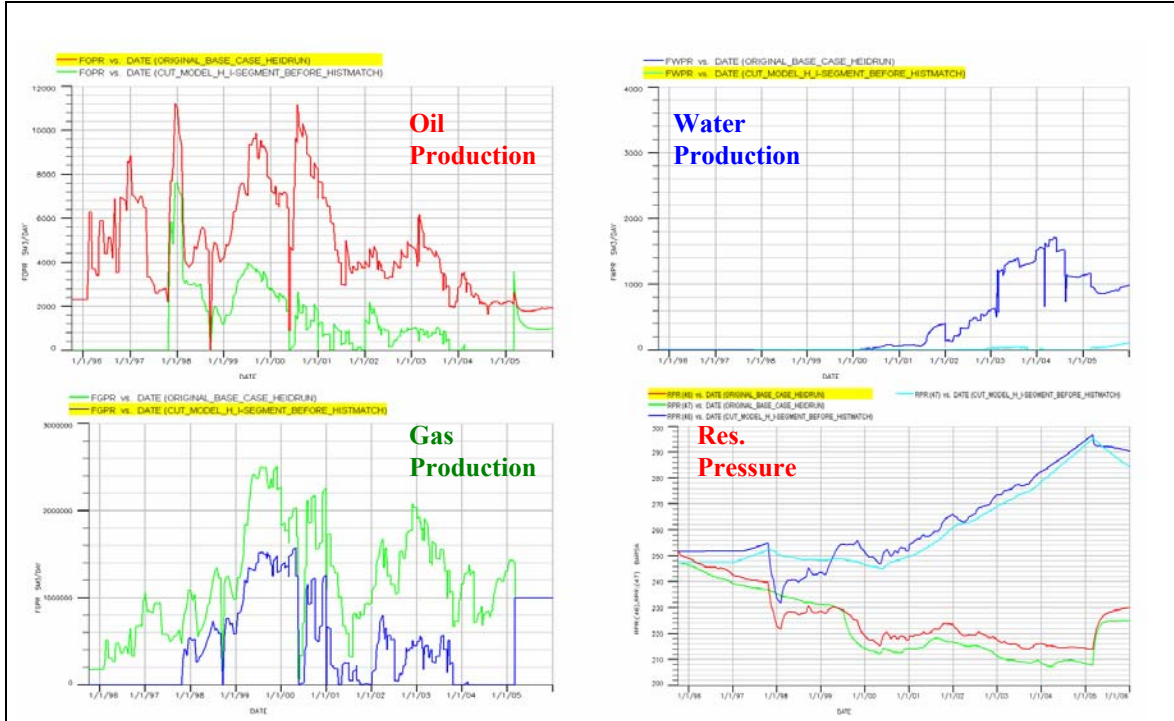
**Figure 39: The Comparison Simulation Result (Before History Matching) from Cut
Model (H and I Segment) with Actual Production from Original Base Case
Heidrun Simulation Model**
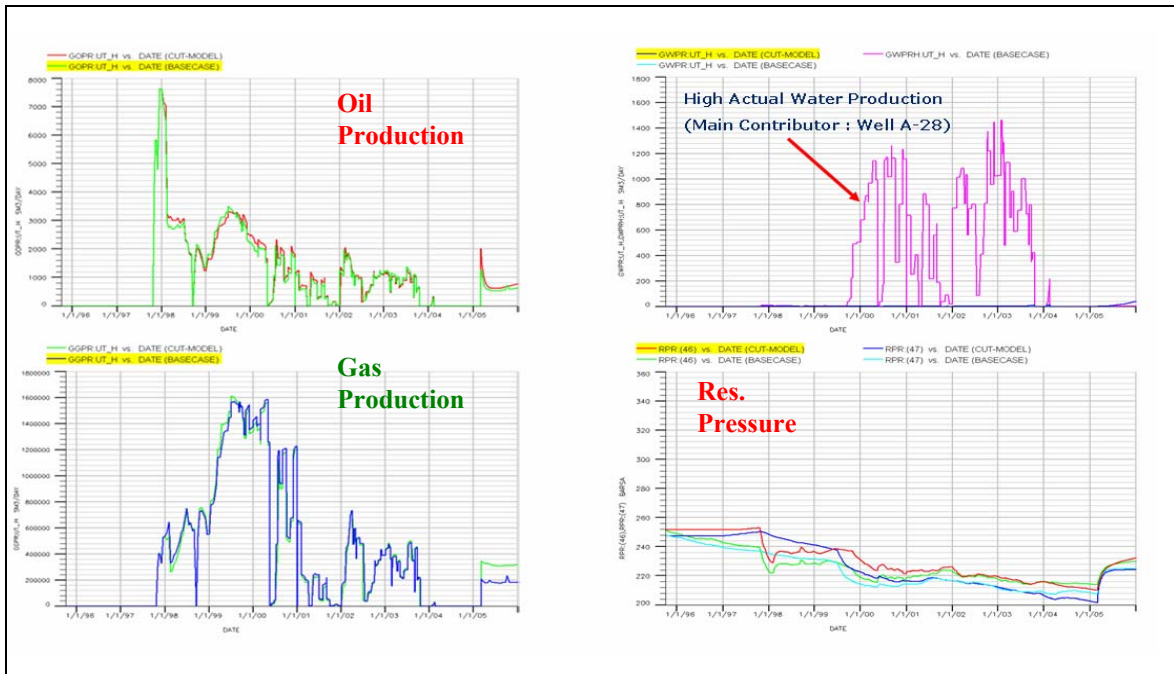
**Figure 40: The History Matching Result (H Segment) after Cutting
Water Injection Rate 50%**
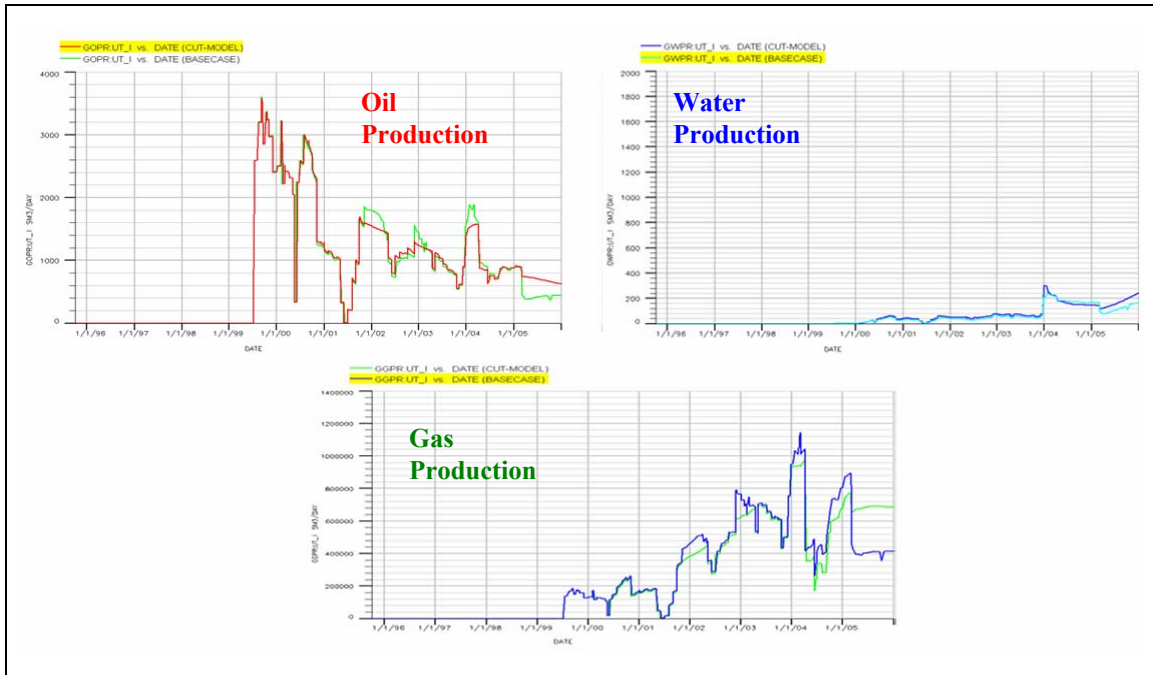
Figure 41: The History Matching Result (I Segment) after Cutting Water Injection Rate 50%
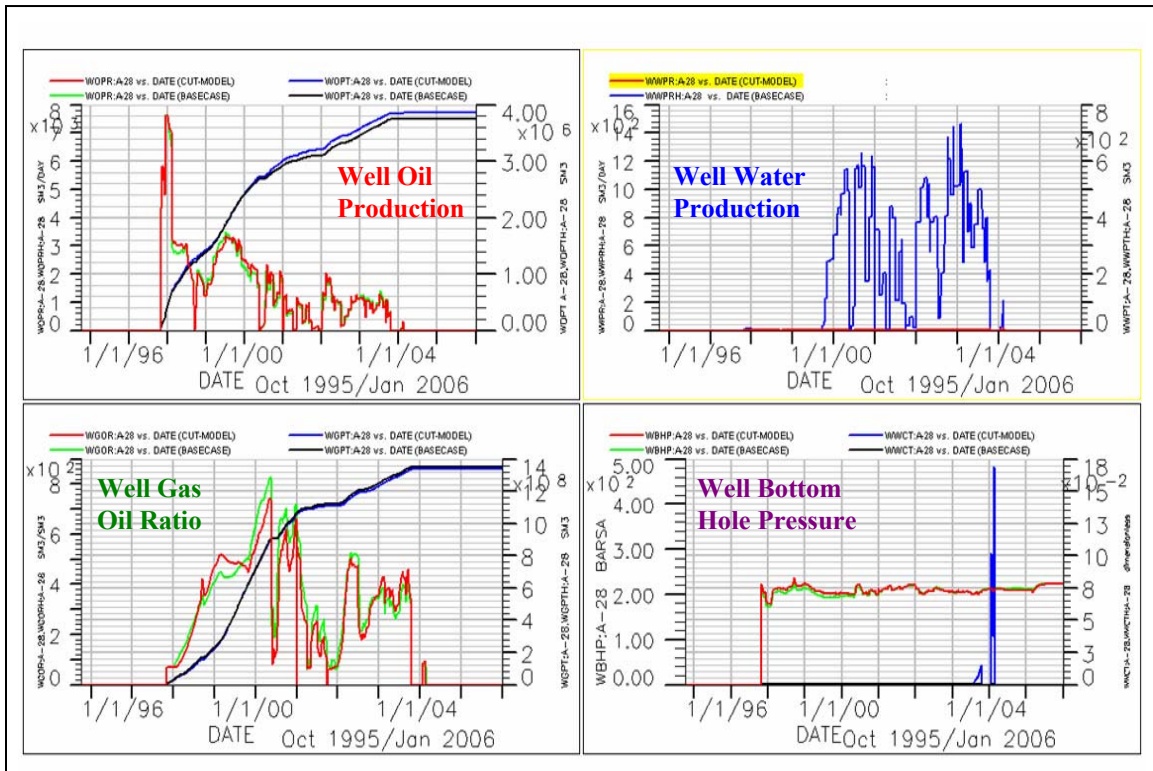
Figure 42: The Example Matching Result in Well A-28 after Cutting Water Injection Rate 50%
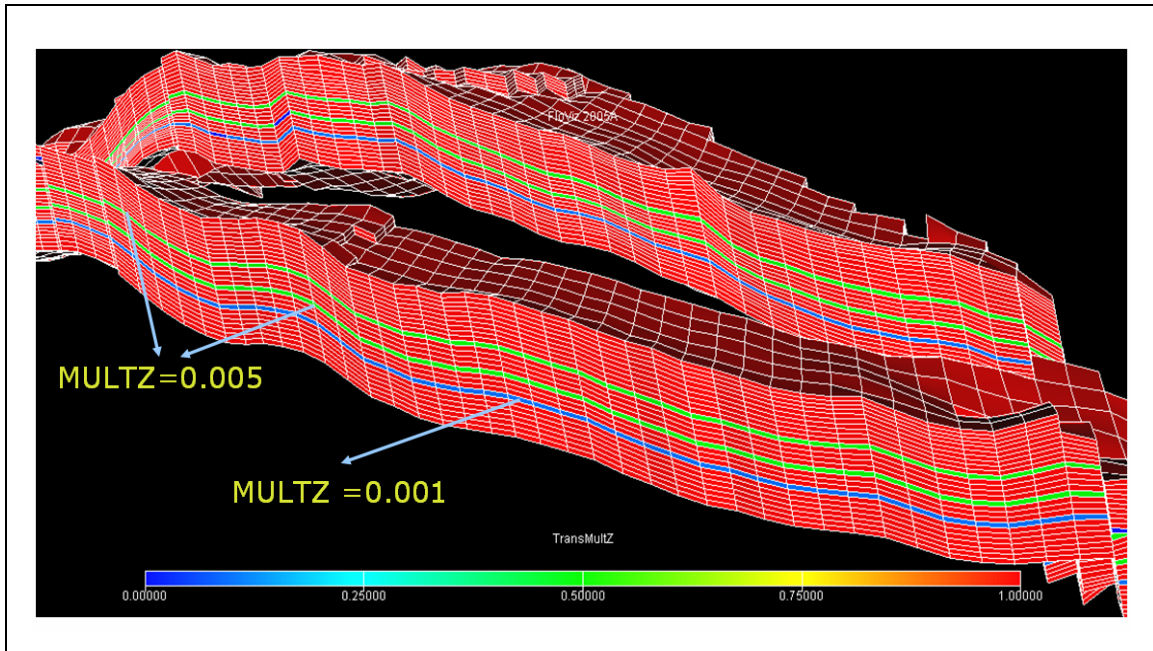
Figure 43: The Visualization of Shale Barrier in Heidrun Simulation Model
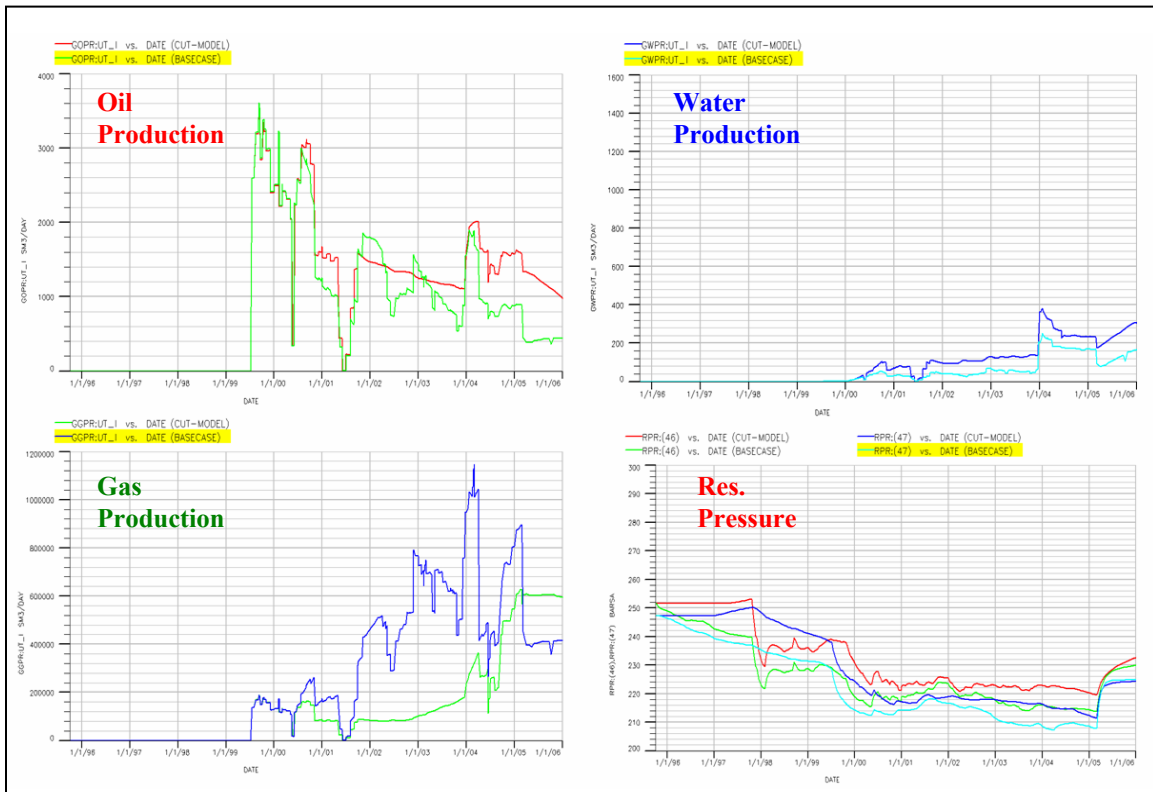
**Figure 44: The History Matching Result after Increasing
MULTZ in Shale Barrier 100 Times**
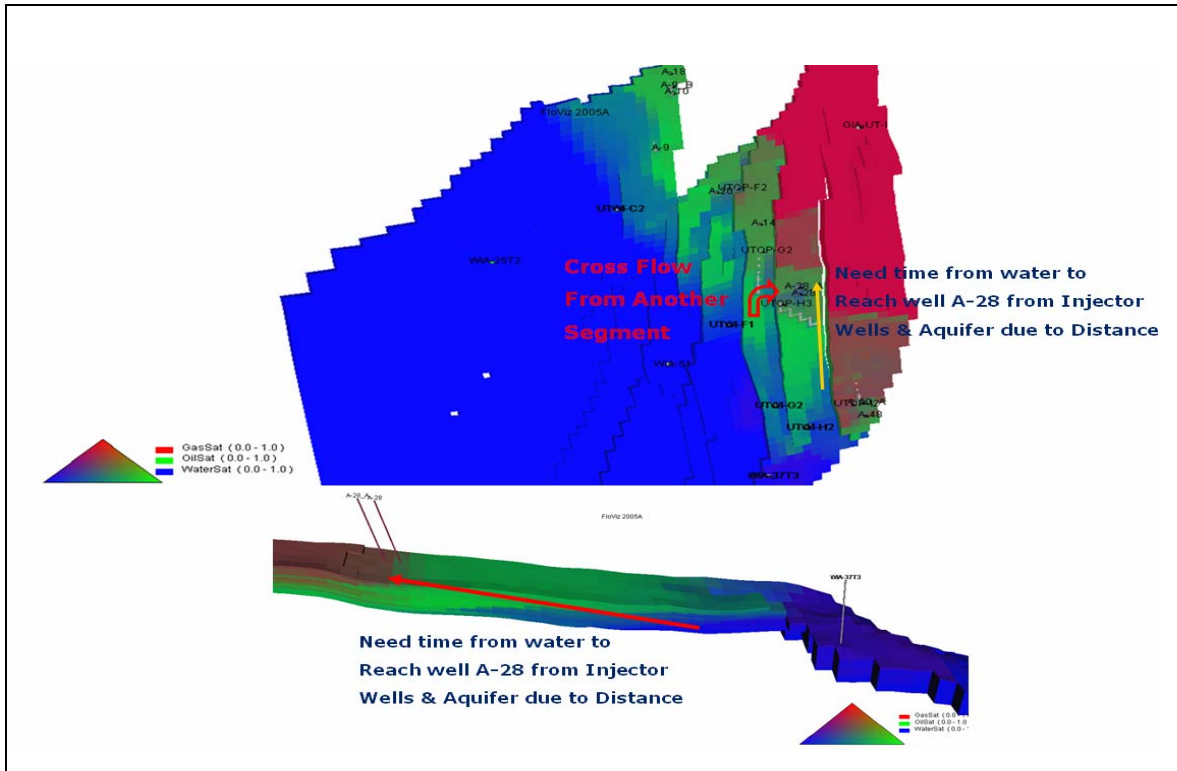
**Figure 45: The Visualization of Possibility Water Cross Flow
From Another Segments to Well A-28**
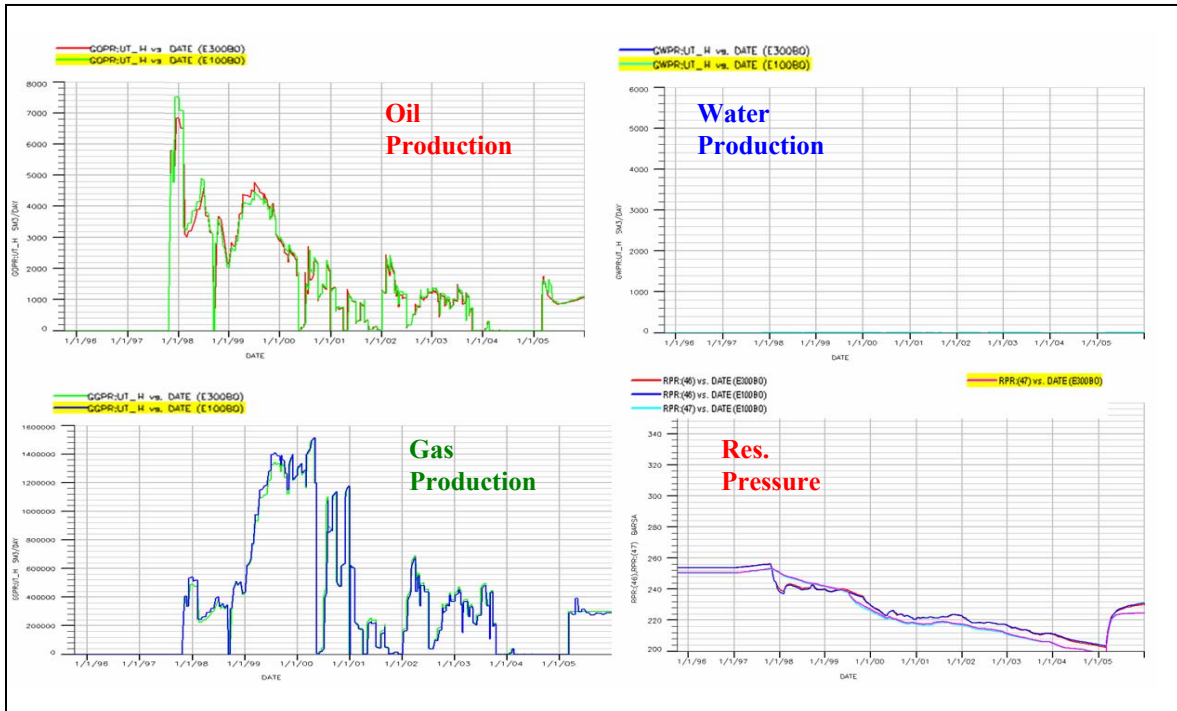
**Figure 46: The Comparison Simulation Result (in H Segment) between Eclipse 100
and Eclipse 300 Black Oil Model**
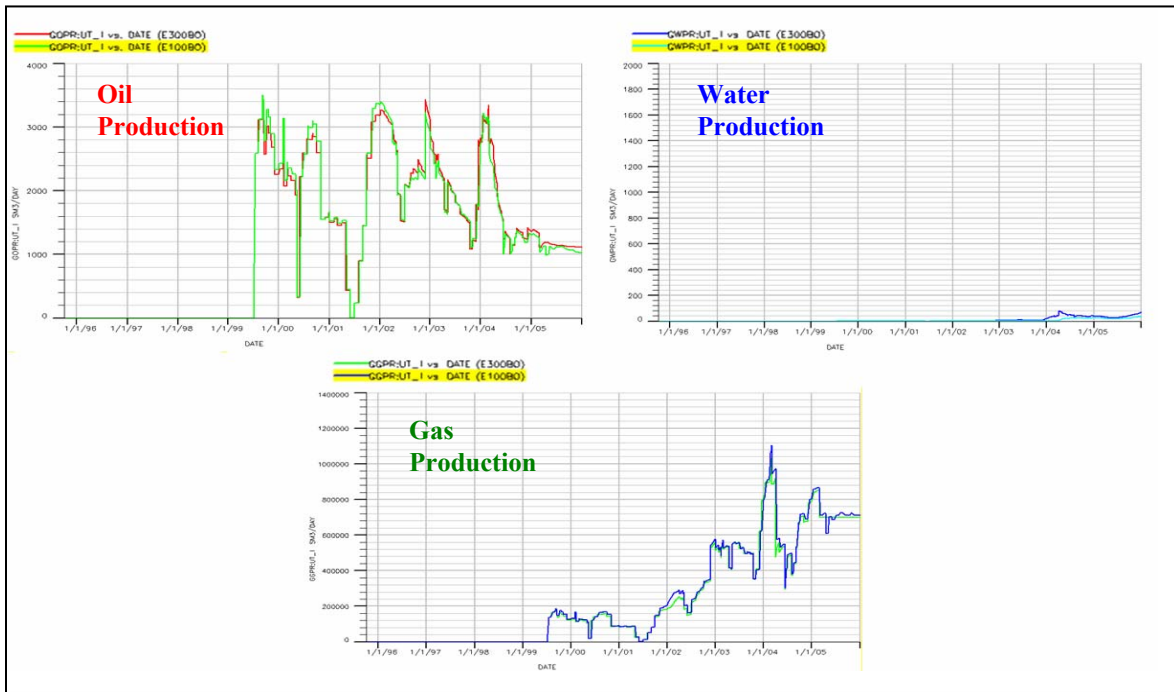
Figure 47: The Comparison Simulation Result (in I Segment) between Eclipse 100 and Eclipse 300 Black Oil Model

Figure 48: The Comparison Simulation Result (for H and I Segment) between Eclipse 300 Compositional and Eclipse 300 Black Oil
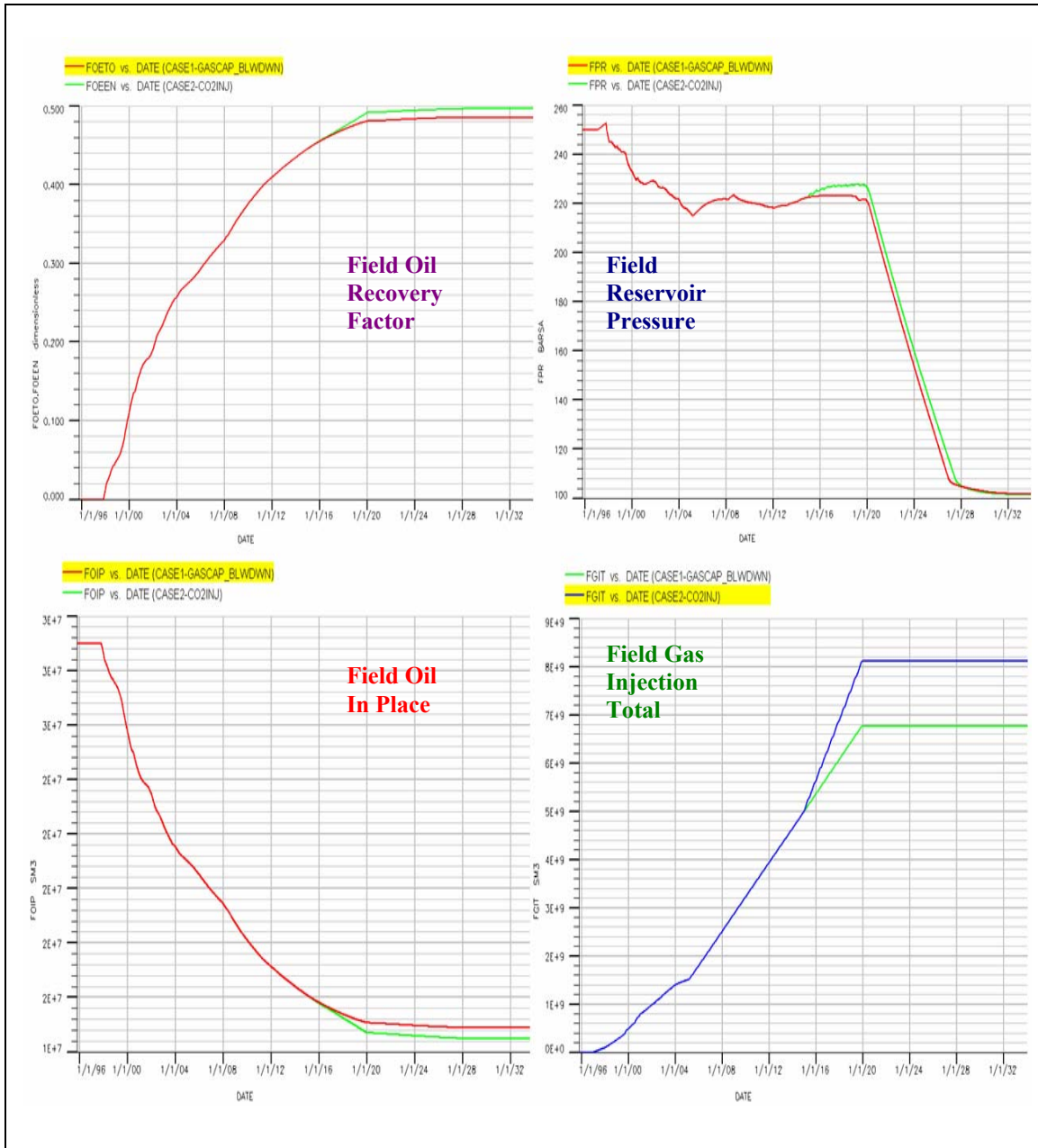
Figure 49: The Comparison Compositional Simulation Result (for OOIP and Pressure) between Gas Blow Down Case (Without CO₂ Injection) and Gas Blow Down Case (With CO₂ Injection) at H and I Segment Heidrun Field
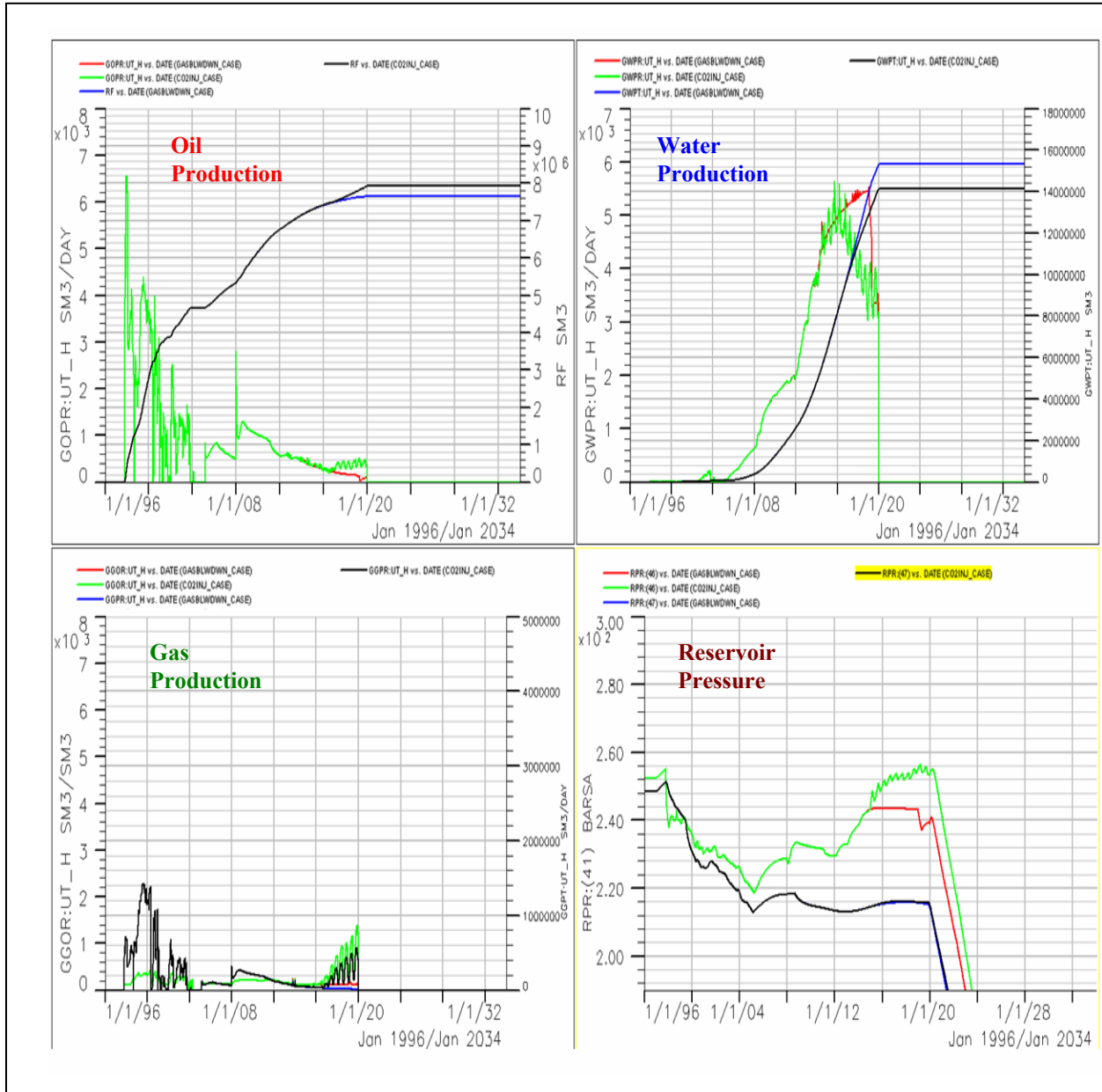
Figure 50: The Comparison Compositional Simulation Result (for Fluid Production) between Gas Blow Down Case (Without CO₂ Injection) and Gas Blow Down Case (With CO₂ Injection) at H Segment Heidrun Field
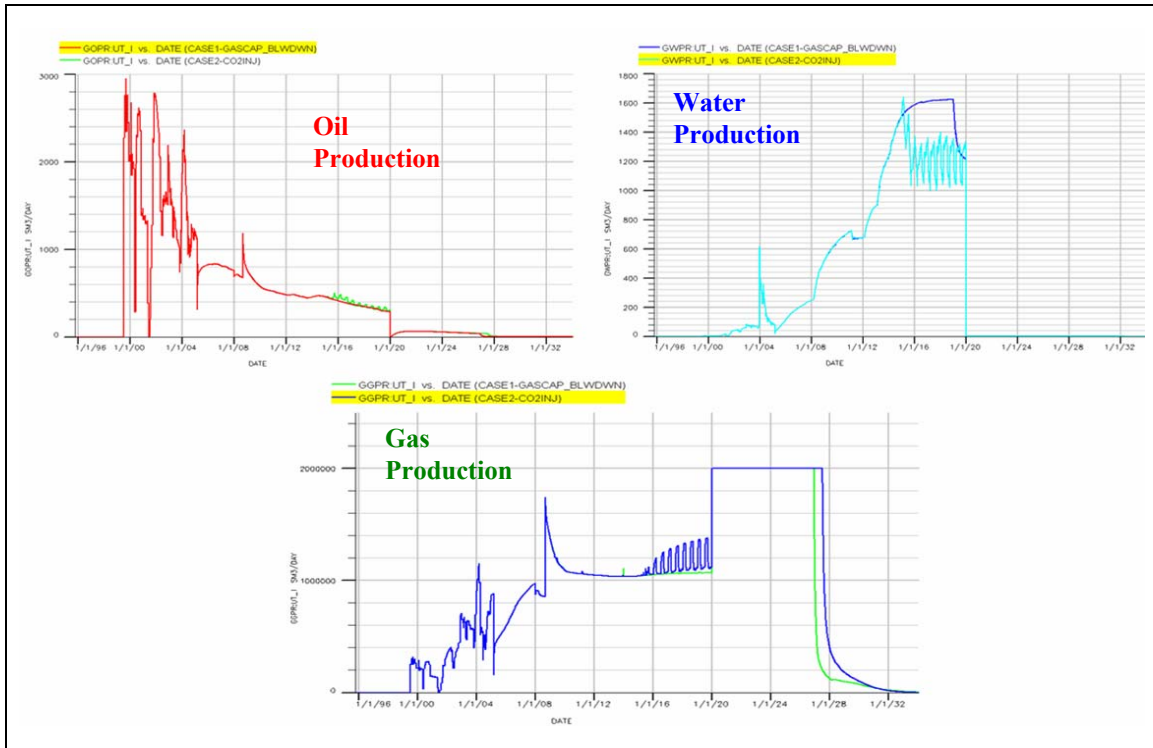
Figure 51: The Comparison Compositional Simulation Result (for Fluid Production) between Gas Blow Down Case (Without CO₂ Injection) and Gas Blow Down Case (With CO₂ Injection) at I Segment Heidrun Field
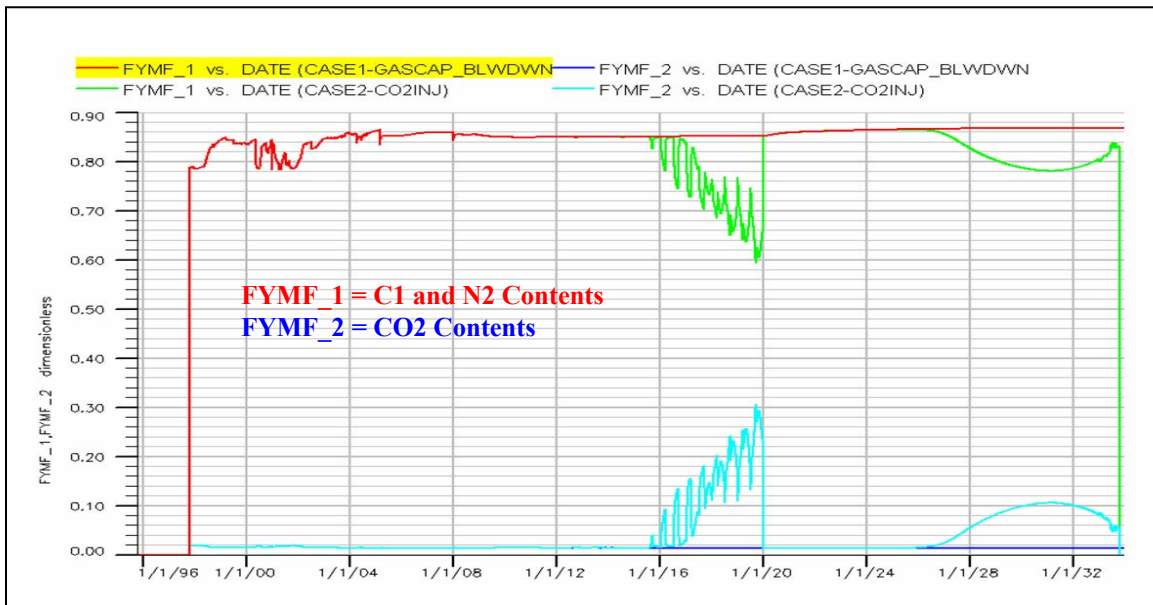
Figure 52: The Comparison Compositional Simulation Result (for CO₂ contents) between Gas Blow Down Case (Without CO₂ Injection) and Gas Blow Down Case (With CO₂ Injection) at H and I Segment Heidrun Field
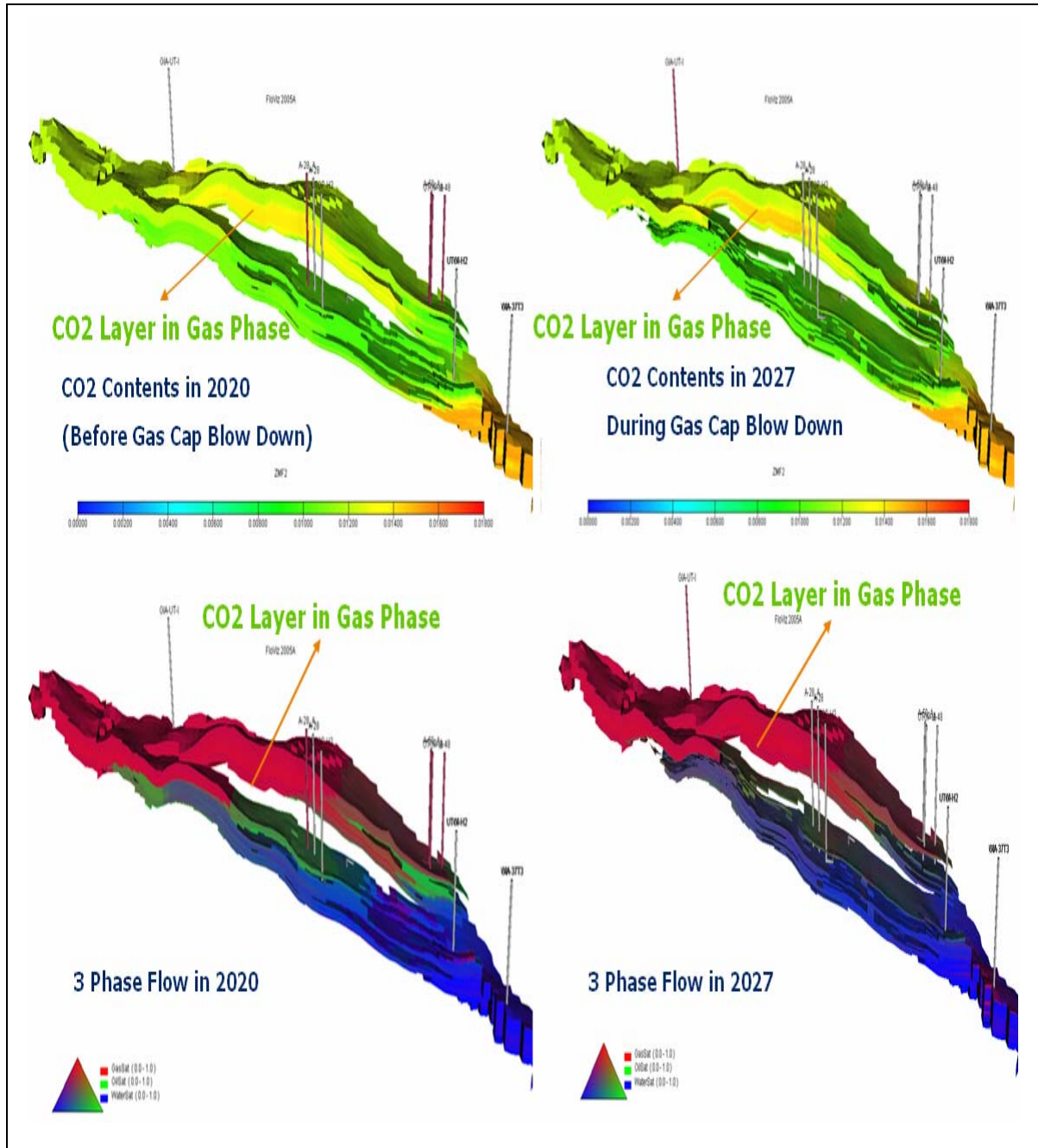
Figure 53: The Visualization of CO₂ contents and 3 Phase Flow during Gas Blow-down Period Case (Without CO₂ Injection)
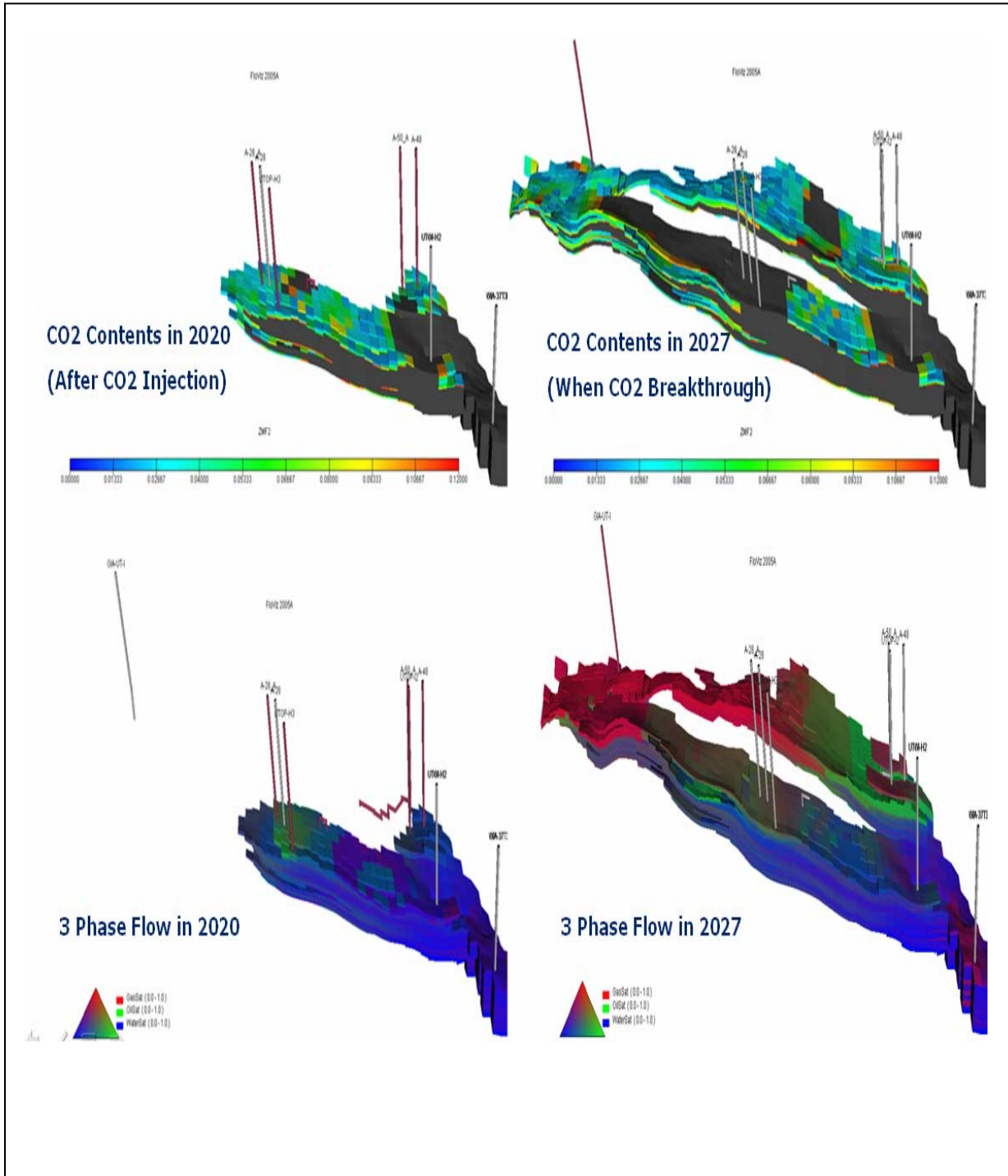
Figure 54: The Visualization of CO₂ contents and 3 Phase Flow during Gas Blow Down Period Case (With CO₂ Injection)
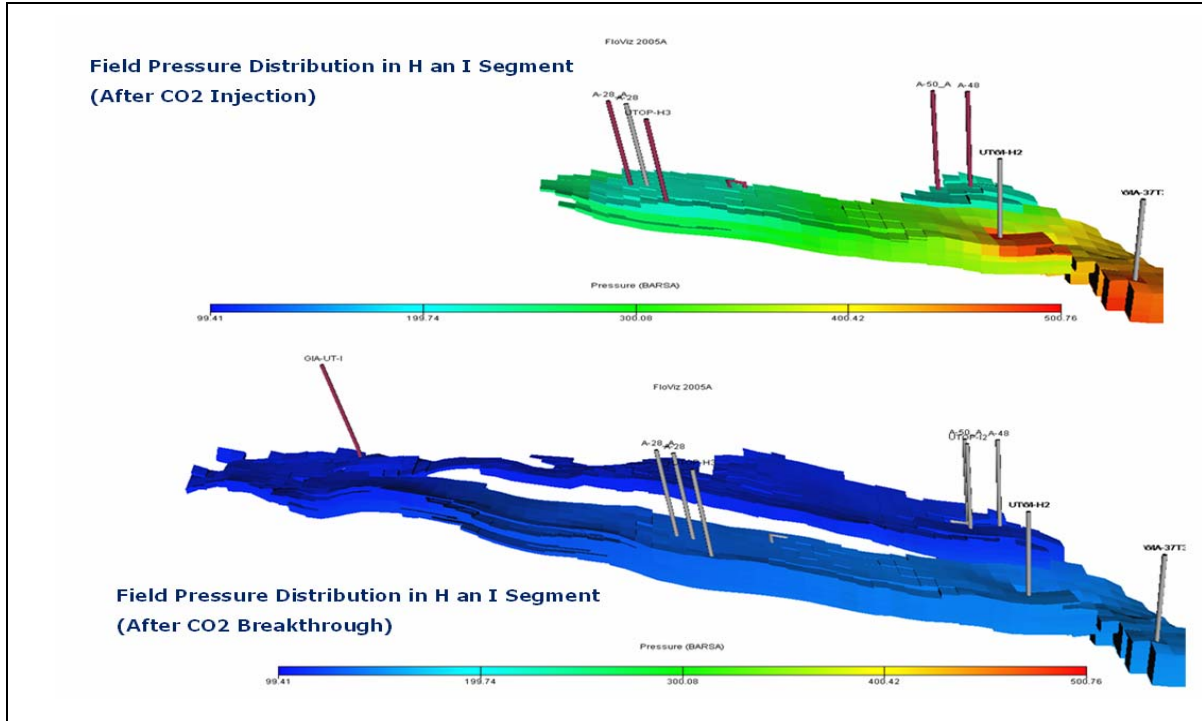
Figure 55: The Visualization of Field Pressure Distribution after CO₂ Injection and after CO₂ Breakthrough at H and I Segment Heidrun Model
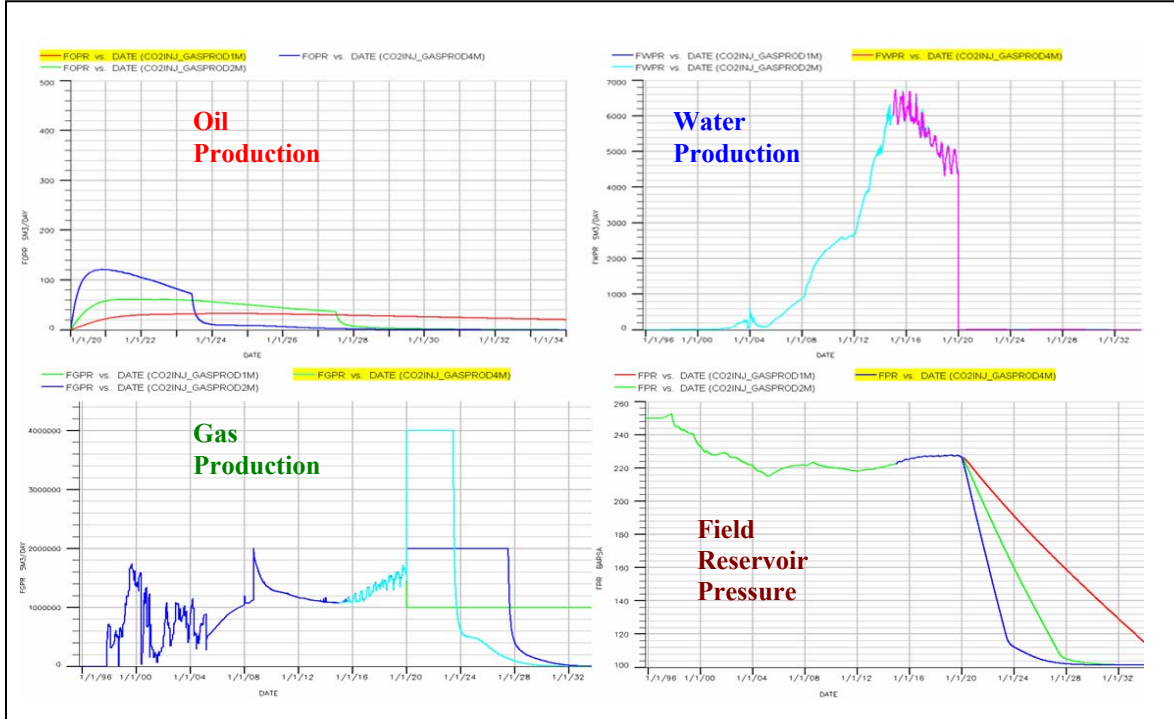
Figure 56: The Comparison Compositional Simulation Result in Field Production for Sensitivity Study CO₂ Injection to Gas Production Rate
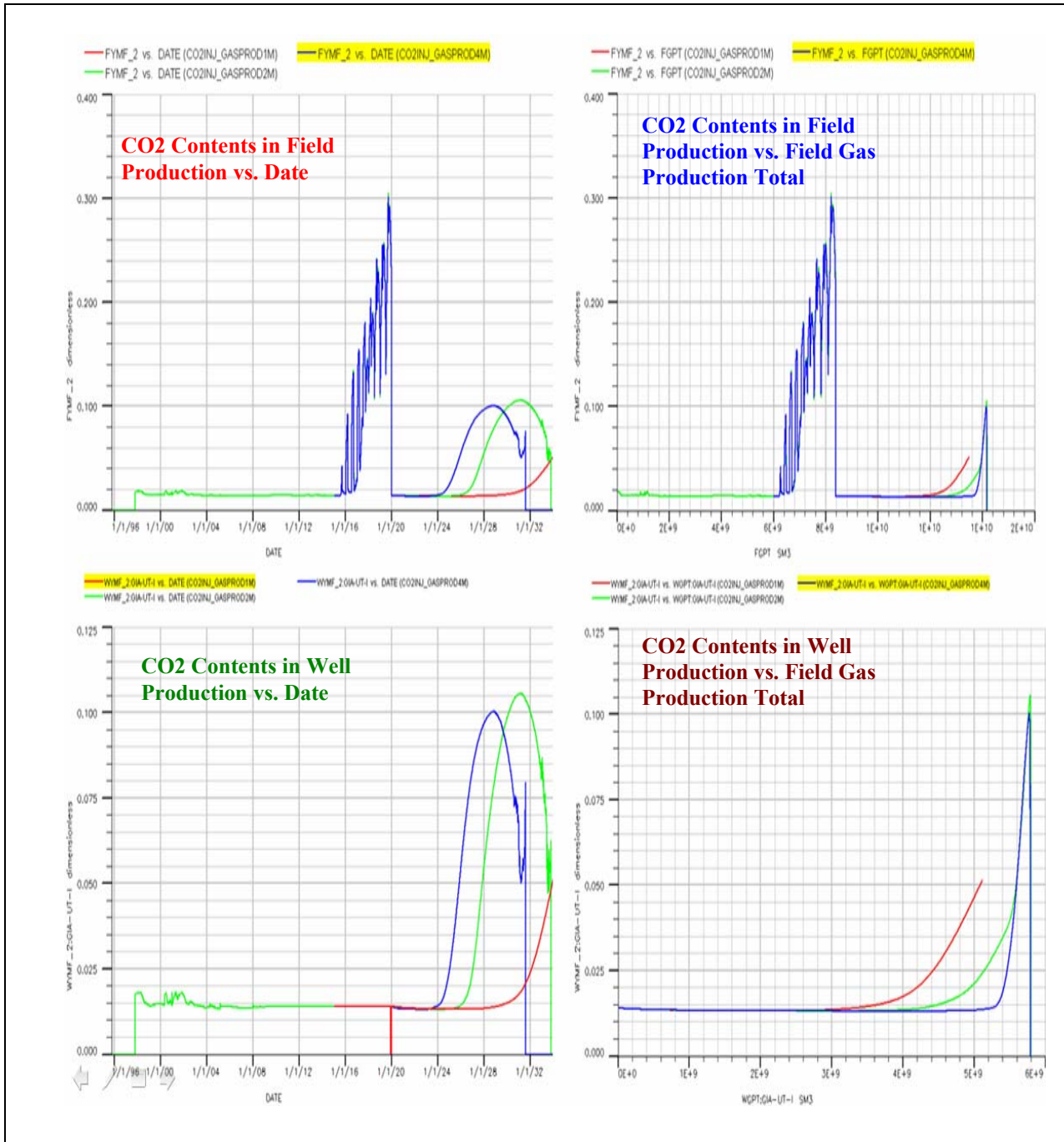
Figure 57: The Comparison Compositional Simulation Result in CO₂ Contents for Sensitivity Study CO₂ Injection to Gas Production Rate
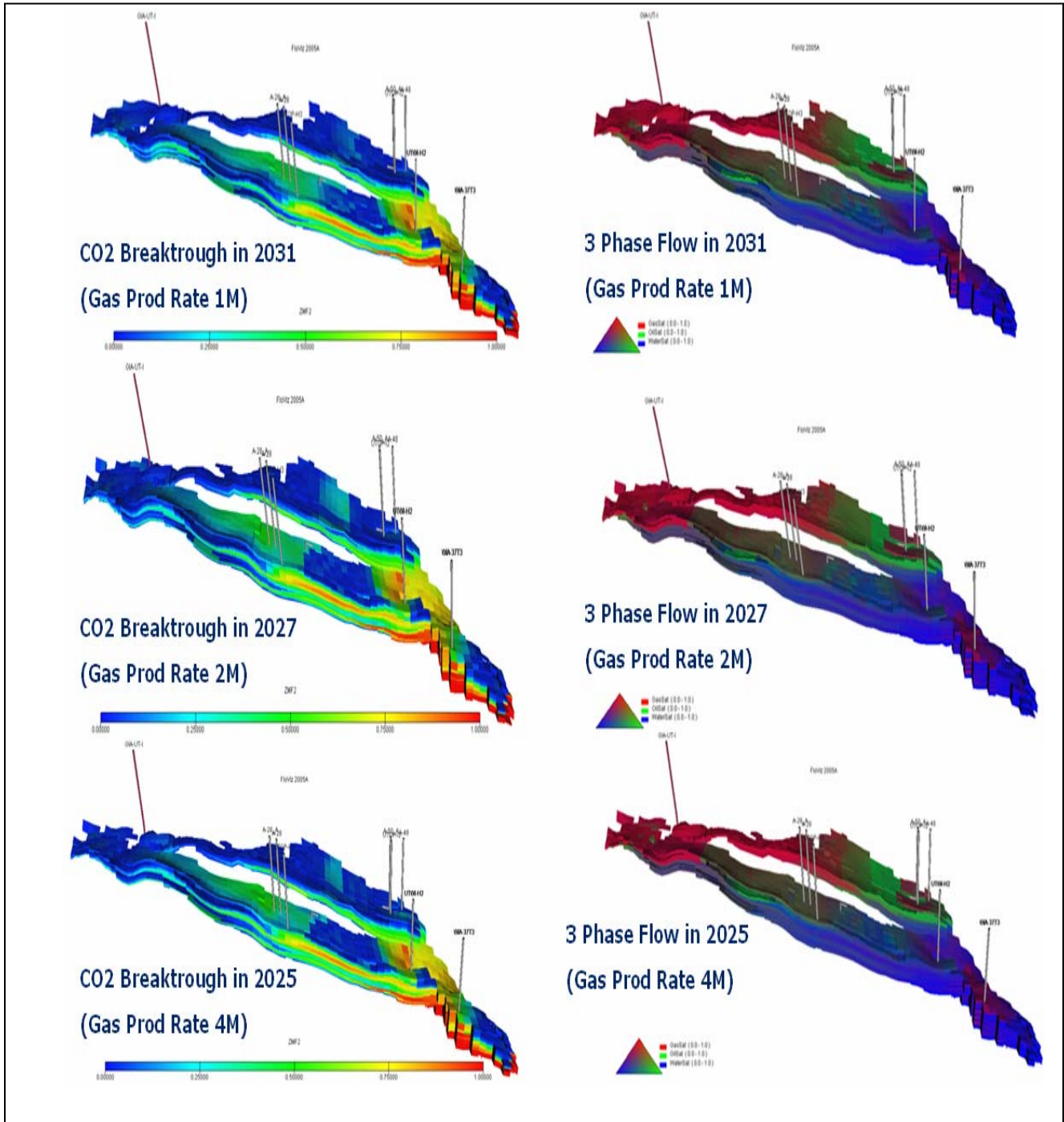
Figure 58: The Visualization of CO_2 contents and 3 Phase Flow in Sensitivity Study CO_2 Injection to Gas Production Rate
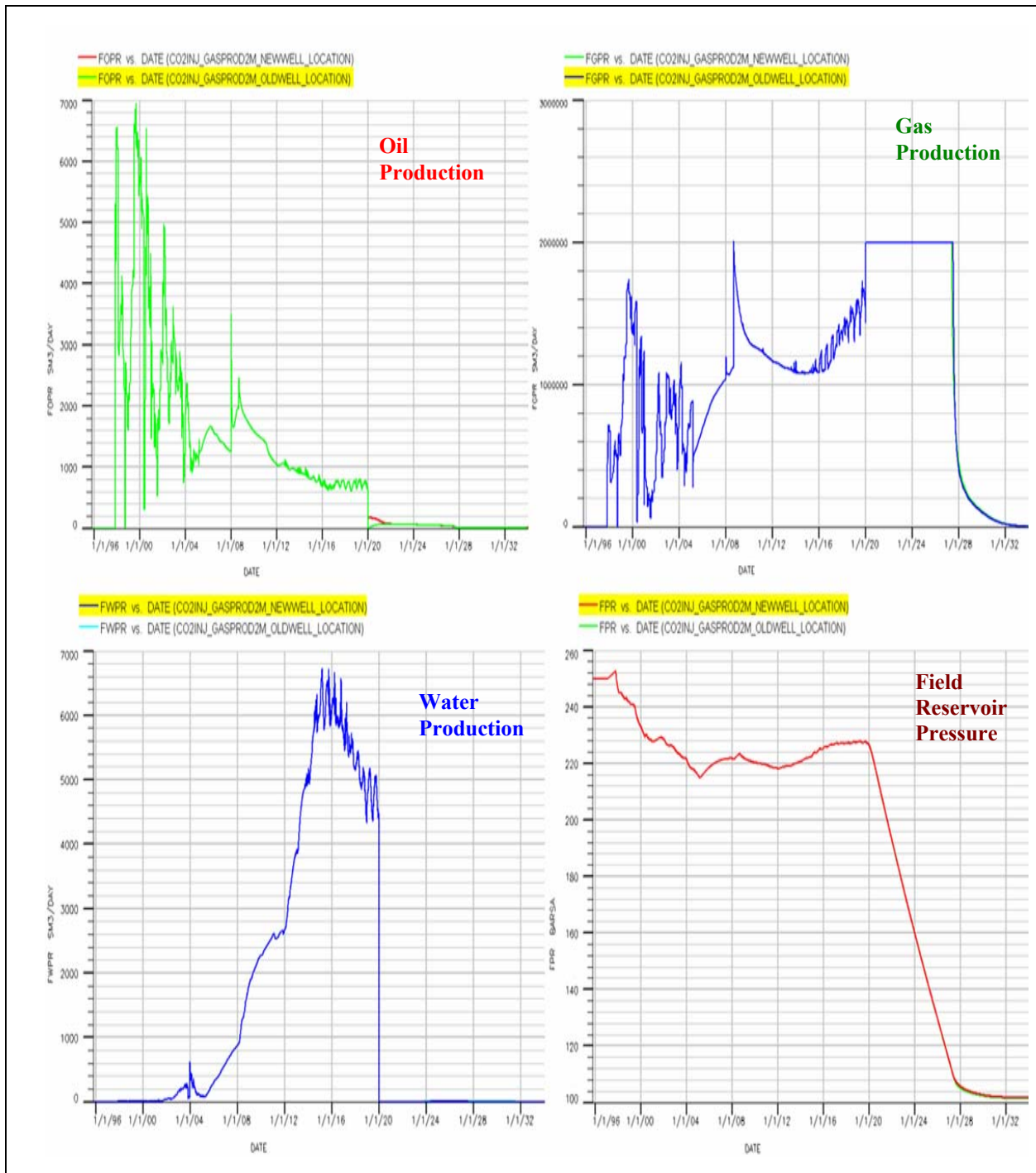
Figure 59: The Comparison Compositional Simulation Result in Field Production for Sensitivity Study CO₂ Injection to Gas Producer Well Location
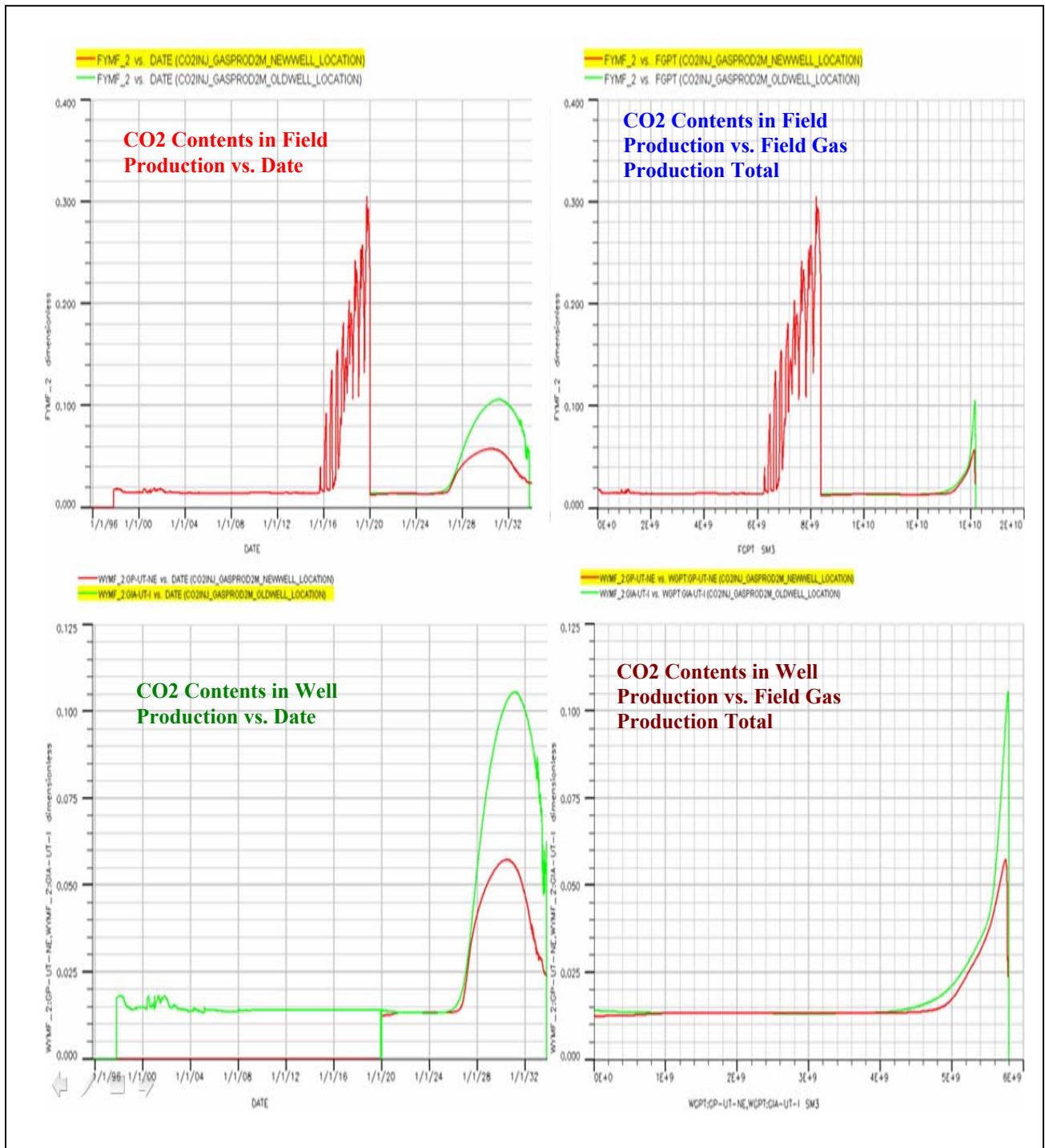
Figure 60: The Comparison Compositional Simulation Result in CO₂ Contents for Sensitivity Study CO₂ Injection to Gas Producer Well Location
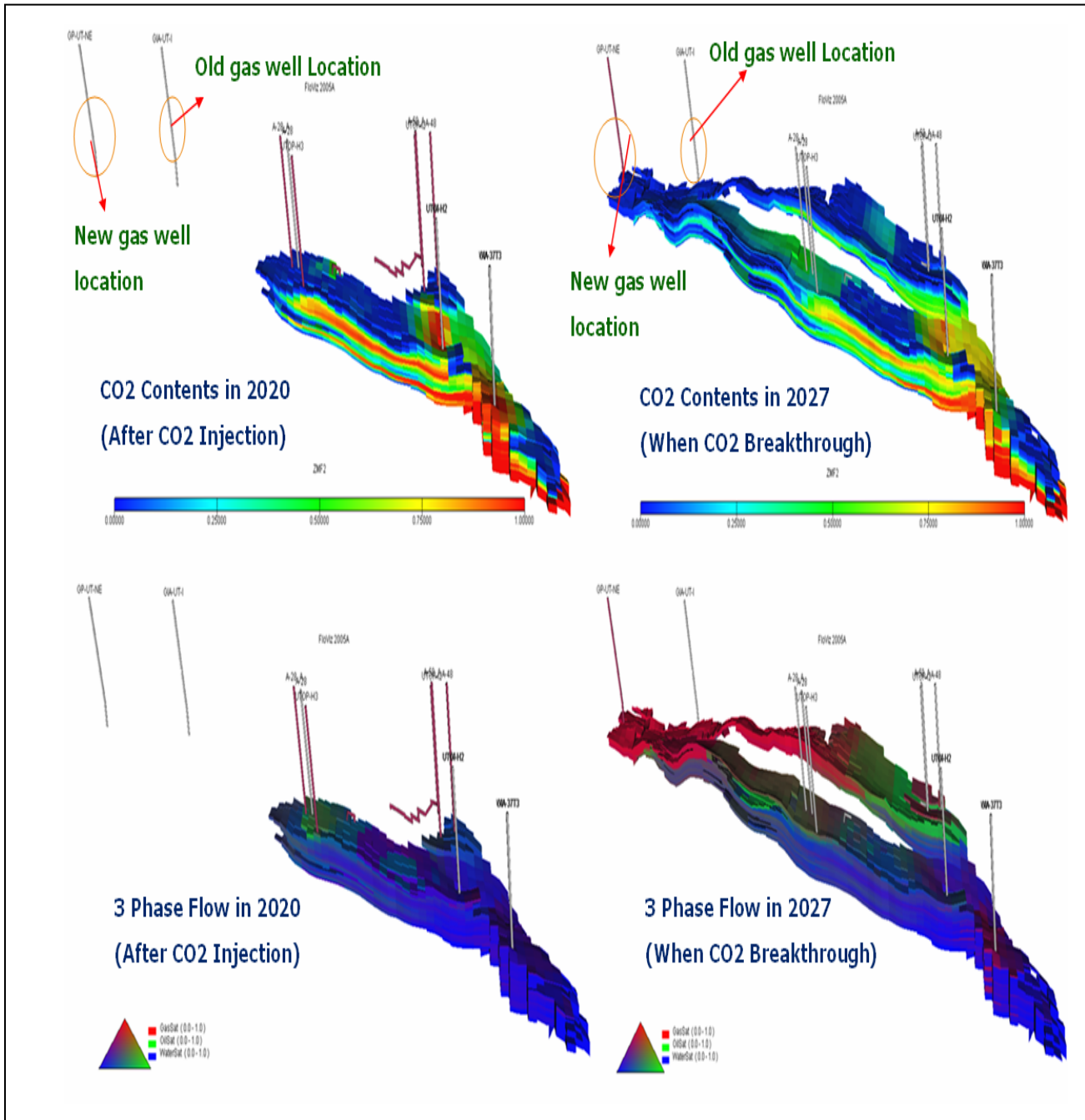
Figure 61: The Visualization of CO₂ contents and 3 Phase Flow in Sensitivity Study CO₂ Injection to Gas Producer Well Location
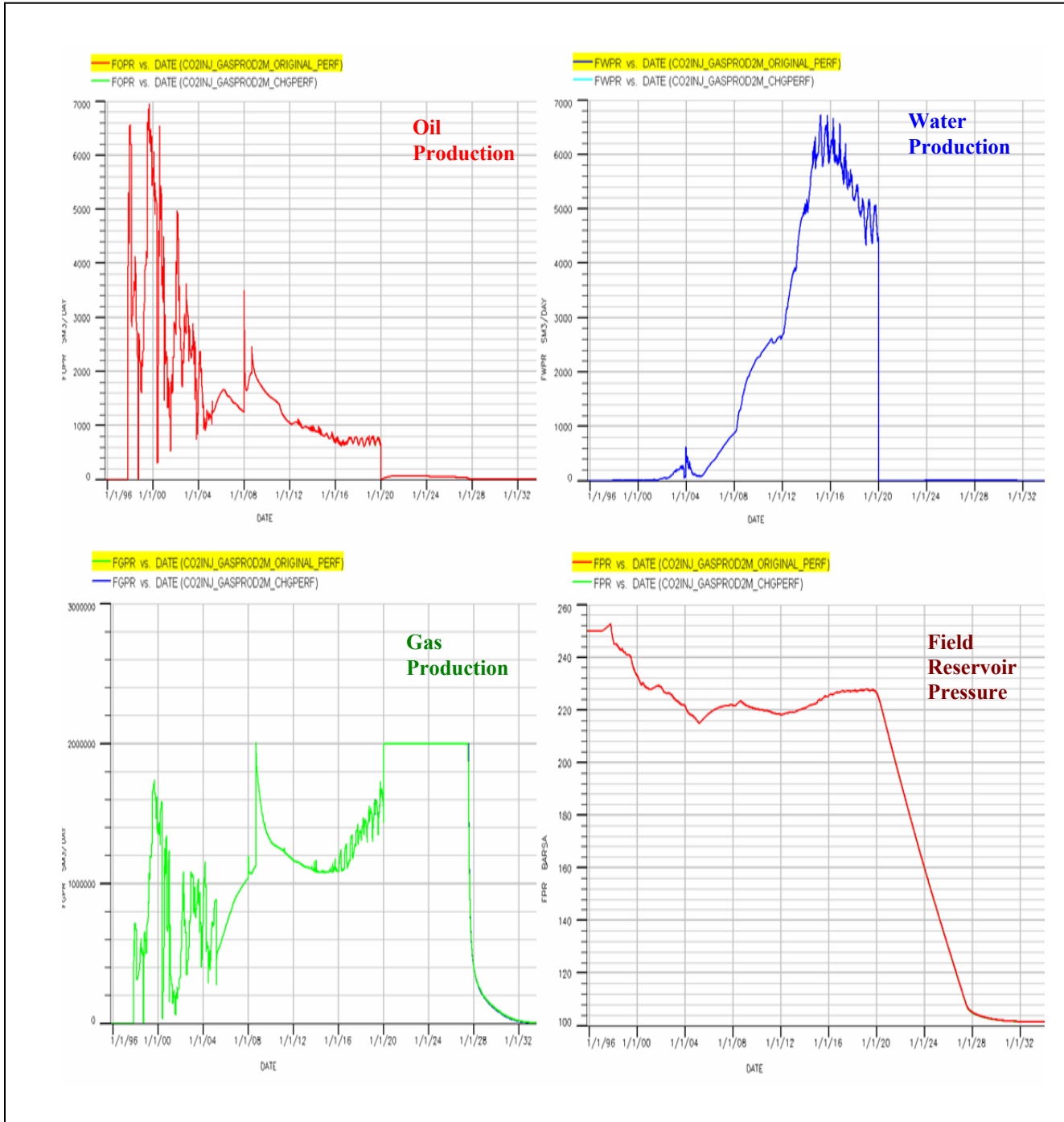
Figure 62: The Comparison Compositional Simulation Result in Field Production for Sensitivity Study CO₂ Injection to Perforation Interval
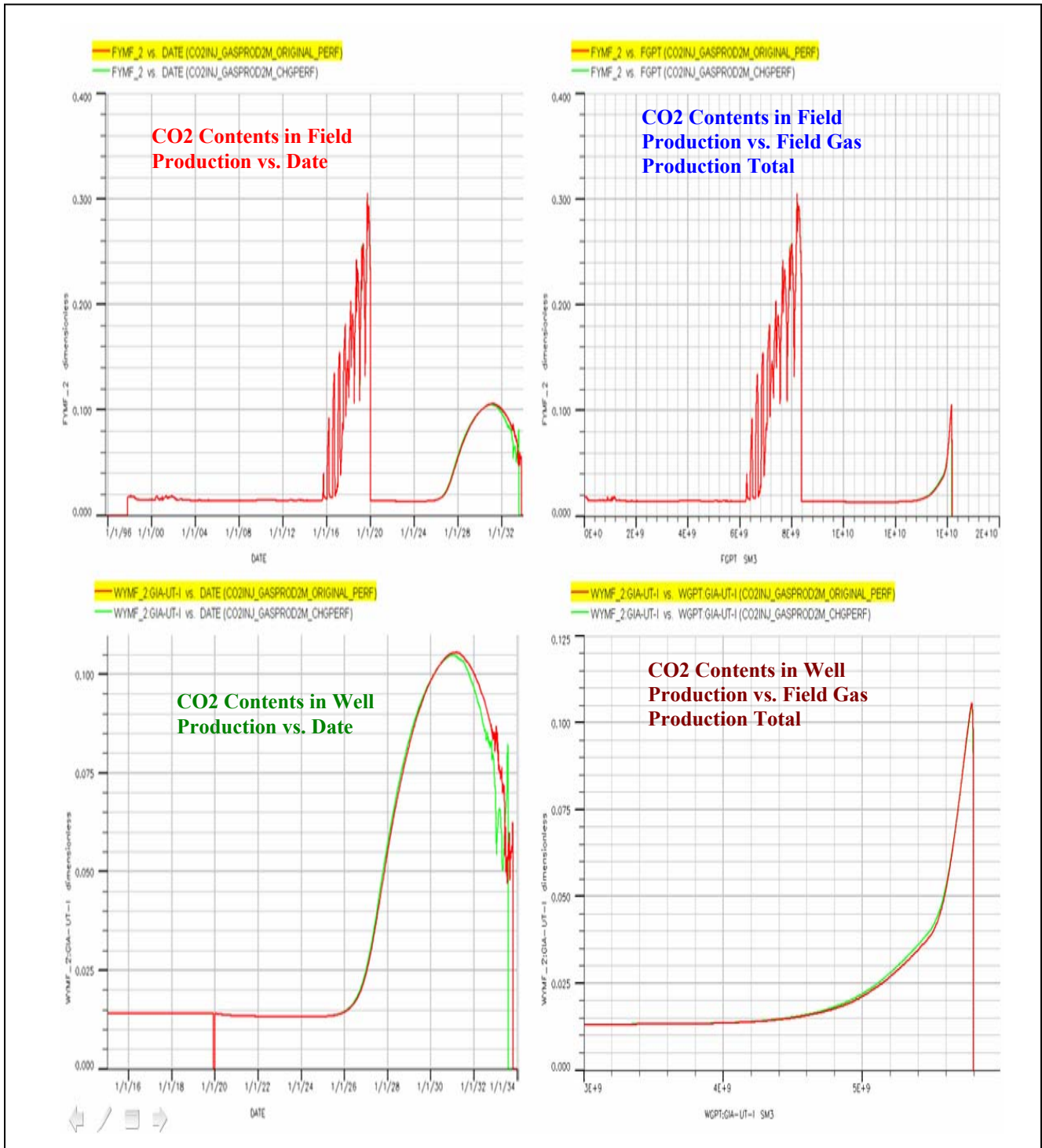
Figure 63: The Comparison Compositional Simulation Result in CO₂ Contents for Sensitivity Study CO₂ Injection to Perforation Interval
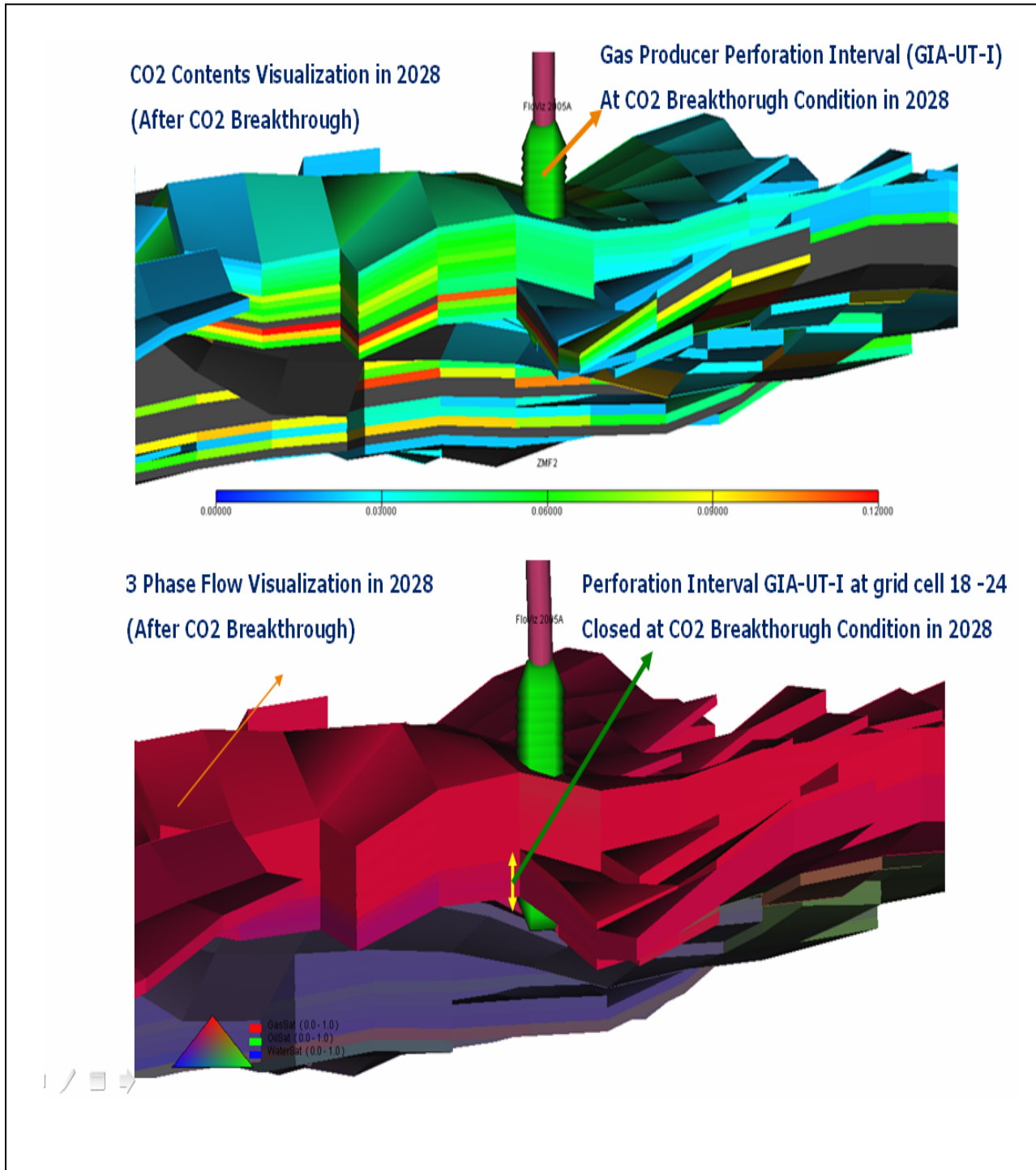
Figure 64: The Visualization of CO₂ contents and 3 Phase Flow in Sensitivity Study CO₂ Injection to Perforation Interval
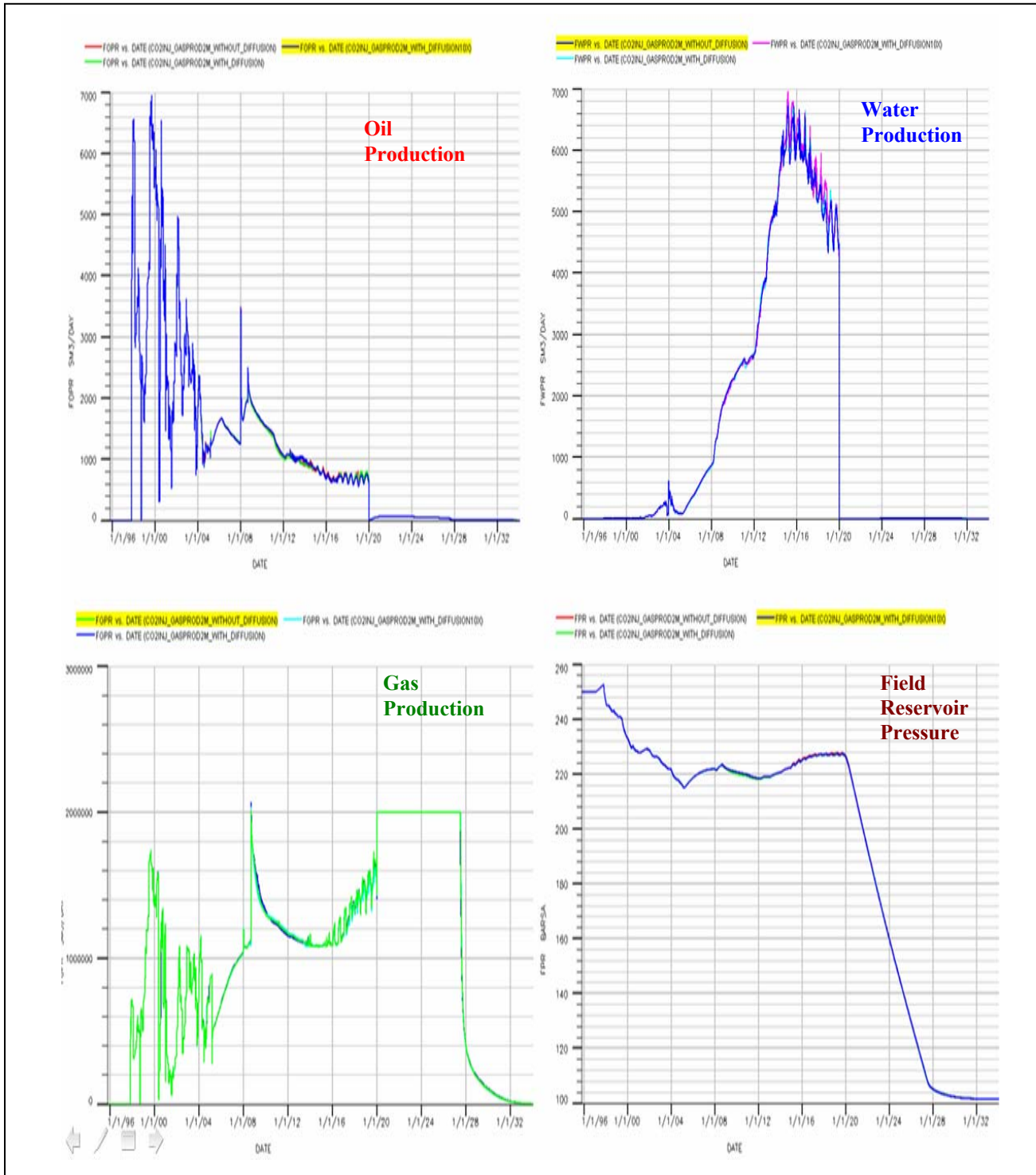
**Figure 65: The Comparison Compositional Simulation Result in Field Production
for Sensitivity Study CO₂ Injection to Diffusion Effect**
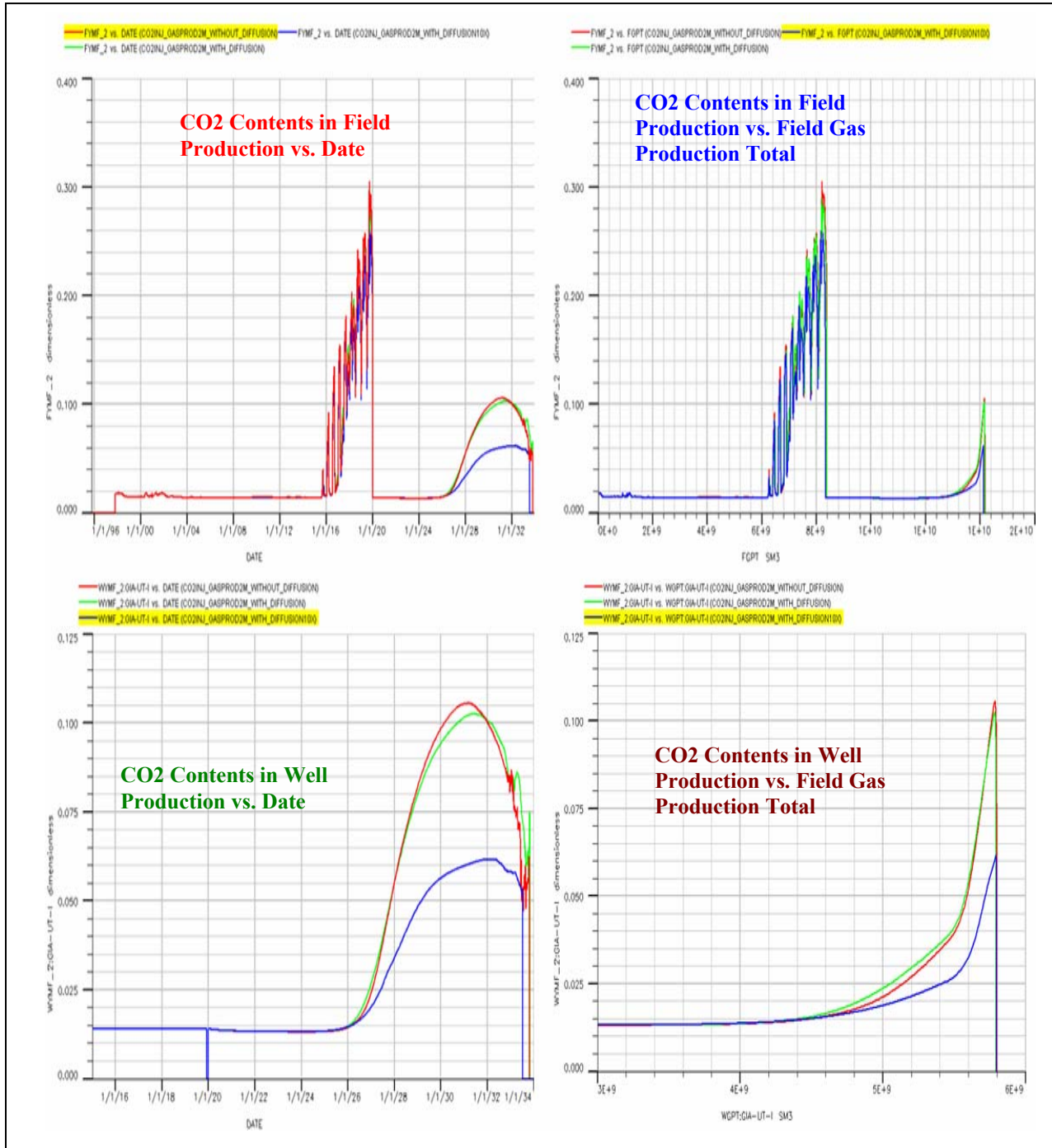
Figure 66: The Comparison Compositional Simulation Result in CO₂ Contents for Sensitivity Study CO₂ Injection to Diffusion Effect
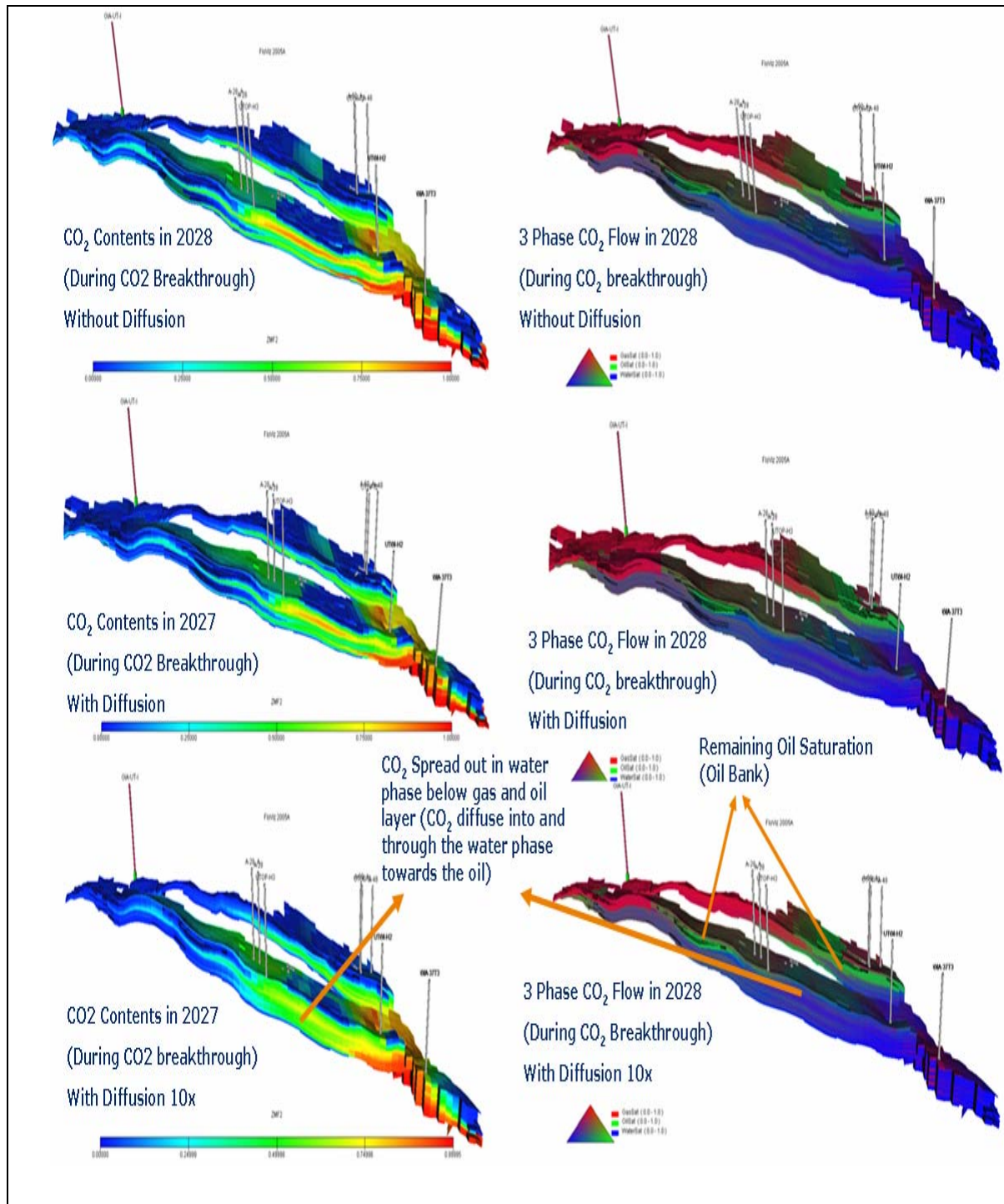
Figure 67: The Visualization of CO₂ contents and 3 Phase Flow in Sensitivity Study CO₂ Injection to Diffusion Effect

APPENDIX B

Example Eclipse 300 Compositional Program for CO₂ Injection with Gas Production Rate=4 M Sm³/day during gas Blow Down Period

```
-- This Heidrun Base Case Simulation was modified by Zein 2006-04-07:

--Modifications:
-- Change Critical Initial Water Saturation from Water Zone from 0.99
to 0.2, Add block summary
-- Put Additonal keyword to replace WLIFT in E-100 (Add keyword
ACTIONW)
-- Change Tuning, add VECTABLE to get faster performance and create
compostion vs Depth (SOLVD)
-- Disable GECON and GCONPROD, Put Constraint BHP in Producer, Put Max
Injection Rate for Updip Injection
-- PUT WCONPROD as DEFAULT FOR WELL A-28_A and ADD KEYWORD WELOPEN WHEN
WE START PRODUCING WELL A-28_A
-- * Shut all connections of the WAG injector GIA-37T3 in periods where
the twin injector is injecting water and vice versa.
--*Turn off debugging information from non-linear solver (argument 8 in
DEBUG3)
-- CHANGE BHP CONSTRAINT in PRODUCER WELL PREDICTION PART (FROM 100 to
210 BAR)
--ADD WINJMULT KEYWORD to GIVE FRACTURE EFFECT IN INJECTIVITY WELL
INJECTOR
-- BLOWDOWN GAS CAP IN YEAR 2020 FROM NEW INFILL GAS PRODUCER(GIA-UT-
I2) AND Use Restart file (TSTEP 195) to run Pred Case
--ADD ZMF KEYWORD TO KNOW TOTAL COMPONENT MOL FRACTIONS
--ADD KEYWORD NOMIX(NO INTERPOLATION THREE PHASE in RELPERM) AND
NODPCDT (NO MAX RATE CHANGE CAP PRESSURE)
-- HEIDRUN SEGMENT MODEL C-HI UPPER TILJE
-- KRIEGED GEOMODEL 2005
--
--
-- This run will provide an initialization of water saturation through
-- restart from the run Pd_Pc_WI-NOSIM at reportstep 0
-- (this run initialize with primary drainage capillary pressure.
-- The SWCR include file is commented out as well as other endpoints
files
-- Restart report every 3 months
-- MULTPV corrections from geomodel
-- Simulation with hysteresis
-- Simulation with Pc=0

-- *************************************************
RUNSPEC

TITLE
 Upper Tilje segment model 2005, primary network drainage data

-- Data-sjekk om ikke kommentert bort
```

```
--NOSIM

METRIC

START
   1 'OCT' 1995  /

AIM

-- choose parallell processing
--PARALLEL
--4 DISTRIBUTED /
-- 6 DISTRIBUTED /

---- Memory requirements
--MEMORY
-- 2000  /
---- 350  /

-- ++++++++++++
-- Grid options:
-- ++++++++++++

-- DIM
DIMENS
-- NX    NY    NZ
  97  138   27  /

GRIDOPTS
-- multx-?   NRMULT
    'YES'      200 /
--    'YES'     /

SATOPTS
-- HYSTER  SURFTENS  /
HYSTER   /

--FAULTDIM
--500 /
--  10000 /


-- No LGRs - No grid coarsening
--LGR
-- MAXLGR MAXCLS MCOARS MAMALG MXLALG LSTACK
--     8      0   21023      0      0     10     'NOINTERP' /


-- +++++++++++++++++
-- Misc. dimensions:
-- +++++++++++++++++

REGDIMS
-- NTFIP NMFIPR NRFREG NTFREG
    141     1      0     200  /
```

```
TABDIMS
-- NTSFUN NTPVT NSSFUN NPPVT NTFIP NRPVT
     44     8    300     30    141   208  /


-- ++++++++++++++
-- In/Out options:
-- ++++++++++++++

UNIFIN
UNIFOUT

SAVE
/

-- +++++++++++++++++++
-- PVT modeling options:
-- +++++++++++++++++++

COMPS
23 /

GAS
OIL
WATER

--API
--DISGAS

-- +++++++++++++++++++++++
-- Tracer modeling options:
-- +++++++++++++++++++++++

-- 1 water tracer:
--TRACERS
-- NOTRAC NWTRAC NGTRAC NETRAC Diff/NODiff
--   0      1      0      0      'NODIFF'  /

-- +++++++++++++++++++++++
-- Relperm modeling options:
-- +++++++++++++++++++++++

ENDSCALE
--                 NTENDP NSENDP
 'NODIR' 'REVERS'    1      20  /



-- +++++++++++++++++++++++
-- Aquifer modeling options:
-- +++++++++++++++++++++++

AQUDIMS
-- MXNAQN MXNAQC NIFTBL NRIFTB NANAQU NCAMAX
     35    500     0      0      0      0   /
```

```
-- +++++++++++++++++++++
-- Equilibration options:
-- +++++++++++++++++++++

EQLDIMS
-- NTEQUL NDPRVD NDRXVD NTTRVD NSTRVD
     43    100    20     1      20   /

EQLOPTS
 'QUIESC' /


-- +++++++++++++++++++++
-- Well modeling options:
-- +++++++++++++++++++++

WELLDIMS
-- NWMAXZ NCWMAX NGMAXZ NWGMAX
    150    60     50     20   /

-- VFP tables:

VFPPDIMS
-- MXMFLO MXMTHP MXMWFR MXMGFR MXMALQ NMMVFT
    14     7      6      8      7      55   /

-- Wellbore friction:

--FRICTION
-- NWFRIC  NWFRIB
--     3        1   /

-- PI changes vs WCT:

--PIMTDIMS
--NTPIMT  NPPIMT
--1         6     /

-- Scale deposition:

SCDPDIMS
-- NTSCDP NPSCDP NTSCDA NPSCDA
     1      9      1      5   /

-- Actions:

ACTDIMS
-- #actions #lines(50) #characters(80)
--     4  50    80  /
     10  50    132 /

-- +++++++++++++++++++++
-- Options for numerics:
-- +++++++++++++++++++++
```

```
NSTACK
  35 /

OPTIONS3
 32* 1 /

--DEBUG3
--7* 1 /

VECTABLE
2000 /



HWELLS
-- No interpolation of relative permeabilities near "critical points".
NOMIX
-- No limit on the rate of change in capillary pressure
NODPCDT
--NPROCX
--4 /

-- PSPLITX
--  30 59 /
--  20 40 59 /
--  15 30 45 59 /
-- /

--
**********************************************************************
*****
GRID
--
**********************************************************************
*****

-- +++++++
-- In/Out
-- +++++++

EXTRAPMS
  0    / Warnings dersom PVT ekstrapoleres

MESSAGES
--Warning Problem Error     Warning Problem Error
-- 2* 10000000   10000     100   3* 10000000   10000     10 /
 2* 10000000   10000     100   3* 10000000   10000     100  /

INIT

GRIDFILE
 0 1 /
```

```
-- +++++++++++++++++++++++++++++++++
-- Grid and properties from geomodel:
--
--   Includes fixes where simgrid
--   doesn't represent geomodel well
--   and fixes of errors in geomodel
--   Some fixes go in the EDIT section
---+++++++++++++++++++++++++++++++++

NOECHO

--Grid geometry:

INCLUDE
 '../../include/grid/UT_Fine_Model.grdecl' /

-- Inactivation of any kind is contained in this file:
-- 1) eroded blocks
-- 2) tower blocks at "reverse" faults
-- 3) false volumes east of the fault HeidrunEast
-- 4) Kritt in FGH
-- 5) strange blocks along edges
-- 6) X - N South connection
-- 7) Remove 10 deepest layers (AARe 1.10 and below) and Viking
-- 8) Restore 10 deepest layers of Aare 1 in Segments K and MS
-- 9) Area outside segments C-I

INCLUDE
 '../../include/grid/actnum_UT.inc' /

RPTGRID
 ALLNNC PART /

--Grid geometry fixes:

--"Repair" the ramp near A-48:

--INCLUDE
-- '../../include/grid/ramp-a-48_UT.nnc' /

--"Repair" poorly represented corner north in EFG area:

INCLUDE
 '../../include/grid/ef-g_UT.nnc' /

-- ++++++++++++++

--Porosity:

INCLUDE
 '../../include/grid_prop/krieged/poro_UT.inc' /

--Permeablity:

INCLUDE
```

```
 '../../include/grid_prop/krieged/perm_UT.inc' /

-- Ny PERMZ etter HM, oensker lavere KVKH, se HM logg paa g-disk
INCLUDE
 '../../include/grid_prop/krieged/permz.inc' /


-- +++++++++++++++++
-- NO Permeability fixes beacuse of new property model
-- +++++++++++++++++


-- +++++++++++++++++++++++++++++++
-- Pinchouts and small gridblocks:
-- +++++++++++++++++++++++++++++++

MINPV
 400 /

-- Generate pinch out connections using the properties of the removed
cells:
PINCH
0.1 'GAP' 1* /



-- +++++++++
-- Barriers:
-- +++++++++
-- Justert ifm HM, se sim logg for details, Robert 19.05.05
EQUALS
'MULTZ' 0.005   1 97 1 138   11  11    / T.3.3 -> T.3.2
'MULTZ' 0.005   1 97 1 138   16  16    / T.3.2.3 -> T.3.2.2
'MULTZ' 0.001   1 97 1 138   20  20    / T.3.2.2 -> T.3.2.1
/

--
+++++++++++++++++++++++++++++++++++++++++++++++++++++++++++++++++++++++++
+++
-- Include MULTZ=0 to close off vertical connections across staircase
faults:
--
+++++++++++++++++++++++++++++++++++++++++++++++++++++++++++++++++++++++++
+++

INCLUDE
 '../../include/grid_prop/krieged/multz_UT_FF03_conv.grdecl' /

-- +++++++++
-- Aquifer:
-- +++++++++

INCLUDE
 '../../include/grid/aquifer_UT.inc' /


-- +++++++++++++++++++
-- Various HM changes:
```

```
-- +++++++++++++++++++


--****
-- Defining faults in D and E segment to introduce transm. multipliers.
ebak
INCLUDE
 '../../include/grid/de_UT.faults' /

--INCLUDE
-- '../../include/grid/multpv-oilandgas_UT.inc' /

INCLUDE
 '../../include/grid_prop/krieged/multnum_UT.inc' /

INCLUDE
 '../../Zein/include/grid/EQLNUM13_14_43.MULTPV' /

--
************************************************************************
******
EDIT
--
************************************************************************
******

--NOWARN

-- Include Havana generated EDITNNC's for fault seal:

INCLUDE
 '../../include/grid_prop/krieged/faultseal_1_2_UT.inc' /

INCLUDE
 '../../include/grid_prop/krieged/faultseal_if_UT.inc' /

--WARN

-- +++++++++++++++++++
-- Various HM changes:
-- +++++++++++++++++++

--    Close off to the south of C-4H (ebak)

EQUALS
 'TRANY'  0.    30 97 129 129 1 27 /
/


--****
-- Multiplying faults defined by FAULT for HM of A-52 (and D
producers).
-- further studies are neede. EBAK
--MULTFLT
-- 'DE_NORTH' 0.1 /
```

```
-- 'DE_SOUTH' 0.1 /
-- 'E_XS1' 0.1 /
-- 'D_W1' 0.1 / Stenger litt for aa forhindre at vannet stikker rett
opp til A-35
-- 'D_NORTH_W1' 0.1 / Stenger litt for aa forhindre at vannet stikker
rett opp til A-35
-- 'D_XS6' 0.1 / Stenger litt for aa forhindre at vannet stikker rett
opp til A-35
-- 'D_NORTH_W3' 10. / Aapner for aa faa mer vann til A-50
--/

--
-- ++++++++++
-- UT hist.match 18.5.05, RF: stenger komm. mellom FIPNUM 60 (A-37
omraadet) og 43-44 (UT-EF)
-- ++++++++++'


MULTREGT
43 60 0.0 /
44 60 0.0 /
/




--
-- ++++++++++
-- Grid fixes:
-- ++++++++++'

-- Fjerne kontaktpunkt ost-vest C-E og legge til kontaktpunkt nord-soer
C-E  -dk
-- NB !! dette er egentlig ikke noe HM punkt
--       Disse justeringene fjernes naar vi har
--       en riktigere representasjon av CDEM krysset
--NOWARN
INCLUDE
 '../../include/edit/tilje_ce_hi_UT.inc' /
--WARN

--
*********************************************************************
******
PROPS
--
*********************************************************************
******

TOLCRIT
 1.E-20 /

-- ++++++++++++++++++++++++++++++++++++++
-- Initial and critical water saturations:
-- ++++++++++++++++++++++++++++++++++++++
```

```
INCLUDE
--'../../include/grid_prop/2A_SWAT.inc' /
--'../../include/grid_prop/2A_SWAT-E300.inc' /
'../include/grid/SWCR_2AQUIFER.GRDECL' /

MAXVALUE
 'SWCR' 0.60 1  97 1 138  1  27 / Alle
/

-- ++++++++++++++++
-- Other endpoints:
-- ++++++++++++++++

COPY
 'SWCR'  'SWL'  /
 'SWCR' 'SGU' /
/

MULTIPLY
    'SGU'  -1      /
/
ADD
    'SGU'   1      /
/

COPY
 'SWCR'  'ISWCR' /
 'SWCR' 'ISWL' /
 'SGU' 'ISGU' /
/

-- +++++++++
-- Relperm:
-- +++++++++

EHYSTR
-- 1*  4  2*  BOTH  NEW  DRAIN  OIL  /
  1*  4  2*  BOTH  NEW  BOTH  OIL  /

INCLUDE
 '../../include/relperm/Tilje_pSw_h_Pc=0.swof'  /

INCLUDE
 '../../include/relperm/Tilje_network_h_Pc=0.sgof'  /


-- Gammel relperm
--INCLUDE
-- '../../include/relperm/relperm-base.inc'  /


-- +++++++++
-- PVT:
-- +++++++++
```

```
--APIGROUP
-- 1 /

--NOWARN
INCLUDE
--'../../include/pvt/FF01-API.PVT'  /
--'../../include/pvt/FF01-API_E300BO_ZW.PVT'  /
--'../../include/pvt/PVT3.NC23'  /
'../include/PVT3-UT14_15.NC23'  /
--WARN


-- +++++++++
-- Tracers:
-- +++++++++

TRACER
 'SW' 'WAT' /
/

RPTPROPS
  PCG  PCW  /
/

KVTABLE
-- P    C1N2      CO2       C2 ... osv
  1.0  4.32E+02  6.53E+01 1.88E+01 3.46E+00 1.00E+00 3.11E-01 8.82E-02
2.37E-02 2.97E-03 14*1.62E-05/1
  1.0  4.32E+02  6.53E+01 1.88E+01 3.46E+00 1.00E+00 3.11E-01 8.82E-02
2.37E-02 2.97E-03 14*1.62E-05/2
  1.0  4.32E+02  6.53E+01 1.88E+01 3.46E+00 1.00E+00 3.11E-01 8.82E-02
2.37E-02 2.97E-03 14*1.62E-05/3
  1.0  4.32E+02  6.53E+01 1.88E+01 3.46E+00 1.00E+00 3.11E-01 8.82E-02
2.37E-02 2.97E-03 14*1.62E-05/4
  1.0  4.32E+02  6.53E+01 1.88E+01 3.46E+00 1.00E+00 3.11E-01 8.82E-02
2.37E-02 2.97E-03 14*1.62E-05/5
  1.0  4.32E+02  6.53E+01 1.88E+01 3.46E+00 1.00E+00 3.11E-01 8.82E-02
2.37E-02 2.97E-03 14*1.62E-05/6
  1.0  4.32E+02  6.53E+01 1.88E+01 3.46E+00 1.00E+00 3.11E-01 8.82E-02
2.37E-02 2.97E-03 14*1.62E-05/7
  1.0  4.32E+02  6.53E+01 1.88E+01 3.46E+00 1.00E+00 3.11E-01 8.82E-02
2.37E-02 2.97E-03 14*1.62E-05/8

--
************************************************************************
******
REGIONS
--
************************************************************************
******
INCLUDE
 '../../include/grid_prop/krieged/satnum_UT_hyster.inc' /

INCLUDE
```

```
  '../../include/grid_prop/krieged/imbnum_UT.inc' /

-- Gammel relperm
--INCLUDE
-- '../../include/grid_prop/krieged/satnum_UT.inc' /

INCLUDE
 '../../include/grid_prop/krieged/eqlnum_UT.inc' /

INCLUDE
 '../../include/grid_prop/krieged/fipnum_UT.inc' /


--
++++++++++++++++++++++++++++++++++++++++++++++++++++++++++++++++++++++++++
+++
-- Aquifer:
--
++++++++++++++++++++++++++++++++++++++++++++++++++++++++++++++++++++++++++
+++

EQUALS
 'SATNUM' 1    1 3 138 138 1 27 /
 'EQLNUM' 43   1 3 138 138 1 27 /
 'FIPNUM' 141 1 3 138 138 1 27 /
/

--
*************************************************************************
******
SOLUTION
--
*************************************************************************
******

RPTRST
-- PRES   PCOG  PCOW  /
 'BASIC=4' SWAT SOIL SGAS RS ZMF /

-- Contacts, and API and RS vs. depth:


INCLUDE
--'../../include/equil/equil-base.inc'      /
'../../include/equil/equil-base-e300bo-entire-ut.inc' /

-- Treshold pressures:
--INCLUDE
--'../../include/equil/thpres.inc'  /

--INCLUDE
--  '../../include/equil/real_01/explicit_thpres.inc'  /

RESTART
-- '../2B_Pd_Imb_Pc_WAG/2B_Pd_Imb_Pc_WAG_2-NOSIM' 0 /
```

```
-- '../2B_Pd_Imb_Pc_WI/2B_Pd_Imb_Pc_WI' 0 /
'2C_PD_PC0_FIPNUM-14-15-43_CUTINJ50_E300COMP_PREDBLWDWN_CO2INJREV' 195
/

-- Initial tracer concentration:
-- DIM
TBLKFSW
 361422*0 /

-- ++++++++
-- In/Out:
-- ++++++++

RPTSOL
 'FIP=2' 'RESTART=2' 'FIPRESV' 'SOLVD' 'PSAT' 'PART' /

-- RPTRST
--  'BASIC=5 ' 'FREQ=6' / Skriver ut restartdata hver 3. mnd.
-- -- 'BASIC=4' 'FREQ=1'/ Skriver ut restartdata hvert aar.

FIELDSEP
  1 4* 1 / K-values
/

--
**********************************************************************
******
SUMMARY
--
**********************************************************************
******

INCLUDE
 '../../include/summary/basic-e300comp-ZW_UT.summary' /

INCLUDE
 '../include/summary/block.summary' /


--
**********************************************************************
******
SCHEDULE
--
**********************************************************************
******
SKIPREST

-- ++++++++
-- PVT:
-- ++++++++

--DRSDT
--0.0  /
```

```
GINJGAS
 FIELD GV FIELD /
/
-- ++++++++
-- In/Out:
-- ++++++++

RPTSCHED
--   'FIP=2' 'NEWTON=2' 'WELSPECS' 'FIPRESV' 'WELLS=2' /
    'FIP=2' 'WELSPECS' 'FIPRESV' 'WELLS=2' /

--RPTRST
--   'BASIC=5' 'FREQ=6' /

-- +++++++++
-- Numerics:
-- +++++++++


-- Tuning justert ifm aa faa HYSTERESE kjoeringer til aa gaa
--
TUNING
--  TSINIT TSMAXZ TSMINZ TSMCHP TSFMAX TSFMIN TSFCNV TFDIFF THRUPT
TMAXWC
--def 1.0  365.0   0.1   0.15    3.0   0.3    0.1   1.25   1E20
N/A
--     1.0   10.0    4*                         0.3   1.5    2*   /
--     1.0   30.0    0.1   0.15    3.0   0.5    0.5   1.2      2*   /
     1.0   5.0    0.1   0.15    1.1   0.5    0.5   1.2      2*   /
--  TRGTTE TRGCNV TRGMBE TRGLCV XXXTTE XXXCNV XXXMBE XXXLCV XXXWFL
TRGFIP TRGSFT
--def 0.1   1E-3   1E-7   1E-4   10.0   0.01   1E-6   1E-3   1E-3
0.025  0.
--     0.5    0.10   3.0E-7  0.002  10.0   1.0    3E-6   0.01 /
/     0.1   1E-4   3E-7   1E-4   10.0   0.1    3E-6   0.01 /
--  NEWTMX NEWTMN LITMAX LITMIN MXWSIT MXWPIT DDPLIM DDSLIM TRGDPR
XXXDPR
--def 12     1     25     1      8      8      1E6    1E6    1E6
1E6
--     20     1     40     1*     25     5* /
     12     1     40     1*     25     5* /
-- ++++++++++++++
-- Well modelling:
-- ++++++++++++++

INCLUDE
 '../../include/vfp/vfp-2005.inc' /

--SKIPREST
-- +++++++++++++++++++
-- Time dependent data:
-- +++++++++++++++++++


INCLUDE
```

```
--  '../../include/schedule/REFCASE_UT_WI_BHP_CON.SCH' /
--'../../include/schedule/NEW-ZEIN-E300COMP-CUTINJ50.SCH' /
'../../include/schedule/NEW-E300COMP-
CUTINJ50_DEPLPRED_BLOWDWN4M_CO2INJREV.SCH' /


-- Writing time-dependent data to a save file for fast restart:
END
```

APPENDIX C

Heidrun EOS Model in Eclipse 300 format for 23 Components

```
-- 2006-03-10: Insert composition vs. depth for EQLNUM 14 and 15.
-- Assume same oil and gas compositions at the GOC as for EQLNUM=1

-- Generated with PVTsim version 14.0.2 at 01.04.2005 15:48:55
-- Fluid Properties Generated Using PVTsim
-- Number of components:
NCOMPS
23 /
-- Equation of state
EOS
SRK /
-- Reservoir temperature (C)
RTEMP
     85.00 /
-- Standard Conditions (C and bara)
STCOND
   14.99999   1.01325  /
-- Component names
CNAMES
N2-C1
CO2
C2
C3
C4
C5
C6
C7
C8-C9
C10-C11
C12-C13
C14-C15
C16-C17
C18-C19
C20-C21
C22-C23
C24-C25
C26-C29
C30-C33
C34-C38
C39-C44
C45-C54
C55-C80   /
-- Tc (K)
TCRIT
   190.093
   304.200
   305.400
   369.800
```

```
    419.710
    465.531
    507.400
    529.093
    563.131
    610.312
    644.725
    674.177
    700.938
    727.991
    757.897
    780.763
    801.253
    832.272
    871.639
    913.214
    961.694
   1026.940
   1148.000 /
-- Pc (Bar)
PCRIT
    45.9031
    73.7646
    48.8387
    42.4552
    37.5089
    33.7860
    29.6882
    34.1960
    28.6681
    24.8714
    22.4745
    20.9476
    19.5671
    18.1726
    17.0976
    16.4578
    16.0155
    15.4631
    14.9483
    14.5760
    14.2887
    14.0715
    13.9606 /
-- Omega
ACF
    0.00826
    0.22500
    0.09800
    0.15200
    0.18754
    0.24039
    0.29600
    0.45538
    0.51368
```

```
      0.56813
      0.63794
      0.70269
      0.76710
      0.83667
      0.91348
      0.97158
      1.02217
      1.09499
      1.17800
      1.24864
      1.30248
      1.31218
      1.10118 /
-- OmegaA
OMEGAA
      0.42747
      0.42747
      0.42747
      0.42747
      0.42747
      0.42747
      0.42747
      0.42748
      0.42748
      0.42748
      0.42748
      0.42748
      0.42748
      0.42748
      0.42748
      0.42748
      0.42748
      0.42748
      0.42748
      0.42748
      0.42748
      0.42748
      0.42748 /
-- OmegaB
OMEGAB
      0.08664
      0.08664
      0.08664
      0.08664
      0.08664
      0.08664
      0.08664
      0.08664
      0.08664
      0.08664
      0.08664
      0.08664
      0.08664
      0.08664
```

```
        0.08664
        0.08664
        0.08664
        0.08664
        0.08664
        0.08664
        0.08664
        0.08664
        0.08664 /
-- Molecular weights
MW
     16.0990
     44.0098
     30.0698
     44.0968
     58.1237
     72.1506
     84.9000
     91.7000
    111.4084
    138.6959
    165.3078
    190.9893
    217.4537
    247.4959
    282.6944
    311.2517
    337.7326
    379.3851
    435.6645
    497.8649
    573.8897
    680.2564
    884.4301 /
-- Boiling points (K)
TBOIL
    111.321
    194.650
    184.600
    231.100
    269.072
    305.573
    341.900
    365.100
    401.517
    450.523
    491.765
    529.587
    564.109
    591.737
    617.435
    641.896
    664.404
    696.016
    731.290
```

```
     765.285
     803.046
     852.110
     932.795 /
-- Critical volumes (m3/kg-mole)
VCRIT
       0.099
       0.094
       0.148
       0.203
       0.258
       0.305
       0.370
       0.454
       0.503
       0.500
       0.577
       0.661
       0.760
       0.880
       1.024
       1.143
       1.256
       1.438
       1.686
       1.966
       2.315
       2.818
       3.836 /
-- Critical Z-factors
ZCRIT
     0.28730
     0.27414
     0.28465
     0.28029
     0.27684
     0.26612
     0.26037
     0.35253
     0.30778
     0.24515
     0.24185
     0.24694
     0.25505
     0.26431
     0.27795
     0.28988
     0.30190
     0.32138
     0.34769
     0.37747
     0.41374
     0.46446
     0.56107 /
-- Volume translation/co-volume
```

```
SSHIFT
  0.021163
  0.110743
  0.058382
  0.080639
  0.095238
  0.117137
  0.140024
  0.052946
  0.115028
  0.143217
  0.145473
  0.133762
  0.120123
  0.105107
  0.078971
  0.054872
  0.030479
 -0.008186
 -0.062339
 -0.122307
 -0.194485
 -0.291357
 -0.460098 /
-- Parachors (dyn/cm)
PARACHOR
    77.004
    78.000
   108.900
   151.900
   188.425
   229.964
   271.000
   273.878
   320.987
   384.560
   446.812
   506.656
   568.666
   638.901
   721.334
   787.946
   849.933
   948.634
  1080.064
  1226.132
  1404.508
  1656.502
  2153.060 /

-- Binary interaction coefficients for SRK
BIC
  0.1194
  0.0003  0.1200
  0.0004  0.1200  0.0000
```

```
 0.0004   0.1200   0.0000   0.0000
 0.0004   0.1200   0.0000   0.0000   0.0000
 0.0004   0.1200   0.0000   0.0000   0.0000   0.0000
-0.0217   0.1000   0.0000   0.0000   0.0000   0.0000   0.0000
-0.0217   0.1000   0.0000   0.0000   0.0000   0.0000   0.0000   0.0000
-0.0217   0.1000  -0.0386  -0.0386   0.1000   0.1000   0.0000   0.0000
0.0000
-0.0217   0.1000  -0.0386  -0.0386   0.1000   0.1000   0.0000   0.0000
0.0000   0.0000
-0.0217   0.1000  -0.0386  -0.0386   0.1000   0.1000   0.0000   0.0000
0.0000   0.0000
 0.0000
-0.0217   0.1000  -0.0386  -0.0386   0.1000   0.1000   0.0000   0.0000
0.0000   0.0000
 0.0000   0.0000
 0.0004   0.1000  -0.0386  -0.0386   0.1000   0.1000   0.0000   0.0000
0.0000   0.0000
 0.0000   0.0000   0.0000
 0.0004   0.1000  -0.0386  -0.0386   0.1000   0.1000   0.0000   0.0000
0.0000   0.0000
 0.0000   0.0000   0.0000   0.0000
 0.0004   0.1000  -0.0386  -0.0386   0.1000   0.1000   0.0000   0.0000
0.0000   0.0000
 0.0000   0.0000   0.0000   0.0000   0.0000
 0.0004   0.1000  -0.0386  -0.0386   0.1000   0.1000   0.0000   0.0000
0.0000   0.0000
 0.0000   0.0000   0.0000   0.0000   0.0000   0.0000
 0.0004   0.1000  -0.0386  -0.0386   0.1000   0.1000   0.0000   0.0000
0.0000   0.0000
 0.0000   0.0000   0.0000   0.0000   0.0000   0.0000   0.0000
 0.0440   0.1000  -0.0386  -0.0386   0.1000   0.1000   0.0000   0.0000
0.0000   0.0000
 0.0000   0.0000   0.0000   0.0000   0.0000   0.0000   0.0000   0.0000
 0.0440   0.1000  -0.0386  -0.0386   0.1000   0.1000   0.0000   0.0000
0.0000   0.0000
 0.0000   0.0000   0.0000   0.0000   0.0000   0.0000   0.0000   0.0000
0.0000
 0.0440   0.1000  -0.0386  -0.0386   0.1000   0.1000   0.0000   0.0000
0.0000   0.0000
 0.0000   0.0000   0.0000   0.0000   0.0000   0.0000   0.0000   0.0000
0.0000   0.0000
 0.0440   0.1000  -0.0386  -0.0386   0.1000   0.1000   0.0000   0.0000
0.0000   0.0000
 0.0000   0.0000   0.0000   0.0000   0.0000   0.0000   0.0000   0.0000
0.0000   0.0000
 0.0000
 0.0440   0.1000  -0.0386  -0.0386   0.1000   0.1000   0.0000   0.0000
0.0000   0.0000
 0.0000   0.0000   0.0000   0.0000   0.0000   0.0000   0.0000   0.0000
0.0000   0.0000
 0.0000   0.0000
/
BICS
 0.1194
 0.0003   0.1200
```

```
   0.0004   0.1200   0.0000
   0.0004   0.1200   0.0000   0.0000
   0.0004   0.1200   0.0000   0.0000   0.0000
   0.0004   0.1200   0.0000   0.0000   0.0000   0.0000
  -0.0217   0.1000   0.0000   0.0000   0.0000   0.0000   0.0000
  -0.0217   0.1000   0.0000   0.0000   0.0000   0.0000   0.0000   0.0000
  -0.0217   0.1000  -0.0386  -0.0386   0.1000   0.1000   0.0000   0.0000
0.0000
  -0.0217   0.1000  -0.0386  -0.0386   0.1000   0.1000   0.0000   0.0000
0.0000   0.0000
  -0.0217   0.1000  -0.0386  -0.0386   0.1000   0.1000   0.0000   0.0000
0.0000   0.0000
   0.0000
  -0.0217   0.1000  -0.0386  -0.0386   0.1000   0.1000   0.0000   0.0000
0.0000   0.0000
   0.0000   0.0000
   0.0004   0.1000  -0.0386  -0.0386   0.1000   0.1000   0.0000   0.0000
0.0000   0.0000
   0.0000   0.0000   0.0000
   0.0004   0.1000  -0.0386  -0.0386   0.1000   0.1000   0.0000   0.0000
0.0000   0.0000
   0.0000   0.0000   0.0000   0.0000
   0.0004   0.1000  -0.0386  -0.0386   0.1000   0.1000   0.0000   0.0000
0.0000   0.0000
   0.0000   0.0000   0.0000   0.0000   0.0000
   0.0004   0.1000  -0.0386  -0.0386   0.1000   0.1000   0.0000   0.0000
0.0000   0.0000
   0.0000   0.0000   0.0000   0.0000   0.0000   0.0000
   0.0004   0.1000  -0.0386  -0.0386   0.1000   0.1000   0.0000   0.0000
0.0000   0.0000
   0.0000   0.0000   0.0000   0.0000   0.0000   0.0000   0.0000
   0.0440   0.1000  -0.0386  -0.0386   0.1000   0.1000   0.0000   0.0000
0.0000   0.0000
   0.0000   0.0000   0.0000   0.0000   0.0000   0.0000   0.0000   0.0000
   0.0440   0.1000  -0.0386  -0.0386   0.1000   0.1000   0.0000   0.0000
0.0000   0.0000
   0.0000   0.0000   0.0000   0.0000   0.0000   0.0000   0.0000   0.0000
0.0000
   0.0440   0.1000  -0.0386  -0.0386   0.1000   0.1000   0.0000   0.0000
0.0000   0.0000
   0.0000   0.0000   0.0000   0.0000   0.0000   0.0000   0.0000   0.0000
0.0000   0.0000
   0.0440   0.1000  -0.0386  -0.0386   0.1000   0.1000   0.0000   0.0000
0.0000   0.0000
   0.0000   0.0000   0.0000   0.0000   0.0000   0.0000   0.0000   0.0000
0.0000   0.0000
   0.0000
   0.0440   0.1000  -0.0386  -0.0386   0.1000   0.1000   0.0000   0.0000
0.0000   0.0000
   0.0000   0.0000   0.0000   0.0000   0.0000   0.0000   0.0000   0.0000
0.0000   0.0000
   0.0000   0.0000
/
-- LBC coefficients
LBCCOEF
```

```
       0.1023000     0.0233640     0.0585330     -0.0407580     0.0093324 /



ZMFVD
-- fangst
2281.4 0.8616657808  0.01226535306  0.05244599468  0.02028041964
0.022681707      0.01122011488   0.003397206034 0.004116986718
       0.00620510587 0.002528109425 0.001596423353 0.0009189308498
0.0004180440655 0.0001691082923 4.951613802E-005
       2.278395387E-005 1.075106663E-005 6.595722935E-006 9.429791311E-
007 2.06472326E-007 3.423045219E-008 5.429492413E-009
        1.356126031E-009

2281.5 0.4425082337   0.009896766408 0.05835009495 0.03512719583
0.02623017037 0.01633603789 0.01384698849 0.02753746472
       0.0598094026   0.04286831797  0.04539006171 0.04394886433
0.03370394422 0.02728639565 0.01676913834 0.01439133982 0.01235086663
       0.01969671461 0.01450759629   0.01288424951 0.01018133984
0.00934941577 0.007029400372

2393 0.4328286957 0.009840196586 0.05848115694 0.03547070843
0.02632052796 0.01646032985 0.01409027999 0.02808056007 0.06105122807
     0.04380086729 0.04640091716 0.0449409086 0.03447068796
0.0279105581 0.01715379887 0.01472183886 0.01263466905 0.02014950913
     0.01484116974 0.0131805093 0.01041544993 0.009564397561
0.007191034873 /
--
-- Kritt

2283.6 0.4425082337 0.009896766408 0.05835009495 0.03512719583
0.02623017037 0.01633603789 0.01384698849 0.02753746472 0.0598094026
  0.04286831797 0.04539006171 0.04394886433 0.03370394422 0.02728639565
0.01676913834 0.01439133982 0.01235086663 0.01969671461
  0.01450759629 0.01288424951 0.01018133984 0.00934941577
0.007029400372

2393 0.4328286957 0.009840196586 0.05848115694 0.03547070843
0.02632052796 0.01646032985 0.01409027999 0.02808056007
       0.06105122807 0.04380086729 0.04640091716 0.0449409086
0.03447068796 0.0279105581 0.01715379887 0.01472183886 0.01263466905
       0.02014950913 0.01484116974 0.0131805093 0.01041544993
0.009564397561 0.007191034873/ Kritt

 1.0 1.0 22*0 / dummy
 1.0 1.0 22*0 / dummy
 1.0 1.0 22*0 / dummy
 1.0 1.0 22*0 / dummy
 1.0 1.0 22*0 / dummy
 1.0 1.0 22*0 / dummy
-- Upper Tilje
2310 0.4425082337 0.009896766408 0.05835009495 0.03512719583
0.02623017037 0.01633603789 0.01384698849 0.02753746472 0.0598094026
       0.04286831797 0.04539006171 0.04394886433 0.03370394422
0.02728639565 0.01676913834 0.01439133982 0.01235086663 0.01969671461
```

```
      0.01450759629 0.01288424951 0.01018133984 0.00934941577
0.007029400372

2395 0.4328286957 0.009840196586 0.05848115694 0.03547070843
0.02632052796 0.01646032985 0.01409027999 0.02808056007
        0.06105122807 0.04380086729 0.04640091716 0.0449409086
0.03447068796 0.0279105581 0.01715379887 0.01472183886 0.01263466905
        0.02014950913 0.01484116974 0.0131805093 0.01041544993
0.009564397561 0.007191034873/
--
 1.0 1.0 22*0 / dummy 10
 1.0 1.0 22*0 / dummy
 1.0 1.0 22*0 / dummy
 1.0 1.0 22*0 / dummy

2299.9 0.8616657808  0.01226535306  0.05244599468  0.02028041964
0.022681707      0.01122011488   0.003397206034 0.004116986718
        0.00620510587 0.002528109425 0.001596423353 0.0009189308498
0.0004180440655 0.0001691082923 4.951613802E-005
        2.278395387E-005 1.075106663E-005 6.595722935E-006 9.429791311E-
007 2.06472326E-007 3.423045219E-008 5.429492413E-009
         1.356126031E-009

2300.0 0.4425082337  0.009896766408 0.05835009495 0.03512719583
0.02623017037 0.01633603789 0.01384698849 0.02753746472
        0.0598094026   0.04286831797  0.04539006171 0.04394886433
0.03370394422 0.02728639565 0.01676913834 0.01439133982 0.01235086663
        0.01969671461 0.01450759629  0.01288424951 0.01018133984
0.00934941577 0.007029400372

2393 0.4328286957 0.009840196586 0.05848115694 0.03547070843
0.02632052796 0.01646032985 0.01409027999 0.02808056007 0.06105122807
        0.04380086729 0.04640091716 0.0449409086 0.03447068796
0.0279105581 0.01715379887 0.01472183886 0.01263466905 0.02014950913
        0.01484116974 0.0131805093 0.01041544993 0.009564397561
0.007191034873 / 14

2304.9 0.8616657808  0.01226535306  0.05244599468  0.02028041964
0.022681707      0.01122011488   0.003397206034 0.004116986718
        0.00620510587 0.002528109425 0.001596423353 0.0009189308498
0.0004180440655 0.0001691082923 4.951613802E-005
        2.278395387E-005 1.075106663E-005 6.595722935E-006 9.429791311E-
007 2.06472326E-007 3.423045219E-008 5.429492413E-009
         1.356126031E-009

2305.0 0.4425082337  0.009896766408 0.05835009495 0.03512719583
0.02623017037 0.01633603789 0.01384698849 0.02753746472
        0.0598094026   0.04286831797  0.04539006171 0.04394886433
0.03370394422 0.02728639565 0.01676913834 0.01439133982 0.01235086663
        0.01969671461 0.01450759629  0.01288424951 0.01018133984
0.00934941577 0.007029400372

2393 0.4328286957 0.009840196586 0.05848115694 0.03547070843
0.02632052796 0.01646032985 0.01409027999 0.02808056007 0.06105122807
```

```
      0.04380086729 0.04640091716 0.0449409086 0.03447068796
0.0279105581 0.01715379887 0.01472183886 0.01263466905 0.02014950913
      0.01484116974 0.0131805093 0.01041544993 0.009564397561
0.007191034873 / 15


 1.0 1.0 22*0 / dummy
 1.0 1.0 22*0 / dummy
 1.0 1.0 22*0 / dummy
 1.0 1.0 22*0 / dummy
 1.0 1.0 22*0 / dummy 20
 1.0 1.0 22*0 / dummy
 1.0 1.0 22*0 / dummy
 1.0 1.0 22*0 / dummy
 1.0 1.0 22*0 / dummy
 1.0 1.0 22*0 / dummy
 1.0 1.0 22*0 / dummy
 1.0 1.0 22*0 / dummy
 1.0 1.0 22*0 / dummy
 1.0 1.0 22*0 / dummy
 1.0 1.0 22*0 / dummy 30
 1.0 1.0 22*0 / dummy
 1.0 1.0 22*0 / dummy
 1.0 1.0 22*0 / dummy
 1.0 1.0 22*0 / dummy
 1.0 1.0 22*0 / dummy
 1.0 1.0 22*0 / dummy
 1.0 1.0 22*0 / dummy
 1.0 1.0 22*0 / dummy
 1.0 1.0 22*0 / dummy
 1.0 1.0 22*0 / dummy 40
 1.0 1.0 22*0 / dummy
 1.0 1.0 22*0 / dummy
 1.0 1.0 22*0 / dummy
--  1.0 1.0 22*0 / dummy
--  1.0 1.0 22*0 / dummy
--  1.0 1.0 22*0 / dummy
--  1.0 1.0 22*0 / dummy
--  1.0 1.0 22*0 / dummy
--  1.0 1.0 22*0 / dummy
--  1.0 1.0 22*0 / dummy 50
--  1.0 1.0 22*0 / dummy
--  1.0 1.0 22*0 / dummy
--  1.0 1.0 22*0 / dummy
--  1.0 1.0 22*0 / dummy
--  1.0 1.0 22*0 / dummy
--  1.0 1.0 22*0 / dummy
--  1.0 1.0 22*0 / dummy
--  1.0 1.0 22*0 / dummy
--  1.0 1.0 22*0 / dummy 60
--  1.0 1.0 22*0 / dummy
--  1.0 1.0 22*0 / dummy
--  1.0 1.0 22*0 / dummy
--  1.0 1.0 22*0 / dummy
--  1.0 1.0 22*0 / dummy
```

```
--  1.0 1.0 22*0 / dummy
--  1.0 1.0 22*0 / dummy
--  1.0 1.0 22*0 / dummy
--  1.0 1.0 22*0 / dummy
--  1.0 1.0 22*0 / dummy 70
--  1.0 1.0 22*0 / dummy
--  1.0 1.0 22*0 / dummy
--  1.0 1.0 22*0 / dummy
--  1.0 1.0 22*0 / dummy
--  1.0 1.0 22*0 / dummy
--  1.0 1.0 22*0 / dummy
```